

REPORT NO.  
UCB/EERC-89/12  
NOVEMBER 1989

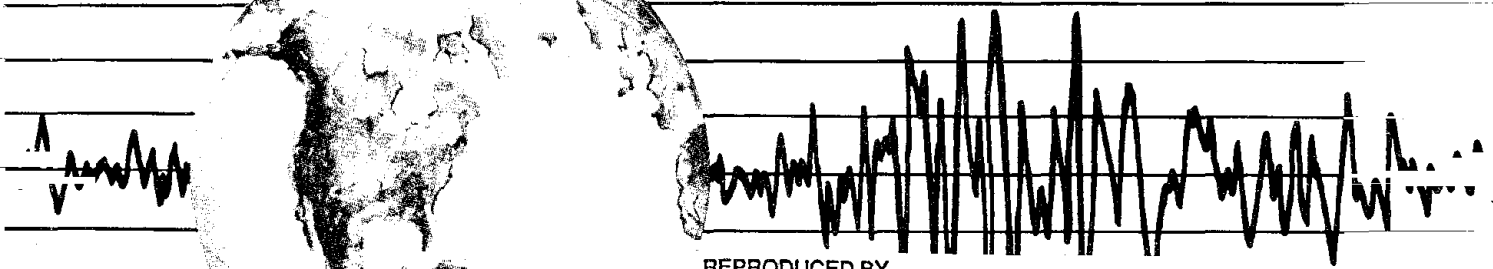
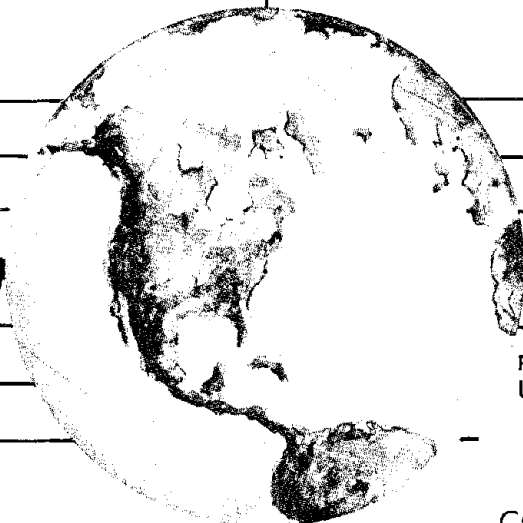
EARTHQUAKE ENGINEERING RESEARCH CENTER

# ADAP-88

## A COMPUTER PROGRAM FOR NONLINEAR EARTHQUAKE ANALYSIS OF CONCRETE ARCH DAMS

by

GREGORY L. FENVES  
SOHEIL MOJTAHEDI  
RICHARD B. REIMER



REPRODUCED BY  
U.S. DEPARTMENT OF COMMERCE  
NATIONAL TECHNICAL  
INFORMATION SERVICE  
SPRINGFIELD, VA 22161

COLLEGE OF ENGINEERING

UNIVERSITY OF CALIFORNIA AT BERKELEY

For sale by the National Technical Information Service, U.S. Department of Commerce, Springfield, Virginia 22161

See back of report for up to date listing of EERC reports.

**DISCLAIMER**

Any opinions, findings, and conclusions or recommendations expressed in this publication are those of the authors and do not necessarily reflect the views of the Sponsors or the Earthquake Engineering Research Center, University of California at Berkeley.

**ADAP-88: A COMPUTER PROGRAM FOR NONLINEAR  
EARTHQUAKE ANALYSIS OF CONCRETE ARCH DAMS**

by

Gregory L. Fenves

Soheil Mojtahedi

Richard B. Reimer

Report No. UCB/EERC-89/12  
Earthquake Engineering Research Center  
College of Engineering  
University of California at Berkeley

November 1989

*ia*

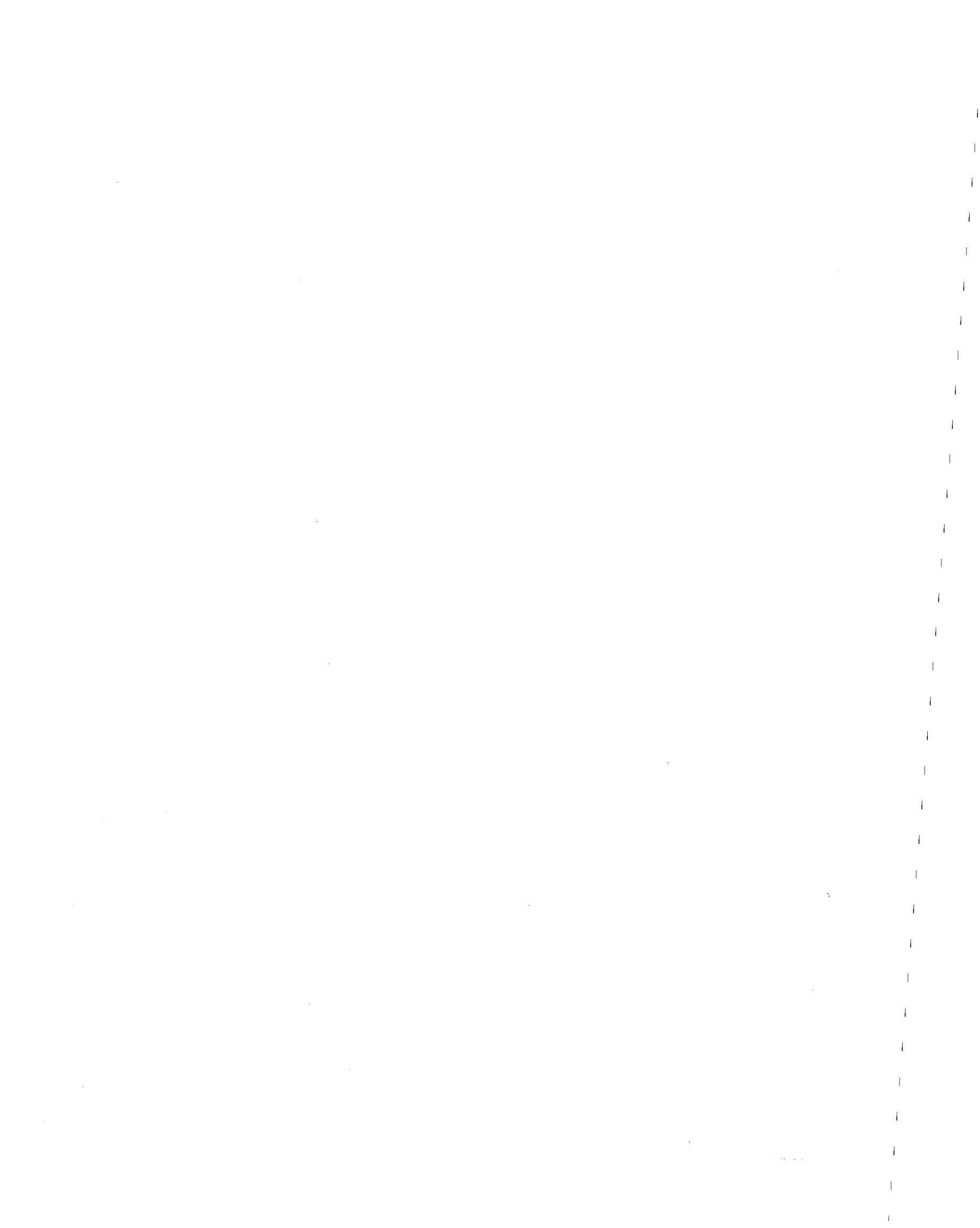


## ABSTRACT

The modeling and dynamic analysis of concrete arch dams, the impounded water, and foundation rock is an important step in the earthquake safety evaluation of such systems. Sophisticated methods of earthquake analysis assuming linear elastic response have been developed. An analysis assuming an arch dam is an elastic monolithic structure usually shows large tensile stresses in the arch direction. Because arch dams are constructed as cantilever monoliths, the joints between the monoliths cannot develop the tensile stress predicted in a linear analysis. In reality, the joints can be expected to open and close during an earthquake, releasing arch stresses and redistributing forces.

In this study, a nonlinear joint element is implemented in a finite element computer program and it is used to model the opening and closing of contraction joints in concrete arch dams. The joint element is combined with shell, solid, and fluid finite elements to model a complete arch dam system. Special consideration is given to resolving the stress distribution near the joints by using a refined mesh of solid elements. A numerical procedure for solving the equations of motion recognizes that the nonlinearity in the model is restricted to the joints. The monoliths between contraction joint elements are modeled as linear substructures: this provides a significant reduction of computation in the iterative solution of the nonlinear equations of motion. A study of the finite element modeling shows that the joint opening mechanism reduces the effective vibration frequency of a structure and demonstrates the same qualitative trends observed in the experimental testing of an arch rib. The results of an earthquake analysis of a typical concrete arch dam indicate the expected release of arch tension stresses and subsequent redistribution of forces.

The computer program ADAP-88 implements the nonlinear joint element and solution procedure along with shell, solid, and fluid elements for modeling an arch dam system. The program includes a finite element mesh generator. Experience with the program has shown its computational efficiency.



## ACKNOWLEDGEMENTS

The research and computer program development described in this report was supported by a cooperative industrial effort. Four organizations provided support for the project: County of Los Angeles, Department of Public Works, Los Angeles, CA; Electric Power Research Institute, Palo Alto, CA; Harza Engineering Company, Chicago, IL; and Pacific Gas and Electric Company, San Francisco, CA. The organization and technical representatives of the sponsors are listed below. The cooperation of these organizations and individuals is greatly appreciated.

Sponsor	Organization Representative	Technical Representative
County of Los Angeles, Department of Public Works	Roger W. Burger	Robert J. Kroll
Electric Power Research Institute	Douglas I. Morris	Douglas I. Morris
Harza Engineering Company	Roman P. Wengler	C.H. Yeh
Pacific Gas and Electric Company	Ronald G. Domer	Charles S. Ahlgren

Professor Ray W. Clough provided the motivation for the research in addition to offering thoughtful suggestions. Dr. Yusof Ghanaat participated in many of the project meetings and contributed valuable advice. Mr. Satinder P. Singh conducted several of the tests of the joint element and performed the analysis of Big Tujunga Dam. Professor E.L. Wilson contributed advice and several subroutines used in the computer program.

Additional support from the National Science Foundation under Grant No. BCS-8896121 to the first author is also acknowledged.

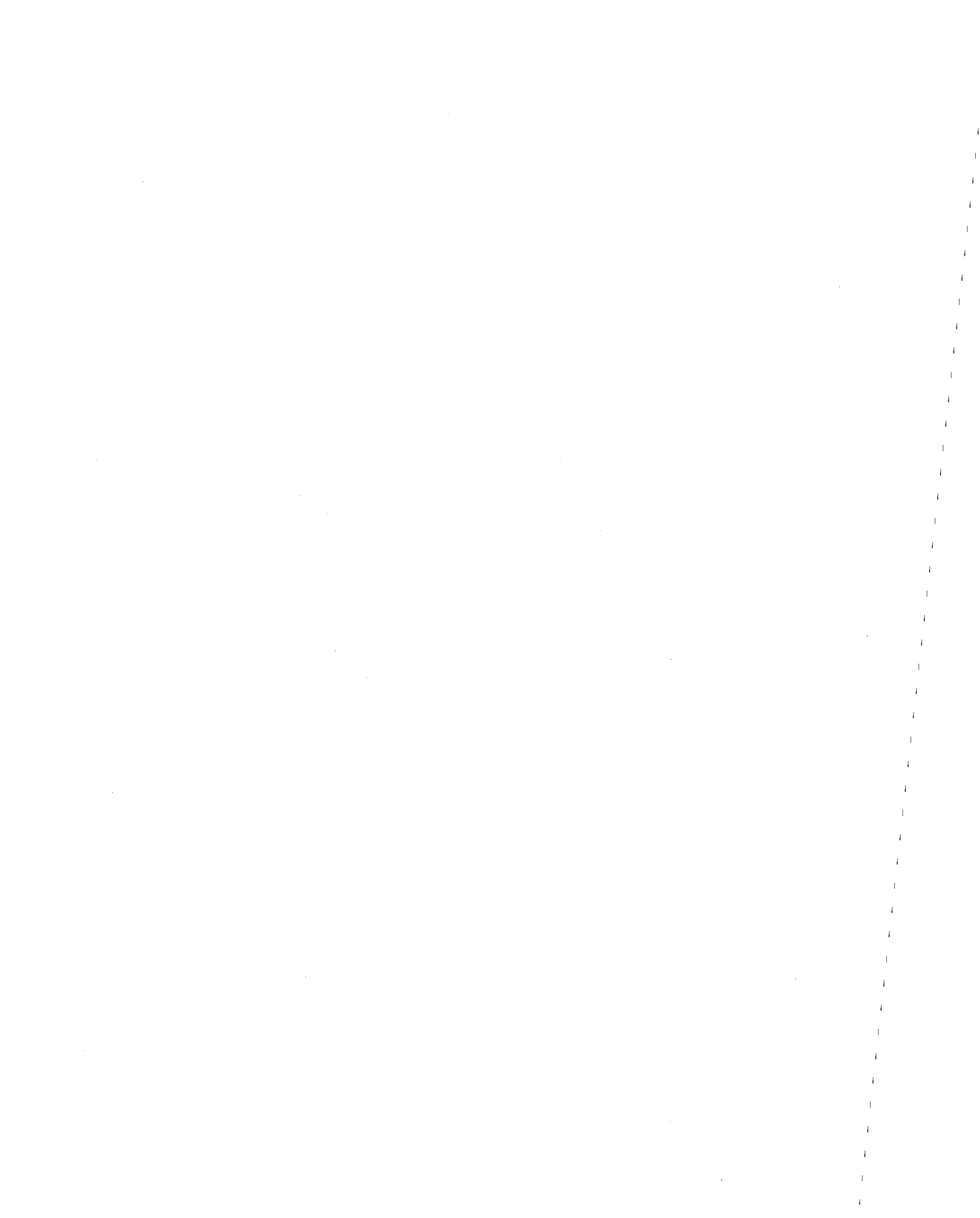




## TABLE OF CONTENTS

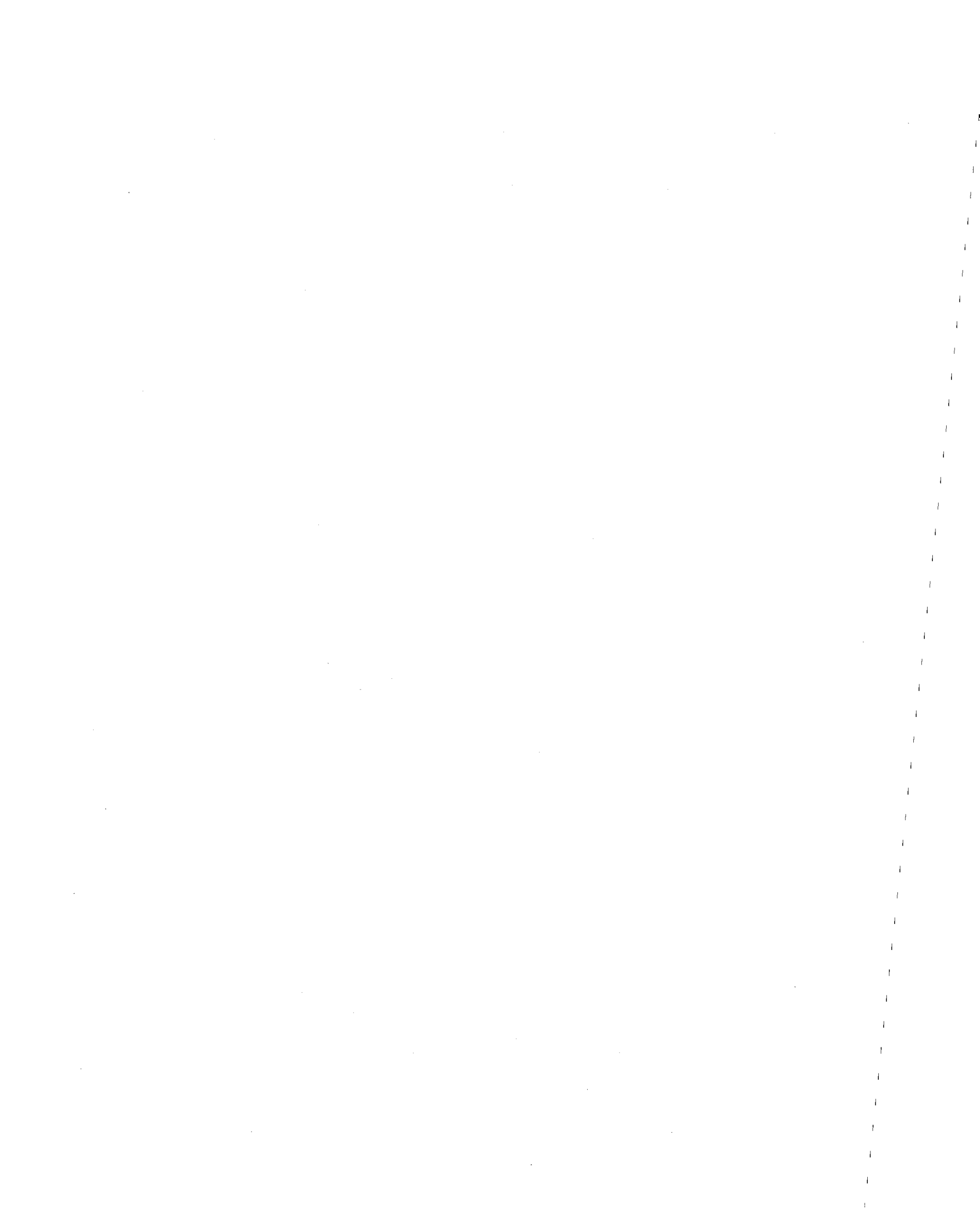
ABSTRACT .....	i
ACKNOWLEDGEMENTS .....	iii
TABLE OF CONTENTS .....	v
LIST OF TABLES.....	ix
LIST OF FIGURES.....	xi
1. INTRODUCTION.....	1
1.1 Objectives of the Study.....	2
1.2 Summary of Previous Work.....	2
1.3 Organization of Report .....	3
2. FINITE ELEMENT MODEL FOR ARCH DAMS .....	5
2.1 Introduction.....	5
2.2 Nonlinear Joint Element.....	5
2.2.1 Element Geometry .....	7
2.2.2 Kinematics.....	8
2.2.3 Force–Displacement Relationship.....	9
2.2.4 Restoring Forces and Tangent Stiffness Matrix.....	10
2.2.5 Numerical Integration of Element Matrices .....	11
2.3 Shell and Solid Elements.....	12
2.4 Transition Between Contraction Joint Elements and Thick Shell Elements.....	12
2.5 Finite Element Mesh Generation .....	12
2.6 Static Analysis.....	14
3. DYNAMIC ANALYSIS OF NONLINEAR SYSTEMS WITH LINEAR SUBSTRUCTURES .....	17
3.1 Introduction.....	17
3.2 Substructure Solution Procedure.....	17
3.2.1 Linear Substructure.....	17
3.2.2 Nonlinear Substructure.....	20
3.2.3 Initial Conditions.....	22
3.2.4 Effective Load for Earthquake Ground Motion .....	23
3.2.5 Discussion of the Procedure.....	23

## TABLE OF CONTENTS (cont'd)

3.3 Effective Force for Linear Substructures.....	24
3.4 Algorithm for the Numerical Procedure .....	26
3.5 Effect of Static Response.....	28
4. DAM-WATER INTERACTION AND DAM-FOUNDATION	
INTERACTION.....	29
4.1 Introduction.....	29
4.2 Dam-Water Interaction .....	29
4.2.1 Equations of Motion for Incompressible Fluids.....	29
4.2.2 Fluid-Structure Coupling.....	32
4.2.3 Solution Procedures for Coupled Equations of Motion .....	34
4.2.4 Selection of Solution Method.....	35
4.3 Dam-Foundation Interaction.....	37
5. STUDY OF CONTRACTION JOINT MODEL.....	39
5.1 Introduction.....	39
5.2 Cantilever Beam.....	39
5.3 Experimental and Analytical Response of an Arch Rib.....	48
5.3.1 Experimental Model of Arch Rib.....	48
5.3.2 Finite Element Model of Arch Rib .....	50
5.3.3 Ground Motion.....	50
5.3.4 Comparison of Experimental and Analytical Response .....	51
5.3.5 Comparison of Joint Opening .....	53
5.3.6 Discussion of Response Comparison .....	54
5.4 Summary.....	57
6. EARTHQUAKE ANALYSIS OF BIG TUJUNGA DAM .....	59
6.1 Introduction.....	59
6.2 Finite Element Model and Ground Motion.....	59
6.3 Static Response.....	63
6.4 Earthquake Response.....	65
7. CONCLUSIONS.....	81
8. REFERENCES .....	83

TABLE OF CONTENTS (cont'd)

APPENDIX A: USER GUIDE FOR ADAP-88.....	85
A.1 Introduction .....	85
A.2 Mesh Generation.....	85
A.2.1 Mesh Generation Concepts.....	85
A.2.2 Generation of Dam Mesh.....	87
A.2.3 Generation of Foundation Mesh.....	89
A.3 Parameters for Joint Elements.....	91
A.4 Static Analysis .....	91
A.5 Earthquake Analysis.....	92
A.6 Description of Input Data .....	93
A.7 Description of Earthquake Response Output.....	101
A.7.1 Nodal Point Displacements.....	101
A.7.2 Joint Element Displacements.....	102
A.7.3 Stresses in 3-D Solid Elements.....	103
A.7.4 Stresses in 3-D Shell Elements.....	104
A.7.5 Stresses in Thick Shell and Transition Elements .....	105
A.8 Saving Response Histories and Response Envelopes.....	107
A.8.1 Response Histories.....	107
A.8.2 Response Envelopes .....	107
A.9 Installation of ADAP-88 Program.....	107
A.9.1 Dynamic Storage Allocation.....	107
A.9.2 Mesh Plotting .....	108
APPENDIX B: USER GUIDE FOR RESVOR.....	109
B.1 Introduction .....	109
B.2 Description of Input Data .....	109



## LIST OF TABLES

TABLE 4.1	Effect of Incompressible Added Mass of Water on Vibration Frequencies of Morrow Point Dam .....	36
TABLE 5.1	Vibration Frequencies of Experimental and Analytical Models of Arch Rib.....	50
TABLE 5.2	Cases of El Centro Ground Motion Applied to Experimental and Analytical Models of Arch Rib.....	51
TABLE 6.1	Cases for Earthquake Analysis of Big Tujunga Dam .....	62
TABLE 6.2	Vibration Frequencies of Big Tujunga Dam with Flexible Foundation Rock .....	63
TABLE A.1	Parameters for Foundation Mesh Generation .....	90
TABLE A.2	Natural Coordinates of Integration Points for Joint Element.....	103
TABLE A.3	Stress Components in 3-D Solid Elements .....	103
TABLE A.4	Stress Components in 3-D Shell Elements.....	105
TABLE A.5	Natural Coordinates of Integration Points for Thick Shell and Transition Elements .....	106
TABLE A.6	Stress Components in Thick Shell and Transition Elements .....	106



## LIST OF FIGURES

FIGURE 2.1	Finite Element Model of Arch Dam .....	6
FIGURE 2.2	Nonlinear Joint Element .....	7
FIGURE 2.3	Stress–Relative Displacement Relationship for Joint Element .....	10
FIGURE 2.4	Location of Contraction Joints at Crest .....	14
FIGURE 3.1	Schematic Representation of Linear and Nonlinear Substructures	18
FIGURE 4.1	Dam and Water Domains .....	30
FIGURE 4.2	Coupling of Dam and Water Finite Element Models .....	33
FIGURE 5.1	Finite Element Model of Cantilever Beam with Joint at Support ..	39
FIGURE 5.2	Vertical Displacement at Free End of Cantilever Beam Due to Harmonic Support Acceleration with $f=48$ Hz.....	41
FIGURE 5.3	Joint Displacement at Fixed End of Cantilever Beam Due to Harmonic Support Acceleration with $f=48$ Hz.....	42
FIGURE 5.4	Vertical Displacement at Free End of Cantilever Beam Due to Harmonic Support Acceleration with $f=80$ Hz.....	43
FIGURE 5.5	Joint Displacement at Bottom of Fixed End of Cantilever Beam Due to Harmonic Support Acceleration with $f=80$ Hz.....	44
FIGURE 5.6	Illustration of the Effect of the Frequency Ratio on the Dynamic Amplification for Harmonic Support Acceleration of a Single Degree-of-Freedom System.....	45
FIGURE 5.7	Normal Stress and Joint Displacement at Support of Cantilever Beam with Axial Thrust of 5 kip Due to Harmonic Support Acceleration of $f=80$ Hz .....	46
FIGURE 5.8	Response of Cantilever Beam with Axial Thrust of 2 kip Due to Harmonic Support Acceleration of $f=80$ Hz .....	47
FIGURE 5.9	Scaled Model of Arch Rib on Shaking Table (Niwa and Clough, 1980).....	48
FIGURE 5.10	Elastic Vibration Modes Determined from Free Vibration Tests (Niwa and Clough, 1980).....	49
FIGURE 5.11	Finite Element Model of Arch Rib.....	49
FIGURE 5.12	First Antisymmetric Response of Finite Element Model of Arch Rib, Cases 1 and 2 .....	52
FIGURE 5.13	First Antisymmetric Response of Experimental Model of Arch Rib, Cases 1 and 2 (Niwa and Clough, 1980).....	53

## LIST OF FIGURES (cont'd)

FIGURE 5.14	First Antisymmetric Response of Finite Element Model of Arch Rib, Peak Ground Acceleration 0.740 g, Case 3.....	54
FIGURE 5.15	First Antisymmetric Response of Models of Arch Rib, Biaxial Excitation, Case 4.....	55
FIGURE 5.16	Joint Opening Ratio for Models of Arch Rib, Peak Ground Acceleration 0.152 g, Case 2 .....	56
FIGURE 5.17	First Antisymmetric Response of Finite Element Model of Arch Rib with Small Tangential Joint Stiffness, Peak Ground Acceleration 0.152 g, Case 2 .....	57
FIGURE 6.1	Plan of Big Tujunga Dam .....	60
FIGURE 6.2	Finite Element Mesh of Big Tujunga Dam with Three Contraction Joints (Foundation Rock Mesh Not Shown).....	61
FIGURE 6.3	Ground Motion for Earthquake Analysis of Big Tujunga Dam, as Scaled from Lake Hughes No. 12 Records.....	64
FIGURE 6.4	Pseudo–Acceleration Spectra for Ground Motion Used in Earthquake Analysis of Big Tujunga Dam .....	65
FIGURE 6.5	Envelopes of Maximum Arch Stresses (in psi) in Big Tujunga Dam Due to Static Loads with One–Third Reservoir.....	66
FIGURE 6.6	Envelopes of Maximum Cantilever Stresses (in psi) in Big Tujunga Dam Due to Static Loads with One–Third Reservoir .....	67
FIGURE 6.7	Envelopes of Maximum Arch Stresses (in psi) in Big Tujunga Dam Due to Static Loads with Full Reservoir.....	68
FIGURE 6.8	Envelopes of Maximum Cantilever Stresses (in psi) in Big Tujunga Dam Due to Static Loads with Full Reservoir .....	69
FIGURE 6.9	Regions of Joint Opening in Big Tujunga Dam Due to Static Loads .....	70
FIGURE 6.10	Envelopes of Maximum Arch Stresses (in psi) in Big Tujunga Dam Due to Ground Motion with One–Third Reservoir.....	71
FIGURE 6.11	Envelopes of Maximum Cantilever Stresses (in psi) in Big Tujunga Dam Due to Ground Motion with One–Third Reservoir .	72
FIGURE 6.12	Envelopes of Maximum Arch Stresses (in psi) in Big Tujunga Dam Due to Ground Motion with Full Reservoir.....	74



## LIST OF FIGURES (cont'd)

FIGURE 6.13	Envelopes of Maximum Cantilever Stresses (in psi) in Big Tujunga Dam Due to Ground Motion with Full Reservoir .....	75
FIGURE 6.14	Displacement at Crest in the Stream Direction of Big Tujunga Dam Due to Ground Motion with Full Reservoir.....	76
FIGURE 6.15	Opening Displacement of Contraction Joints in Big Tujunga Dam Due to Ground Motion with Full Reservoir .....	77
FIGURE 6.16	Maximum Joint Opening in Big Tujunga Dam Due to Ground Motion with Full Reservoir .....	78
FIGURE 6.17	Envelopes of Maximum Stresses (in psi) in Big Tujunga Dam with One Contraction Joint Due to Ground Motion with Full Reservoir (Case 5) .....	79
FIGURE A.1	Plan View of Dam Crest.....	86
FIGURE A.2	Typical Horizontal Section of Dam.....	87
FIGURE A.3	Finite Element Mesh on Reference Surface of Dam.....	88
FIGURE A.4	Projection of Abutment and Foundation Model on X-Z Plane ....	89
FIGURE A.5	Foundation Mesh on Interface of Layers of 3-D Solid Elements..	90
FIGURE A.6	Integration Points for Joint Element.....	102
FIGURE A.7	Stress Points for 3-D Shell Element.....	104
FIGURE A.8	Stress Points for Thick Shell and Transition Elements .....	105



# Chapter 1

## *INTRODUCTION*

Although concrete dams have historically been regarded as safe structures during earthquakes, it is important that owners, designers, and operators have the capability to evaluate the expected seismic performance of proposed and existing dams. The seismic evaluation of a concrete dam generally requires the following steps:

1. Selection of credible and maximum expected earthquake ground motions at the site;
2. Modeling the dam, foundation, and impounded water and performing a dynamic analysis for the postulated ground motions;
3. Evaluation of the dynamic response, including assessment of post-earthquake stability.

The modeling and dynamic analysis of the dam, foundation, and water system is a critical step in the evaluation procedure. Sophisticated methods of dynamic analysis assuming linear elastic response of the system are well established and have been implemented in ADAP (Arch Dam Analysis Program), a widely used computer program for earthquake analysis of concrete arch dams (Clough, et al., 1973). ADAP uses a three-dimensional finite element model of the dam and foundation rock region. The original version of ADAP represented the water impounded in the reservoir as an added mass using an approximation based on Westergaard's development. Although the Westergaard added mass approach is computationally efficient, it does not properly represent the hydrodynamic forces acting on dams. A recent extension to ADAP, included in the program EADAP (Ghanaat and Clough, 1989), uses an added mass matrix computed from a finite element model of the impounded water assuming incompressible fluid (Kuo, 1982).

Earthquake analysis of concrete arch dams assuming linear behavior is important for understanding the general characteristics of the dynamic response including dam-water interaction and dam-foundation interaction effects. An analysis assuming that an arch dam is a monolithic structure invariably shows net tensile stresses in the arch direction: the dynamic tensile stresses in the arch direction exceed the static compressive arch stresses. However, arch dams are constructed as cantilever monoliths separated by contraction joints, and the joints cannot develop the tensile stresses indicated in a linear analysis. The joints can be expected to open and close during an earthquake, producing a significant redistribution of stresses.

The effect of the contraction joint opening mechanism on the earthquake response of an arch dam depends on a number of factors. The loss of arch stiffness lengthens the vibration periods of

the dam, possibly shifting the periods into different regions of the ground motion spectrum, and hence changing the maximum response. The release of arch stresses at the contraction joints precludes vertical cracking of the concrete near the joints and transfer forces to the cantilevers. The cantilever blocks must have sufficient strength to resist the additional forces. Under severe ground motion it is possible for the cantilevers to become overloaded, possibly resulting in crushing or horizontal cracking of the cantilevers. The repeated opening and closing of the contraction joints may degrade the joint and lead to local failure of the concrete. Joint degradation was clearly demonstrated in shaking table tests of a single arch rib, which became unstable after a compressive failure at a joint.

### **1.1 Objectives of the Study**

There is an important need for computing the nonlinear response of concrete arch dams to determine the earthquake behavior when contraction joints open and close. The principal objective of this study is to develop a three-dimensional nonlinear joint element and an efficient numerical procedure for solving the nonlinear equations of motion for such a problem. Because of the acceptance of the computer program ADAP, a nonlinear analysis procedure is implemented in a new version of the program, called ADAP-88. The new program retains ADAP's features for modeling and generating finite element meshes for the dam, foundation rock, and impounded water.

Another objective of this work is to compare the analytical response of arch dams including joint opening with the response of an arch dam model tested on a shaking table. Finally, a typical concrete arch dam is analyzed to ascertain the effects of the contraction joint mechanism on the earthquake response of the dam.

### **1.2 Summary of Previous Work**

The joint mechanism in arch dams was described by Clough (Clough, 1980). The observations led to experimental testing of an arch dam model to determine the effect of joint opening. In a series of shaking table studies at the Earthquake Engineering Research Center at the University of California at Berkeley (Niwa and Clough, 1980), a single segmental arch rib was subjected to support motion to simulate the opening and closing of the joints between the segments. The tests showed that joint opening suppresses tensile stresses in the arch direction of the rib, but significantly increases compressive stresses. For large amplitude excitation, the arch rib failed by crushing of the material in the reduced contact area of the joints.

The importance of the joint opening mechanism has led to two analytical research efforts. In the first study, a smeared crack representation of the joints was developed along with an approximate method for achieving equilibrium in the numerical solution (Kuo, 1982). The analysis demonstrated reduction in arch stresses and transfer of load to the cantilevers. In the most

complete work to date, a discrete joint model represented by nonlinear springs was developed (Dowling and Hall, 1989). The spring stiffnesses (rotational and normal to the joint) were obtained from a separate two-dimensional analysis of a typical arch. The impounded water was modeled as an incompressible fluid. The analysis demonstrated that contraction joint opening, particularly in the upper portions of the joint, is significant in arch dam response even under moderate earthquake ground motion. Also, large compressive stresses in the closed portion of the joint were indicated.

### **1.3 Organization of Report**

The finite elements necessary for earthquake analysis of arch dams are described in Chapter 2. The chapter presents the formulation for the joint element in addition to summarizing the elements used for modeling the dam body and foundation region. Chapter 3 presents the substructure formulation for dynamic analysis of systems with local nonlinearities. Chapter 4 describes the methods for including dam-water interaction, assuming incompressible water, and dam-foundation rock interaction. A study of the joint element and solution procedure is presented in Chapter 5, where the experimental response of an arch rib is compared with the numerical response. The earthquake analysis of a typical dam, Big Tujunga, is given in Chapter 6 with the emphasis on the effect of the joint opening mechanism on the response. Chapter 7 presents the conclusions of the study. Appendices A and B are guides for the users of the computer program ADAP-88.



# Chapter 2

## *FINITE ELEMENT MODEL FOR ARCH DAMS*

### 2.1 Introduction

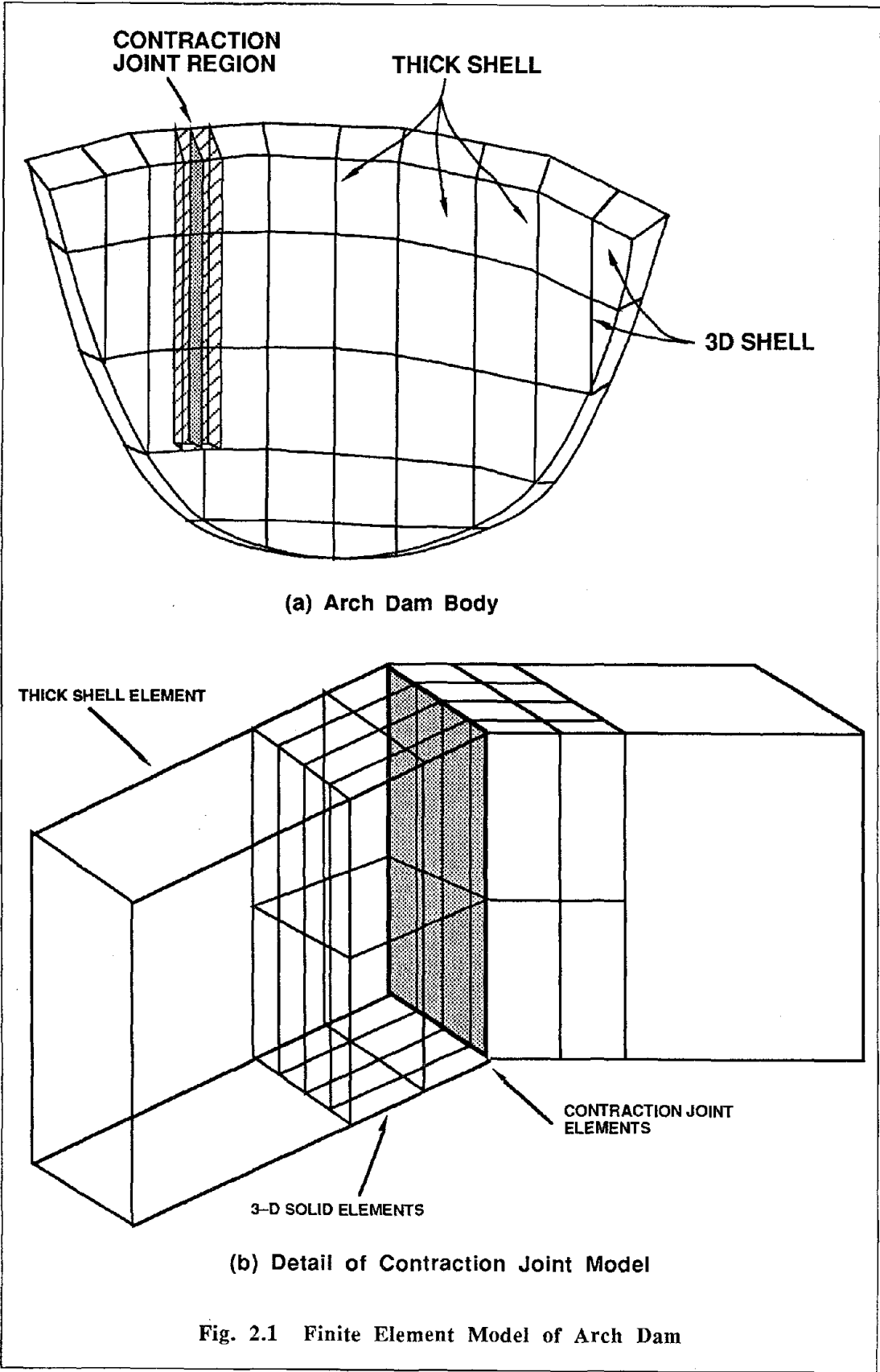
This chapter presents the finite element model used for the earthquake analysis of concrete arch dams. The elements used to model the dam body and foundation rock are the same as in the original version of ADAP (Clough, et al., 1973). The cantilevers are modeled by two types of shell elements. A three-dimensional shell element is used near the abutments and a thick shell element is used in the cantilevers away from the abutments. The foundation of the dam is modeled by three-dimensional solid elements.

The major new feature in ADAP-88 is an element to model the opening and closing of contraction joints. The element has a nonlinear force-displacement relationship which must be accounted for in the solution for dynamic response. To represent the local behavior and stress concentration near the contraction joints, a portion of the cantilever adjacent to the joints is modeled with three-dimensional solid elements. Figure 2.1 shows a typical finite element model of an arch dam. The program includes a finite element mesh generator with the capability to develop models representing a wide range of arch dam configurations.

### 2.2 Nonlinear Joint Element

The nonlinear joint element models the opening and closing of contraction joints in an arch dam. The element develops a resisting force due to relative deformation at the joint. The joint does not develop inertial or damping forces, hence the element does not have mass or damping.

The element described in this section is similar to previous joint elements used in other applications (Ghaboussi, et al., 1973; Goodman, et al., 1968; Mojtahedi, et al., 1988). A summary of joint elements for arch dams is given in a recent paper (Hohberg and Bachman, 1988).





### 2.2.1 Element Geometry

Figure 2.2 shows the eight node joint element. The element consists of two coincident surfaces, in which each surface is defined by four nodes. It is not necessary that the four nodes defining the joint surface lie on a plane.

The geometry of the coincident joint surfaces is described isoparametrically in terms of the nodal coordinates:

$$\mathbf{x} = \sum_{j=1}^4 N_j \mathbf{x}_j \quad (2.1)$$

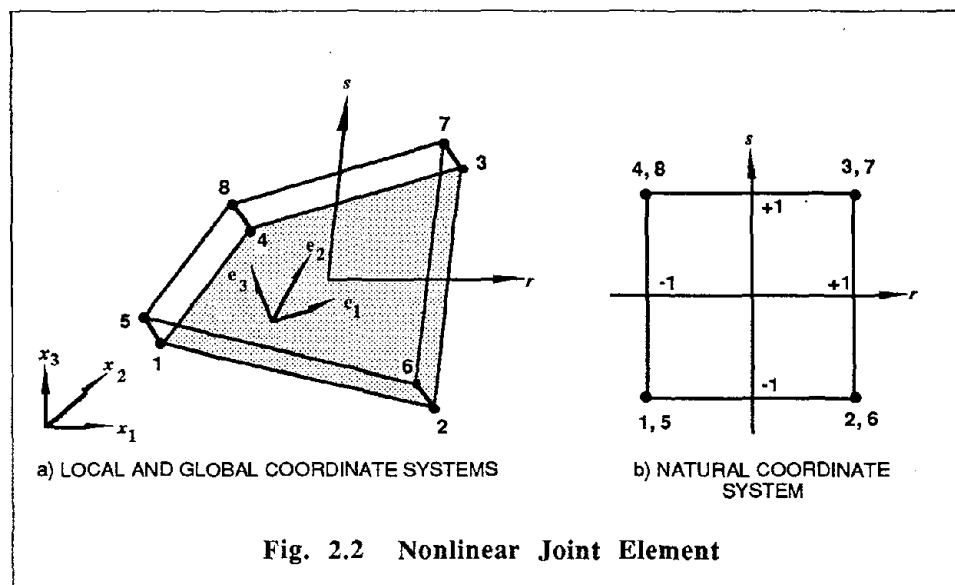
where  $\mathbf{x}$  are the global coordinates of a point on the joint surface and  $\mathbf{x}_j$  are the coordinates of nodes  $j$  and  $j+4$ ,

$$\mathbf{x} = \begin{Bmatrix} x_1 \\ x_2 \\ x_3 \end{Bmatrix} \quad \mathbf{x}_j = \begin{Bmatrix} x_{1j} \\ x_{2j} \\ x_{3j} \end{Bmatrix} \quad (2.2)$$

The shape functions are given in the natural coordinate system,

$$N_j = \frac{1}{4}(1+r_j r)(1+s_j s) \quad j = 1, 2, 3, 4 \quad (2.3)$$

in which  $r_j, s_j$  are the coordinates of node  $j$ .



An orthonormal coordinate system is constructed at every point on the surface of the joint element, as shown in Fig. 2.2. One axis is perpendicular to the surface (axis 3) and two axes are

tangent to the surface (axes 1 and 2). The orthonormal basis is constructed from the three vectors defined as follows (Hughes, 1987):

$$\mathbf{e}_r = \frac{\mathbf{x}_{,r}}{\|\mathbf{x}_{,r}\|} \quad (2.4a)$$

$$\mathbf{e}_s = \frac{\mathbf{x}_{,s}}{\|\mathbf{x}_{,s}\|} \quad (2.4b)$$

$$\mathbf{e}_3 = \frac{\mathbf{e}_r \times \mathbf{e}_s}{\|\mathbf{e}_r \times \mathbf{e}_s\|} \quad (2.4c)$$

in which the comma notation indicates differentiation. The vectors  $\mathbf{e}_r$  and  $\mathbf{e}_s$  can be orthogonalized to define  $\mathbf{e}_1$  and  $\mathbf{e}_2$ :

$$\mathbf{e}_1 = \frac{\sqrt{2}}{2} (\mathbf{e}_\alpha - \mathbf{e}_\beta) \quad (2.5a)$$

$$\mathbf{e}_2 = \frac{\sqrt{2}}{2} (\mathbf{e}_\alpha + \mathbf{e}_\beta) \quad (2.5b)$$

in which,

$$\mathbf{e}_\alpha = \frac{\mathbf{e}_r + \mathbf{e}_s}{\|\mathbf{e}_r + \mathbf{e}_s\|} \quad (2.5c)$$

$$\mathbf{e}_\beta = \frac{\mathbf{e}_3 \times \mathbf{e}_\alpha}{\|\mathbf{e}_3 \times \mathbf{e}_\alpha\|} \quad (2.5d)$$

### 2.2.2 Kinematics

The displacements of the bottom surface (defined by nodes 1 to 4) of the joint and the top surface (defined by nodes 5 to 8) are given by:

$$\mathbf{u}_{bot} = N_1 \mathbf{u}_1 + N_2 \mathbf{u}_2 + N_3 \mathbf{u}_3 + N_4 \mathbf{u}_4 \quad (2.6a)$$

$$\mathbf{u}_{top} = N_1 \mathbf{u}_5 + N_2 \mathbf{u}_6 + N_3 \mathbf{u}_7 + N_4 \mathbf{u}_8 \quad (2.6b)$$

where  $\mathbf{u}_j$  is the displacements of node  $j$ .

The bottom and top surface displacements can be expressed in the orthonormal coordinate system for the surface by:

$$\bar{\mathbf{u}}_{bot} = \mathbf{a} \mathbf{u}_{bot} \quad (2.7a)$$

$$\bar{\mathbf{u}}_{top} = \mathbf{a} \mathbf{u}_{top} \quad (2.7b)$$

where the transformation matrix  $\mathbf{a}$  is a function of the natural coordinates,  $r$  and  $s$ , on the surface of the element:

$$\mathbf{a} = [\mathbf{e}_1 \quad \mathbf{e}_2 \quad \mathbf{e}_3]^T \quad (2.8)$$

The relative displacements between the two surfaces of the joint element are given by:

$$\mathbf{v} = \bar{\mathbf{u}}_{top} - \bar{\mathbf{u}}_{bot} \quad (2.9)$$

Because the relative displacement varies over the surface, the element is able to represent partial opening of the joint.

Substituting Eq. 2.7 and 2.6 into Eq. 2.9 gives the relative displacements between the surfaces in terms of the nodal displacements :

$$\mathbf{v} = \mathbf{B}\mathbf{u} \quad (2.10a)$$

where,

$$\mathbf{u} = [\mathbf{u}_1^T \quad \mathbf{u}_2^T \quad \mathbf{u}_3^T \quad \mathbf{u}_4^T \quad \mathbf{u}_5^T \quad \mathbf{u}_6^T \quad \mathbf{u}_7^T \quad \mathbf{u}_8^T]^T \quad (2.10b)$$

$$\mathbf{B} = [-\mathbf{N}_1 \quad -\mathbf{N}_2 \quad -\mathbf{N}_3 \quad -\mathbf{N}_4 \quad \mathbf{N}_1 \quad \mathbf{N}_2 \quad \mathbf{N}_3 \quad \mathbf{N}_4] \quad (2.10c)$$

and,

$$\mathbf{N}_j = N_j \mathbf{a} \quad (2.10d)$$

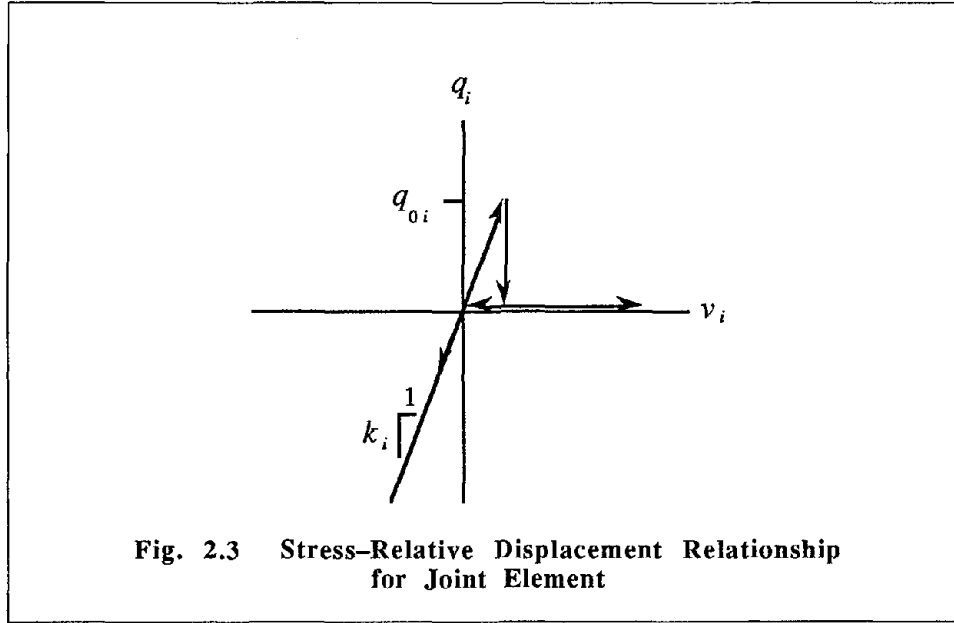
### 2.2.3 Force–Displacement Relationship

The relative displacement,  $\mathbf{v}$  given in Eq. 2.10(a), between the surfaces of the joint produces resisting stresses. The stresses,  $\mathbf{q}$ , in the joint are a nonlinear function of  $\mathbf{v}$  and depend on the state of the joint (closed or open). Because of the orthogonal coordinate system in which  $\mathbf{v}$  is measured, the assumption is made that relative displacement in direction  $i$  only produces stresses in direction  $i$ . In each direction, the joint has a specified tensile strength,  $q_{0i}$ . Once the strength is reached, the joint unloads and the subsequent tensile strength is zero. The stress in the joint is:

$$q_i = \begin{cases} k_i v_i, & v_i \leq q_{0i} / k_i \\ 0, & v_i > q_{0i} / k_i \end{cases} \quad i = 1, 2, 3 \quad (2.11)$$

The nonlinear stress–relative displacement relationship, shown in Fig. 2.3, is characterized by two parameters that are assumed constant for the element:  $q_{0i}$  is the maximum tensile stress the joint can resist before the joint unloads and the relative displacement  $v_i$  increases without resistance;  $k_i$  is the stiffness of the joint when the joint is closed. In a more general application,  $q_{0i}$  could be a specified function of the normal stress or relative displacement to represent friction and interlock.

The element is used in a restrictive form to model opening and closing of contraction joints in arch dams. The stress–displacement relationship in the  $x_3$  direction represents the forces normal to the element during opening and closing of the joint. In the current application of the joint element, tangential displacement between the two surfaces is not allowed.



#### 2.2.4 Restoring Forces and Tangent Stiffness Matrix

Equilibrium between the resisting stresses,  $\mathbf{q}$ , and the nodal forces is given by the principle of virtual displacements:

$$\mathbf{p} = \int_A \mathbf{B}^T \mathbf{q} dA \quad (2.12)$$

where  $\mathbf{p}$  is the vector of nodal forces in the global coordinate system.

The tangent stiffness matrix for the element is needed in the nonlinear solution procedure. Using Eq. 2.12, the tangent stiffness matrix is:

$$\mathbf{k}_T = \frac{\partial \mathbf{p}}{\partial \mathbf{u}} = \int_A \mathbf{B}^T \frac{\partial \mathbf{q}}{\partial \mathbf{v}} \frac{\partial \mathbf{v}}{\partial \mathbf{u}} dA \quad (2.13)$$

Substituting the expressions for  $\mathbf{q}$  from Eq. 2.11 and  $\mathbf{v}$  from Eq. 2.10(a) into Eq. 2.13 gives:

$$\mathbf{k}_T = \int_A \mathbf{B}^T \bar{\mathbf{k}}_T(\mathbf{v}) \mathbf{B} dA \quad (2.14)$$

where  $\bar{\mathbf{k}}_T(\mathbf{v})$  is a diagonal matrix, in which the diagonal terms are:

$$\bar{k}_{Ti} = \begin{cases} k_i, & v_i \leq q_{0i} / k_i \\ 0, & v_i > q_{0i} / k_i \end{cases} \quad i = 1, 2, 3 \quad (2.15)$$

### 2.2.5 Numerical Integration of Element Matrices

The integrals in Eqs. 2.12 and 2.14 for the nodal force vector and the tangent stiffness matrix must be evaluated numerically. The integration over the quadrilateral surface of the element is performed in the natural coordinate system shown in Fig. 2.2(b).

Using the standard transformations of the two dimensional integrals to the natural coordinate system and Gauss integration (Zienkiewics, 1977), the vector of restoring forces and element tangent stiffness matrix can be evaluated from:

$$\mathbf{p} = \sum_l \mathbf{B}^T(r_l, s_l) \mathbf{q}(v_l) |\mathbf{J}(r_l, s_l)| w_l \quad (2.16a)$$

$$\mathbf{k}_T = \sum_l \mathbf{B}^T(r_l, s_l) \bar{\mathbf{k}}_T(v_l) \mathbf{B}(r_l, s_l) |\mathbf{J}(r_l, s_l)| w_l \quad (2.16b)$$

in which the summations are over the Gauss integration points;  $w_l$  is the weight factor for the integration point at  $r_l, s_l$ . In Eq. 2.16,  $|\mathbf{J}(r_l, s_l)|$  is the determinant of the Jacobian of the transformation, where the Jacobian matrix is:

$$\mathbf{J} = \mathbf{x}_{,r} \times \mathbf{x}_{,s} \quad (2.17)$$

The Jacobian matrix can be computed with the normal vector  $\mathbf{e}_3$  in Eq. 2.4.

The number of Gauss integration points used to evaluate Eq. 2.16 depends on the order of the integrands in Eqs. 2.12 and 2.14. If  $\bar{\mathbf{k}}_T$  is constant over the element, the integrands in both expressions are cubic functions of the natural coordinates  $r, s$  for an arbitrary quadrilateral and quadratic functions of  $r, s$  for a parallelogram. In that case, 2x2 Gauss integration, with a total of four points in Eq. 2.16, would exactly evaluate the integrals. In the case of the nonlinear element,  $\bar{\mathbf{k}}_T$  is not constant over the element and higher order integration is necessary to evaluate the integrals more accurately. However, 2x2 Gauss integration produces sufficiently accurate  $\mathbf{p}$  and  $\mathbf{k}_T$  for the general nonlinear joint element.

A computational disadvantage of four point numerical integration is the dependence of the matrix  $\mathbf{B}$  on the surface coordinate system (through the transformation  $\mathbf{a}$ , according to Eq. 2.10). Four point integration would require computing  $\mathbf{a}$  four times at every time step and every iteration, or storing the nine coefficients of  $\mathbf{a}$  at the four points for each joint element. To avoid this computational or storage penalty,  $\mathbf{a}$  is computed only at the centroid of the surfaces. Because the joint surfaces in a reasonable mesh of an arch dam do not have a large curvature over a single element, the normal at the centroid is a good approximation for the normals throughout the element. Four point integration is still performed in Eq. 2.16, but with a constant  $\mathbf{a}$ .

### 2.3 Shell Elements and Solid Elements

A three-dimensional shell element is used to model the portion of the cantilevers near the abutments. It is a 16-node isoparametric element with quadratic displacement and geometry interpolation functions at the dam faces and linear interpolation through the thickness (Ghaboussi, et al., 1971). The element includes incompatible deformation modes to improve the bending behavior.

A thick shell element is used to model the dam away from the abutments. It is similar to the three-dimensional shell element but the sixteen face nodes are reduced to eight mid-surface nodes (Pawsey, 1970). Each mid-surface node has five degrees-of-freedom: three translation and two rotation. The three-dimensional solid element used for the foundation region and near the contraction joints is a standard 8-node isoparametric element with the addition of incompatible deformation modes (Zienkiewics, 1977).

The shell elements only allow isotropic material behavior. Orthotropic material properties can be specified for the solid elements, which may be appropriate for modeling the foundation rock. The complete description of the elements and their use in dam models is given in a report (Clough, et al., 1973).

### 2.4 Transition Between Contraction Joint Elements and Thick Shell Elements

To represent the distribution of forces near the contraction joint elements, the region adjacent to the joints is modeled with three-dimensional solid elements. The solid elements provide a transition between the joint elements and shell elements. The number of solid elements through the thickness of the arch is the same as the number of joint elements through the thickness [see Fig. 2.1(b)]. The number of elements in the arch direction is variable. To maintain compatibility with the shell elements, only two solid elements per shell element are permitted in the vertical direction.

The degrees-of-freedom not common to the thick shell element and the three-dimensional solid elements are kinematically constrained to the displacements of the shell element. The interface through the dam thickness remains plane because of this constraint. The mass of the solid element transition region is lumped at the nodal points for the adjacent shell and contraction joint elements.

### 2.5 Finite Element Mesh Generation

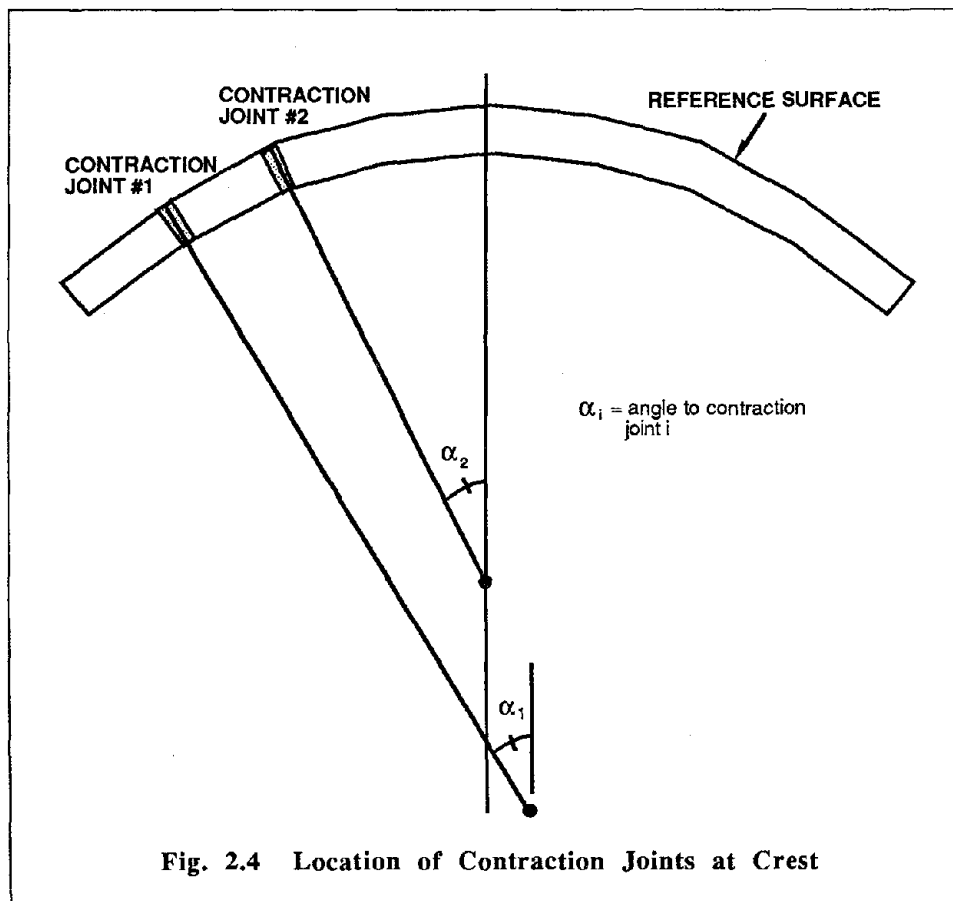
The finite element mesh generation for the dam body and the foundation region is similar to the mesh generation in ADAP. The program generates the nodal points and elements for a three-centered arch dam of arbitrary geometry. The elements in the horizontal and vertical planes are equivalent to the arch and cantilever sections in the trial load method. A complete description of the

mesh generation is given in Appendix A of this report. This section presents a brief description of the procedure and describes the extensions for generating the finite element model of the contraction joints.

The arch and cantilever sections are identified in relation to a vertical reference surface that passes through the upstream edge of the crest. The finite element mesh is defined by a grid of horizontal and vertical lines on the reference surface corresponding to the arch and cantilever sections. At design elevations, the locations of the centers are given in the global coordinate system and the points of compound curvature are measured with respect to a vertical reference plane. The geometry at additional horizontal sections, termed mesh elevations, are obtained from interpolation of geometric information of the design elevations. After defining the grid on the reference surface, the nodal points on the upstream and downstream faces are obtained by radial projection of the reference surface grid. The contraction joints in an arch dam generally follow the geometry defined in the trial load method and the procedure used to generate the finite element mesh for the vertical sections is also used for the geometry of the contraction joints.

When contraction joints are not included, as in ADAP, the reference surface grid is completely determined by the mesh elevations. The locations of the vertical sections are generated from the intersection of the mesh elevation with the abutments. In ADAP-88, a similar procedure is followed for generating the vertical lines but contraction joints are defined by a special procedure. Contraction joint locations are specified by an angle to the reference plane at the crest, as shown in Fig. 2.4. After the contraction joint locations are specified, the mesh generator computes the related abutment elevations for the horizontal lines on the reference surface. All of the abutment elevations corresponding to the contraction joints are included in the finite element model.

When combined with the user-specified mesh elevations, however, an unnecessarily large number of horizontal sections or an inappropriate aspect ratio may result. The mesh generator takes two measures to alleviate this problem. First, the generator disregards the user-specified mesh elevations that are within a specified distance from the elevations corresponding to the contraction joints. The minimum distance is proportional to the smallest element size from the mesh elevations. In the second measure, if the elevations corresponding to a pair of contraction joints at opposite sides of the crown are too close, the elevations are combined to give a nearly horizontal line on the reference surface. The degeneration is allowed only for contraction joint elevations within two consecutive mesh elevations to avoid large slopes.



The finite element mesh for the foundation rock region is more arbitrary than for the dam body. The mesh generator assumes a prismatic shape for the valley. Three different forms of the mesh for the foundation rock can be generated. Appendix A contains a detailed description of the foundation rock mesh generation options.

The mesh for the impounded water is complicated by the irregular geometry of many canyons. To simplify the generation, the water is assumed to be bounded by a cylindrical surface obtained by translating the interface between the dam and canyon in the upstream direction. Usually it is sufficient to extend the water domain a distance equal to three times the dam height. The fluid elements within the water domain are arranged in horizontal layers.

## 2.6 Static Analysis

The solution for the static response of the dam–water–foundation rock system must be available before a nonlinear dynamic analysis can be performed. The static loads are the weight of the dam, temperature changes in the dam, hydrostatic pressure of the impounded water, and silt.



To represent the construction sequence of arch dams, the static response is computed from three models of the dam. Cantilever monoliths are constructed independently and each cantilever transfers its weight to the foundation before the contraction joints are effective in developing arch action. To replicate this process two static analyses are performed for the gravity load on the dam. First, the gravity loads are applied to alternate cantilevers by setting the modulus of elasticity to zero for the remaining cantilevers. The second analysis switches the modulus of elasticity for the remaining cantilevers.

The reservoir of a dam is filled after the contraction joints are grouted so the dam resists hydrostatic loads as a monolithic structure. The static analysis for the hydrostatic load uses the complete dam–foundation rock model. The loads from silt are computed in the same manner. Changes in temperature are also resisted by the dam as a monolithic structure. Uniform or linear temperature changes may be specified. Temperature changes may vary with elevation and through the dam thickness, but they are assumed constant across arch sections.

After the complete static analysis is performed, the state of the joint elements is checked. If any of the joints are open, iteration is performed to find the equilibrium solution consistent with the closed or open state of all the joint elements under static loads.



# Chapter 3

## ***DYNAMIC ANALYSIS OF NONLINEAR SYSTEMS WITH LINEAR SUBSTRUCTURES***

### **3.1 Introduction**

Concrete arch dams with contraction joints may be modeled and analyzed using the substructure approach. Because the cantilevers are assumed to respond in a linear manner it is appropriate to consider the cantilevers as linear substructures. A linear substructure may consist of several adjacent cantilevers, so each contraction joint is not necessarily included in the finite element model. The joints between the substructures are modeled as nonlinear elements that can open and close. The set of joint elements in the finite element model constitute a single nonlinear substructure.

This chapter presents a numerical procedure for the dynamic analysis of nonlinear structural systems with linear substructures. The equations of motion are integrated in a time stepping procedure. Iterations within a time step are performed so that the system is in equilibrium at the end of the time step. The numerical procedure is similar to previous work on systems with local nonlinearities developed by several researchers (Clough and Wilson, 1979; Row and Schrieker, 1983; Row and Schrieker, 1984).

### **3.2 Substructure Solution Procedure**

The solution procedure involves formulating the equations of motion for each linear substructure. A linear substructure is connected to other substructures (linear or nonlinear) at its boundaries. The linear substructures are then combined with the nonlinear substructure using equilibrium and compatibility conditions at the boundaries. Time integration operators are applied to the equations of motion to step through the solution in time. Iterations are performed in each time step to ensure that the system is in equilibrium at the end of every time step.

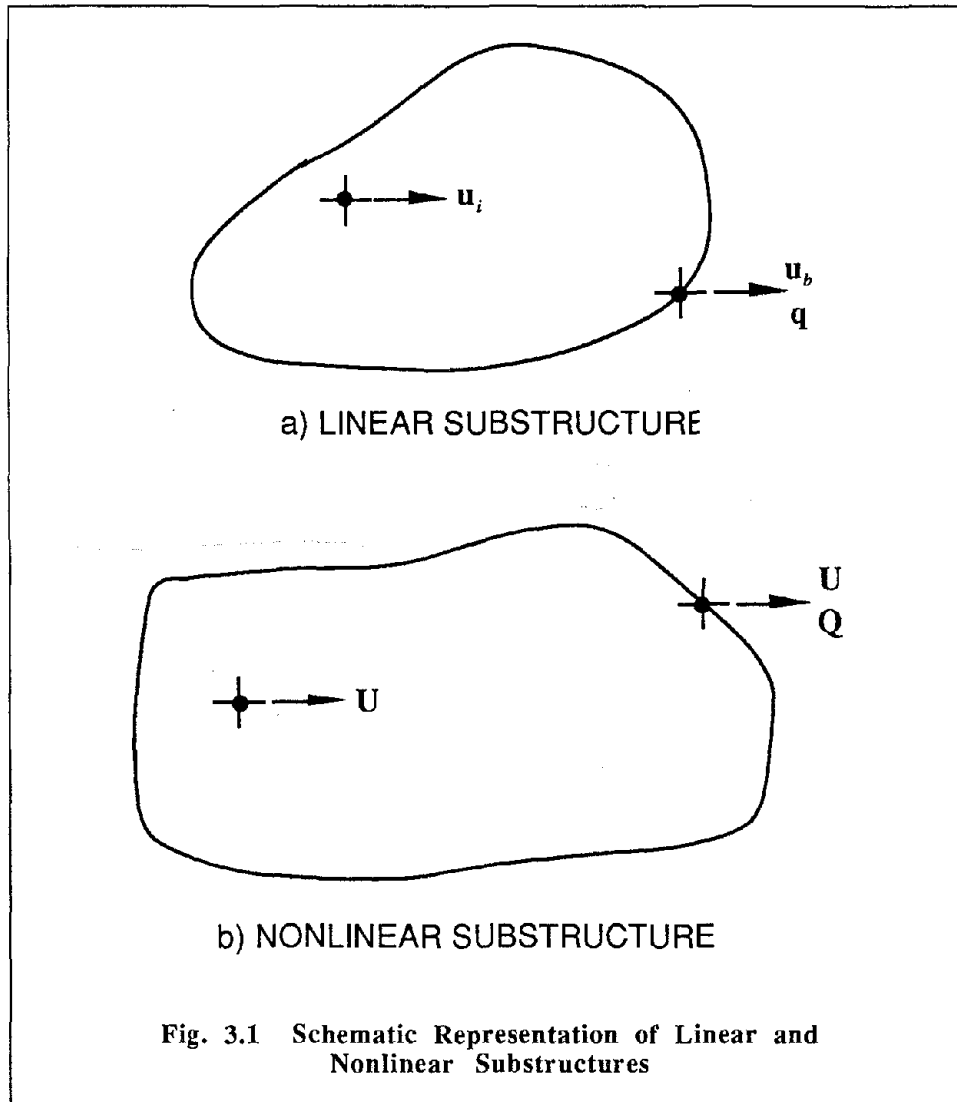
#### *3.2.1 Linear Substructure*

Figure 3.1(a) is a schematic representation of a linear substructure. The equations of motion for the linear substructure are:

$$\mathbf{m}\ddot{\mathbf{u}} + \mathbf{c}\dot{\mathbf{u}} + \mathbf{k}\mathbf{u} = \mathbf{f} + \mathbf{q} \quad (3.1)$$

where  $\mathbf{u}$  is the vector of displacements at the degrees-of-freedom (DOF) in the substructure;  $\mathbf{m}$ ,  $\mathbf{c}$ , and  $\mathbf{k}$ , are the mass, damping, and stiffness matrices, respectively;  $\mathbf{f}$  is the vector of time-dependent loads; and  $\mathbf{q}$  is the vector of forces at the boundary of the substructure. If the response at time  $t_n$  is known, the solution of Eq. 3.1 at time  $t_{n+1}$  is given by:

$$\mathbf{m}\ddot{\mathbf{u}}_{n+1} + \mathbf{c}\dot{\mathbf{u}}_{n+1} + \mathbf{k}\mathbf{u}_{n+1} = \mathbf{f}_{n+1} + \mathbf{q}_{n+1} \quad (3.2)$$



The Newmark time integration method can be used to solve Eq. 3.2 (Hughes, et al., 1979). Applying the approximations for acceleration, the velocity and displacement at time  $t_{n+1}$  are:

$$\dot{\mathbf{u}}_{n+1} = \tilde{\mathbf{u}}_n + \gamma \Delta t \ddot{\mathbf{u}}_{n+1} \quad (3.3a)$$

$$\mathbf{u}_{n+1} = \tilde{\mathbf{u}}_n + \beta \Delta t^2 \ddot{\mathbf{u}}_{n+1} \quad (3.3b)$$

where,

$$\tilde{\mathbf{u}}_n = \dot{\mathbf{u}}_n + \Delta t(1 - \gamma) \ddot{\mathbf{u}}_n \quad (3.3c)$$

$$\tilde{\mathbf{u}}_n = \mathbf{u}_n + \Delta t \dot{\mathbf{u}}_n + \left(\frac{1}{2} - \beta\right) \Delta t^2 \ddot{\mathbf{u}}_n \quad (3.3d)$$

In Eq. 3.3,  $\Delta t = t_{n+1} - t_n$  is the constant time step and  $\beta$  and  $\gamma$  are integration parameters. Solving Eq. 3.3(b) for the acceleration in terms of  $\mathbf{u}_{n+1}$  gives:

$$\ddot{\mathbf{u}}_{n+1} = a_1(\mathbf{u}_{n+1} - \tilde{\mathbf{u}}_n) \quad (3.4)$$

Substituting Eqs. 3.4 and 3.3(a) into Eq. 3.2 gives linear algebraic equations in terms of  $\mathbf{u}_{n+1}$ :

$$\mathbf{k}^* \mathbf{u}_{n+1} = \mathbf{p}_{n+1}^* + \mathbf{q}_{n+1} \quad (3.5)$$

where the effective stiffness matrix and effective load vector are:

$$\mathbf{k}^* = a_1 \mathbf{m} + a_2 \mathbf{c} + \mathbf{k} \quad (3.6a)$$

$$\mathbf{p}_{n+1}^* = \mathbf{f}_{n+1} + \mathbf{m}[a_1 \tilde{\mathbf{u}}_n] + \mathbf{c}[a_2 \tilde{\mathbf{u}}_n - \tilde{\mathbf{u}}_n] \quad (3.6b)$$

In Eqs. 3.4 to 3.6, the scalar constants are:

$$a_1 = \frac{1}{\beta \Delta t^2} \quad a_2 = \frac{\gamma}{\beta \Delta t} \quad (3.7)$$

Equation 3.5 represents a linear relationship between the displacements in the substructure,  $\mathbf{u}_{n+1}$ , and the forces at the boundary of the substructure,  $\mathbf{q}_{n+1}$ . The linear substructure is eventually coupled to the nonlinear substructure through the boundary displacements and forces. The iterative solution of the nonlinear equations of motion for the complete system involves estimates of displacements and boundary forces in the linear substructure. Equation 3.5 is valid for the solution of iteration  $k$  for the response at time  $t_{n+1}$ ,

$$\mathbf{k}^* \mathbf{u}_{n+1}^k = \mathbf{p}_{n+1}^* + \mathbf{q}_{n+1}^k \quad (3.8)$$

because the effective stiffness matrix,  $\mathbf{k}^*$ , and the effective load vector,  $\mathbf{p}_{n+1}^*$ , do not depend on the response at time  $t_{n+1}$ .

The degrees-of-freedom (DOF) in a linear substructure are partitioned into two groups [see Fig. 3.1(a)]:

- Internal DOF which are not connected to other substructures. Quantities associated with internal DOF are denoted by the subscript  $i$ .
- Boundary DOF which are connected to other substructures. Quantities associated with boundary DOF are denoted by subscript  $b$ .

Equation 3.8 can be partitioned into internal and boundary degrees-of-freedom, noting that the vector  $\mathbf{q}$  has non-zero components only at the boundary DOF:

$$\begin{bmatrix} \mathbf{k}_{ii}^* & \mathbf{k}_{ib}^* \\ \mathbf{k}_{bi}^* & \mathbf{k}_{bb}^* \end{bmatrix} \begin{Bmatrix} \mathbf{u}_{i(n+1)}^k \\ \mathbf{u}_{b(n+1)}^k \end{Bmatrix} = \begin{Bmatrix} \mathbf{p}_{i(n+1)}^* \\ \mathbf{p}_{b(n+1)}^* \end{Bmatrix} + \begin{Bmatrix} \mathbf{0} \\ \mathbf{q}_{n+1}^k \end{Bmatrix} \quad (3.9)$$

Solving Eq. 3.9 for the displacements at the internal DOF in terms of displacements at the boundary DOF gives:

$$\mathbf{u}_{i(n+1)}^k = -(\mathbf{k}_{ii}^*)^{-1} [\mathbf{k}_{ib}^* \mathbf{u}_{b(n+1)}^k - \mathbf{p}_{i(n+1)}^*] \quad (3.10)$$

Substituting Eq. 3.10 into the partition of boundary DOF in Eq. 3.9 gives:

$$\bar{\mathbf{k}}^* \mathbf{u}_{b(n+1)}^k = \bar{\mathbf{p}}_{n+1}^* + \mathbf{q}_{n+1}^k \quad (3.11)$$

in which the reduced effective stiffness matrix and reduced effective load vector for the linear substructure are:

$$\bar{\mathbf{k}}^* = \mathbf{k}_{bb}^* - \mathbf{k}_{bi}^* (\mathbf{k}_{ii}^*)^{-1} \mathbf{k}_{ib}^* \quad (3.12a)$$

$$\bar{\mathbf{p}}_{n+1}^* = \mathbf{p}_{b(n+1)}^* - \mathbf{k}_{bi}^* (\mathbf{k}_{ii}^*)^{-1} \mathbf{p}_{i(n+1)}^* \quad (3.12b)$$

Equation 3.11 gives a linear relationship between the displacements and the forces at the boundary of a linear substructure for iteration  $k$  of the response at time  $t_{n+1}$ .

### 3.2.2 Nonlinear Substructure

The complete structural system consists of an arbitrary number of linear substructures and one nonlinear substructure. The nonlinear substructure does not have to be physically contiguous; it may consist of disconnected regions of the system, such as the contraction joints in an arch dam. Figure 3.1(b) shows a schematic representation of the single nonlinear substructure.

The equations of motion for the nonlinear substructure are:

$$\mathbf{M}\ddot{\mathbf{U}} + \mathbf{P}(\dot{\mathbf{U}}, \mathbf{U}) = \mathbf{F} + \mathbf{Q} \quad (3.13)$$

where  $\mathbf{U}$  is the vector of displacements for the nonlinear substructure;  $\mathbf{M}$  is the mass matrix;  $\mathbf{P} = \mathbf{P}(\dot{\mathbf{U}}, \mathbf{U})$  is the vector of restoring forces which is a nonlinear function of velocity and displacements;  $\mathbf{F}$  is the vector of time dependent loads; and  $\mathbf{Q}$  is the vector of forces at the boundary of the nonlinear substructure.

For equilibrium between the nonlinear substructure and the linear substructures, the boundary forces are related by:

$$\mathbf{Q} + \sum \mathbf{q} = \mathbf{0} \quad (3.14)$$

where the summation symbol represents assembly over the linear substructures. For compatibility the displacements at the boundary of a linear substructure are related to the displacements of the nonlinear substructure by:

$$\mathbf{u}_b = \mathbf{a}_b \mathbf{U} \quad (3.15)$$

where  $\mathbf{a}_b$  is a boolean matrix representing the connectivity of the substructures.

If the response at time  $t_n$  is known, the solution of Eq. 3.13 at time  $t_{n+1}$  is given by:

$$\mathbf{M}\ddot{\mathbf{U}}_{n+1} + \mathbf{P}(\dot{\mathbf{U}}_{n+1}, \mathbf{U}_{n+1}) = \mathbf{F}_{n+1} + \mathbf{Q}_{n+1} \quad (3.16)$$

The constant time step  $\Delta t$  and integration parameters  $\beta$  and  $\gamma$  are the same for the nonlinear and linear substructures. The approximation of the response for the nonlinear substructure is the same as for a linear substructure, given in Eq. 3.3, except the response quantities are  $\ddot{\mathbf{U}}$ ,  $\dot{\mathbf{U}}$  and  $\mathbf{U}$ , instead of  $\ddot{\mathbf{u}}$ ,  $\dot{\mathbf{u}}$ , and  $\mathbf{u}$ . Applying the Newmark procedure to Eq. 3.16 gives a system of nonlinear algebraic equations that must be solved iteratively.

The procedure presented in (Hughes, et al., 1979) is used to solve the nonlinear equations of motion, Eq. 3.16. Given the response of iteration  $k$ ,  $\mathbf{U}_{n+1}^k$ , the  $k+1$  iteration is given by the solution of:

$$\mathbf{K}^* \Delta \mathbf{U} = \Delta \mathbf{P}^* \quad (3.17)$$

for the incremental displacement vector,  $\Delta \mathbf{U}$ , where the effective stiffness matrix and the effective load vector for the nonlinear substructure are,

$$\mathbf{K}^* = a_1 \mathbf{M} + a_2 \frac{\partial \mathbf{P}}{\partial \dot{\mathbf{U}}} + \frac{\partial \mathbf{P}}{\partial \mathbf{U}} - \frac{\partial \mathbf{Q}}{\partial \mathbf{U}} \quad (3.18a)$$

$$\Delta \mathbf{P}^* = \mathbf{F}_{n+1} - \mathbf{M}\ddot{\mathbf{U}}_{n+1}^k - \mathbf{P}(\dot{\mathbf{U}}_{n+1}^k, \mathbf{U}_{n+1}^k) + \mathbf{Q}_{n+1}^k \quad (3.18b)$$

After solution of Eq. 3.17, the response for the  $k+1$  iteration is:

$$\mathbf{U}_{n+1}^{k+1} = \mathbf{U}_{n+1}^k + \Delta \mathbf{U} \quad (3.19a)$$

$$\ddot{\mathbf{U}}_{n+1}^{k+1} = a_1 (\mathbf{U}_{n+1}^{k+1} - \tilde{\mathbf{U}}_n) \quad (3.19b)$$

$$\dot{\mathbf{U}}_{n+1}^{k+1} = \tilde{\dot{\mathbf{U}}}_n + \gamma \Delta t \ddot{\mathbf{U}}_{n+1}^{k+1} \quad (3.19c)$$

To start the solution for the response at time  $t_{n+1}$ , the zero iteration is:

$$\mathbf{U}_{n+1}^0 = \tilde{\mathbf{U}}_n \quad (3.20a)$$

$$\dot{\mathbf{U}}_{n+1}^0 = \tilde{\dot{\mathbf{U}}}_n \quad (3.20b)$$

$$\ddot{\mathbf{U}}_{n+1}^0 = \mathbf{0} \quad (3.20c)$$

The iterative solution of Eq. 3.17 is terminated when the vector norms of the unbalanced force,  $\Delta \mathbf{P}^*$ , and the incremental displacement,  $\Delta \mathbf{U}$ , are within acceptable tolerances. The final iterate is the response at time  $t_{n+1}$ .

In Eq. 3.18(a), the gradients of the nonlinear restoring force with respect to the displacement vector and velocity vector are the tangent stiffness matrix and tangent damping matrix, respectively:

$$\mathbf{K}_T = \frac{\partial \mathbf{P}}{\partial \mathbf{U}} \quad (3.21a)$$

$$\mathbf{C}_T = \frac{\partial \mathbf{P}}{\partial \dot{\mathbf{U}}} \quad (3.21b)$$

These matrices are assembled from the tangent stiffness and tangent damping matrices of the elements in the nonlinear substructure. The point in the response at which the gradients are computed depends on the method of iteration, such as Newton–Raphson, modified Newton–Raphson, secant, or initial stiffness.

Using Eqs. 3.11 and 3.14, the boundary force on the nonlinear substructure is assembled from the boundary forces on the linear substructures:

$$\mathbf{Q}_{n+1} = \sum \bar{\mathbf{p}}_{n+1}^* - \sum \bar{\mathbf{k}}^* \mathbf{u}_{b(n+1)}^k \quad (3.22)$$

The gradient of the boundary force with respect to the displacement vector can be obtained by differentiation of Eq. 3.22:

$$\frac{\partial \mathbf{Q}}{\partial \mathbf{U}} = - \sum \bar{\mathbf{k}}^* \quad (3.23)$$

Substituting Eqs. 3.21 and 3.23 into Eq. 3.18(a) gives the effective stiffness matrix of the coupled nonlinear substructure and linear substructures:

$$\mathbf{K}^* = a_1 \mathbf{M} + a_2 \mathbf{C}_T + \mathbf{K}_T + \sum \bar{\mathbf{k}}^* \quad (3.24)$$

Substituting Eq. 3.22 into Eq. 3.18(b) gives the effective load for the nonlinear substructure:

$$\Delta \mathbf{P}^* = \mathbf{F}_{n+1} + \sum \bar{\mathbf{p}}_{n+1}^* - \mathbf{M} \ddot{\mathbf{U}}_{n+1}^k - \mathbf{P}(\dot{\mathbf{U}}_{n+1}^k, \mathbf{U}_{n+1}^k) - \sum \bar{\mathbf{k}}^* \mathbf{u}_{b(n+1)}^k \quad (3.25)$$

The first two terms for  $\Delta \mathbf{P}^*$  in Eq. 3.25 are independent of the iteration, whereas the last three terms depend on the response given by the current iteration for the time step.

### 3.2.3 Initial Conditions

The displacement, velocity, and acceleration at time  $t_0$  are required to start the time integration. The displacement and velocity at  $t_0$  are assumed to be zero, but the extension to the general case is possible. The acceleration for a linear substructure can be obtained from Eq. 3.2 evaluated at  $t_0$ :

$$\mathbf{m} \ddot{\mathbf{u}}_0 = \mathbf{f}_0 + \mathbf{q}_0 \quad (3.26a)$$

or in partitioned form:

$$\begin{bmatrix} \mathbf{m}_{ii} & \mathbf{m}_{ib} \\ \mathbf{m}_{bi} & \mathbf{m}_{bb} \end{bmatrix} \begin{Bmatrix} \ddot{\mathbf{u}}_{i(0)} \\ \ddot{\mathbf{u}}_{b(0)} \end{Bmatrix} = \begin{Bmatrix} \mathbf{f}_{i(0)} \\ \mathbf{f}_{b(0)} \end{Bmatrix} + \begin{Bmatrix} \mathbf{0} \\ \mathbf{q}_0 \end{Bmatrix} \quad (3.26b)$$

Solving Eq. 3.26(b) for the displacements at the internal DOF gives:

$$\ddot{\mathbf{u}}_{i(0)} = -\mathbf{m}_{ii}^{-1} [\mathbf{m}_{ib} \ddot{\mathbf{u}}_{b(0)} - \mathbf{f}_{i(0)}] \quad (3.27)$$



Substituting Eq. 3.27 into the partition of boundary DOF in Eq. 3.26(b) gives:

$$\bar{\mathbf{m}}\ddot{\mathbf{u}}_{b(0)} = \bar{\mathbf{f}}_0 + \mathbf{q}_0 \quad (3.28)$$

in which :

$$\bar{\mathbf{m}} = \mathbf{m}_{bb} - \mathbf{m}_{bi}\mathbf{m}_{ii}^{-1}\mathbf{m}_{ib} \quad (3.29a)$$

$$\bar{\mathbf{f}}_0 = \mathbf{f}_{b(0)} - \mathbf{m}_{bi}\mathbf{m}_{ii}^{-1}\mathbf{f}_{i(0)} \quad (3.29b)$$

For the nonlinear substructure, evaluating Eq. 3.16 at  $t_0$  and using Eq. 3.14 gives:

$$\mathbf{M}\ddot{\mathbf{U}}_0 = \mathbf{F}_0 - \sum \mathbf{q}_0 \quad (3.30)$$

Substituting Eq. 3.28 into Eq. 3.30 gives:

$$(\mathbf{M} + \sum \bar{\mathbf{m}})\ddot{\mathbf{U}}_0 = \mathbf{F}_0 + \sum \bar{\mathbf{f}}_0 \quad (3.31)$$

which can be solved for  $\ddot{\mathbf{U}}_0$ . For each linear substructure,  $\ddot{\mathbf{u}}_0$  can be obtained from Eq. 3.27.

### 3.2.4 Effective Load for Earthquake Ground Motion

Assuming uniform ground motion at the interface between the complete structural system and its supports, the dynamic load on a linear substructure is given by (Clough and Penzien, 1975):

$$\mathbf{f} = -(\mathbf{m}\mathbf{r} + \mathbf{m}_g)\ddot{\mathbf{u}}_g \quad (3.32a)$$

where  $\ddot{\mathbf{u}}_g$  is the vector of the free-field ground acceleration at the supports;  $\mathbf{r}$  is the matrix of direction cosines between the components of the ground motion and the DOF in the substructure, and  $\mathbf{m}_g$  is the mass matrix that couples the DOF in the substructure and the support points. The dynamic load on the nonlinear substructure is:

$$\mathbf{F} = -(\mathbf{M}\mathbf{R} + \mathbf{M}_g)\ddot{\mathbf{u}}_g \quad (3.32b)$$

where similar definitions of the terms apply.

### 3.2.5 Discussion of the Procedure

In the numerical procedure using the substructure approach, the nonlinearities in a system are *a priori* isolated in a single substructure. The other substructures in the system are linear. There are several advantages of using the substructure approach to compute the dynamic response compared to considering the entire system as nonlinear:

- An equilibrium iteration during a time step involves only the degrees-of-freedom in the nonlinear substructure. This simplification results in a substantial reduction of computation for structures with few nonlinear elements compared with linear elements.
- Because the state of the linear substructures does not change, the effective stiffness matrices of the linear substructure are computed once. Only the elements in the nonlinear

substructures must be linearized and their tangent matrices assembled into  $\mathbf{K}^*$  during the equilibrium iteration.

- The restoring forces in the linear substructures and their contribution to the effective load vector,  $\Delta \mathbf{P}^*$ , for the nonlinear substructure are computed in terms of displacements at the boundaries of the linear substructures. This again results in a substantial reduction of computation if the number of boundary DOF in a linear substructure is small compared with the number of interior DOF.

### 3.3 Effective Force for Linear Substructures

At the end of the equilibrium iterations for the response of the nonlinear substructure at time step  $n+1$ , the displacements at the boundary of a linear substructure,  $\mathbf{u}_{b(n+1)}$ , are known. The displacements at the interior DOF of the substructure can be obtained from Eq. 3.10, and the velocity and acceleration at the interior can be obtained from Eq. 3.4. At this point, the response computation for time  $t_{n+1}$  is complete.

The response at the next time step depends on the effective load vector,  $\bar{\mathbf{p}}_{n+1}^*$ , for each linear substructure, as given in Eq. 3.25. Although the solution of the equations of motion using the substructure approach is very efficient, the computation of the effective load vector can be reduced further. The straightforward procedure to compute  $\bar{\mathbf{p}}_{n+1}^*$  is as follows:

- Compute  $\mathbf{p}_{n+1}^*$  using Eqs. 3.6(b) and 3.3
- Reduce  $\mathbf{p}_{n+1}^*$  to give  $\bar{\mathbf{p}}_{n+1}^*$  at the boundary DOF, using Eq. 3.12(b)

Unfortunately, the first step entails a considerable amount of computation because the effective force is obtained by multiplications involving the mass and damping matrices, according to Eq. 3.6(b). The computation of  $\bar{\mathbf{p}}_{n+1}^*$  can be reduced substantially because only the boundary DOF components are needed in the iteration, through Eq. 3.25 (Row and Schriker, 1983).

The computation of the effective load vector for a linear substructure can be modified assuming the damping matrix has the form of Rayleigh damping:

$$\mathbf{c} = b_0 \mathbf{m} + b_1 \mathbf{k} \quad (3.33)$$

where  $b_0$  and  $b_1$  are constant parameters that determine the amount of damping in the linear substructure. Substituting Eq. 3.33 into Eq. 3.6(a) gives the effective stiffness matrix for the substructure:

$$\mathbf{k}^* = (a_1 + a_2 b_0) \mathbf{m} + (1 + a_2 b_1) \mathbf{k} \quad (3.34a)$$

The effective force vector uses the effective stiffness matrix:

$$\mathbf{p}_{n+1}^* = \mathbf{f}_{n+1} + \mathbf{m}[c_1 \ddot{\mathbf{u}}_n - c_2 \ddot{\mathbf{u}}_n] + \mathbf{k}^*[d_1 \dot{\mathbf{u}}_n - d_2 \dot{\mathbf{u}}_n] \quad (3.34b)$$

where  $c_1$ ,  $c_2$ ,  $d_1$ , and  $d_2$ , are constants to be determined. Comparing Eq. 3.34(b) with Eq. 3.6(b), and using Eqs. 3.33 and 3.34(a), provides the values for  $c_1$ ,  $c_2$ ,  $d_1$ , and  $d_2$ . Comparing the terms related to the stiffness matrix,  $\mathbf{k}$ , gives:

$$d_2 = \frac{b_1}{1 + a_2 b_1} \quad d_1 = a_2 d_2 \quad (3.35a)$$

and comparing the terms related to the mass matrix,  $\mathbf{m}$ , gives:

$$c_1 = (a_1 + a_2 b_0)(1 - a_2 d_2) \quad c_2 = b_0 - (a_1 + a_2 b_0) d_2 \quad (3.35b)$$

Using Eq. 3.34(b) for the effective load, Eq. 3.9 can be put in the following form:

$$\begin{bmatrix} \mathbf{k}_{ii}^* & \mathbf{k}_{ib}^* \\ \mathbf{k}_{bi}^* & \mathbf{k}_{bb}^* \end{bmatrix} \begin{Bmatrix} \mathbf{u}_{i(n+1)}^k \\ \mathbf{u}_{b(n+1)}^k \end{Bmatrix} = \begin{Bmatrix} \hat{\mathbf{p}}_{i(n+1)}^* \\ \hat{\mathbf{p}}_{b(n+1)}^* \end{Bmatrix} + \begin{bmatrix} \mathbf{k}_{ii}^* & \mathbf{k}_{ib}^* \\ \mathbf{k}_{bi}^* & \mathbf{k}_{bb}^* \end{bmatrix} \begin{Bmatrix} \tilde{\mathbf{v}}_i \\ \tilde{\mathbf{v}}_b \end{Bmatrix} + \begin{Bmatrix} \mathbf{0} \\ \mathbf{q}_{n+1}^k \end{Bmatrix} \quad (3.36)$$

where the modified effective load vector is,

$$\hat{\mathbf{p}}_{n+1}^* = \mathbf{f}_{n+1} + \mathbf{m}[c_1 \tilde{\mathbf{u}}_n - c_2 \tilde{\mathbf{u}}_n] \quad (3.37)$$

and,

$$\tilde{\mathbf{v}} = d_2(a_2 \tilde{\mathbf{u}}_n - \tilde{\mathbf{u}}_n) \quad (3.38)$$

The solution of Eq. 3.36 for the displacements at the interior DOF gives:

$$\mathbf{u}_{i(n+1)}^k = -(\mathbf{k}_{ii}^*)^{-1} [\mathbf{k}_{ib}^* (\mathbf{u}_{b(n+1)}^k - \tilde{\mathbf{v}}_b) - \hat{\mathbf{p}}_{i(n+1)}^*] + \tilde{\mathbf{v}}_i \quad (3.39)$$

Substituting Eq. 3.39 into Eq. 3.36 gives the relationship between the boundary displacements and the boundary forces for a linear substructure:

$$\bar{\mathbf{k}}^* \mathbf{u}_{b(n+1)}^k = \bar{\mathbf{p}}_{n+1}^* + \mathbf{q}_{n+1}^k \quad (3.40)$$

Eq. 3.40 is the same as Eq. 3.11, but the effective load vector is now:

$$\bar{\mathbf{p}}_{n+1}^* = \bar{\hat{\mathbf{p}}}_{b(n+1)}^* + \bar{\mathbf{k}}^* \tilde{\mathbf{v}}_b \quad (3.41a)$$

where the modified effective force is reduced to the boundary DOF:

$$\bar{\hat{\mathbf{p}}}_{b(n+1)}^* = \hat{\mathbf{p}}_{b(n+1)}^* - \mathbf{k}_{bi}^* (\mathbf{k}_{ii}^*)^{-1} \hat{\mathbf{p}}_{i(n+1)}^* \quad (3.41b)$$

Substituting Eq. 3.41(a) for a linear substructure into Eq. 3.25 for the effective load vector,  $\Delta \mathbf{P}^*$ , for the nonlinear substructure gives:

$$\Delta \mathbf{P}^* = \mathbf{F}_{n+1} + \sum \bar{\hat{\mathbf{p}}}_{b(n+1)}^* - \mathbf{M} \ddot{\mathbf{U}}_{n+1}^k - \mathbf{P}(\dot{\mathbf{U}}_{n+1}^k, \mathbf{U}_{n+1}^k) - \sum \bar{\mathbf{k}}^* (\mathbf{u}_{b(n+1)}^k - \tilde{\mathbf{v}}_b) \quad (3.42)$$

The effort to compute the effective force vector from Eq. 3.37 is considerably less than to compute it from Eq. 3.6(b) because only one matrix-vector multiplication is required. However, an additional response quantity,  $\tilde{\mathbf{v}}$ , must be saved for each linear substructure.

### 3.4 Algorithm for the Numerical Procedure

This section presents the algorithm for solving the equations of motion using the substructure approach. For convenience the pertinent expressions are repeated here with their original equation numbers. The constants in the expressions are given in Eqs. 3.7 and 3.35.

1.0 For each linear substructure:

1.1 Form the effective stiffness matrix:

$$\mathbf{k}^* = (a_1 + a_2 b_0) \mathbf{m} + (1 + a_2 b_1) \mathbf{k} \quad (3.34a)$$

1.2 Reduce the effective stiffness matrix to the boundary DOF:

$$\bar{\mathbf{k}}^* = \mathbf{k}_{bb}^* - \mathbf{k}_{bi}^* (\mathbf{k}_{ii}^*)^{-1} \mathbf{k}_{ib}^* \quad (3.12a)$$

1.3 Assemble  $\bar{\mathbf{k}}^*$  into  $\mathbf{K}^*$

2.0 Assemble  $a_1 \mathbf{M}$  for the nonlinear substructure into  $\mathbf{K}^*$ . This copy of the effective stiffness matrix for the nonlinear substructure does not change.

3.0 Initialize the time integration procedure:

3.1 Compute the initial conditions according to the procedures in Section 3.2.3.

3.2 Set the time step counter,  $n = 0$

4.0 For each time step in the time integration procedure:

4.1 For each linear substructure:

4.1.1 Compute the predictions of velocity and displacement:

$$\tilde{\mathbf{u}}_n = \dot{\mathbf{u}}_n + \Delta t (1 - \gamma) \ddot{\mathbf{u}}_n \quad (3.3c)$$

$$\tilde{\mathbf{u}}_n = \mathbf{u}_n + \Delta t \dot{\mathbf{u}}_n + \left(\frac{1}{2} - \beta\right) \Delta t^2 \ddot{\mathbf{u}}_n \quad (3.3d)$$

and,

$$\tilde{\mathbf{v}} = d_2 (a_2 \tilde{\mathbf{u}}_n - \tilde{\mathbf{u}}_n) \quad (3.38)$$

4.1.2 Compute the modified effective load vector:

$$\hat{\mathbf{p}}_{n+1}^* = \mathbf{f}_{n+1} + \mathbf{m} [c_1 \tilde{\mathbf{u}}_n - c_2 \tilde{\mathbf{u}}_n] \quad (3.37)$$

4.1.3 Reduce the modified effective load vector to the the boundary DOF:

$$\bar{\hat{\mathbf{p}}}_{b(n+1)}^* = \hat{\mathbf{p}}_{b(n+1)}^* - \mathbf{k}_{bi}^* (\mathbf{k}_{ii}^*)^{-1} \hat{\mathbf{p}}_{i(n+1)}^* \quad (3.41b)$$

4.1.4 Assemble  $\bar{\hat{\mathbf{p}}}_{b(n+1)}^*$  into  $\Delta \mathbf{P}^*$

4.2 Assemble  $\mathbf{F}_{n+1}$  into  $\Delta \mathbf{P}^*$

4.3 Initialize equilibrium iterations for the time step:

4.3.1 Set the iteration counter,  $k = 0$

4.3.2 Set the zero iteration:

$$\mathbf{U}_{n+1}^0 = \tilde{\mathbf{U}}_n \quad (3.20a)$$

$$\dot{\mathbf{U}}_{n+1}^0 = \tilde{\dot{\mathbf{U}}}_n \quad (3.20b)$$

$$\ddot{\mathbf{U}}_{n+1}^0 = \mathbf{0} \quad (3.20c)$$

4.4 For each equilibrium iteration:

4.4.1 For each linear substructure compute,

$$\bar{\mathbf{k}}^*(\tilde{\mathbf{v}}_b - \mathbf{u}_{b(n+1)}^k)$$

and assemble into  $\Delta \mathbf{P}^*$

4.4.2 For each element in the nonlinear substructure:

4.4.2.1 Determine the tangent stiffness matrix,  $\mathbf{k}_T$ , and tangent damping matrix,  $\mathbf{c}_T$ , and assemble  $\mathbf{k}_T + a_2 \mathbf{c}_T$  into  $\mathbf{K}^*$

4.4.2.2 Compute the element restoring force and assemble  $-\mathbf{p}(\dot{\mathbf{u}}_{n+1}^k, \mathbf{u}_{n+1}^k)$  into  $\Delta \mathbf{P}^*$

4.4.3 Compute  $-\mathbf{M}\ddot{\mathbf{U}}_{n+1}^k$  and assemble into  $\Delta \mathbf{P}^*$

4.4.4 Solve the following system of equations for  $\Delta \mathbf{U}$ ,

$$\mathbf{K}^* \Delta \mathbf{U} = \Delta \mathbf{P}^* \quad (3.17)$$

4.4.5 Update response of the nonlinear substructure:

$$\mathbf{U}_{n+1}^{k+1} = \mathbf{U}_{n+1}^k + \Delta \mathbf{U} \quad (3.19a)$$

$$\dot{\mathbf{U}}_{n+1}^{k+1} = a_1 (\mathbf{U}_{n+1}^{k+1} - \tilde{\mathbf{U}}_n) \quad (3.19b)$$

$$\ddot{\mathbf{U}}_{n+1}^{k+1} = \tilde{\ddot{\mathbf{U}}}_n + \gamma \Delta t \dot{\mathbf{U}}_{n+1}^{k+1} \quad (3.19c)$$

4.4.6 If the norms of  $\Delta \mathbf{U}$  and  $\Delta \mathbf{P}^*$  are within specified tolerance, go to Step 4.5

4.4.7 Increment the iteration counter,  $k = k+1$ ; repeat Step 4.4

4.5 For each linear substructure:

4.5.1 Compute the displacement at the interior DOF:

$$\mathbf{u}_{i(n+1)} = -(\mathbf{k}_{ii}^*)^{-1} [\mathbf{k}_{ib}^* (\mathbf{u}_{b(n+1)} - \tilde{\mathbf{v}}_b) - \hat{\mathbf{p}}_{i(n+1)}^*] + \tilde{\mathbf{v}}_i \quad (3.39)$$

4.5.2 Compute the acceleration and velocity at all DOF:

$$\ddot{\mathbf{u}}_{n+1} = a_1 (\mathbf{u}_{n+1} - \tilde{\mathbf{u}}_n) \quad (3.4)$$

$$\dot{\mathbf{u}}_{n+1} = \tilde{\dot{\mathbf{u}}}_n + \gamma \Delta t \ddot{\mathbf{u}}_{n+1} \quad (3.3a)$$

4.6 Increment the time step counter,  $n = n+1$ ; repeat Step 4.

### 3.5 Effect of Static Response

The static response must be considered in the nonlinear dynamic response. In the solution procedure described above,  $\mathbf{u}$  are the dynamic displacements relative to the displacements  $\mathbf{u}_s$  due to the static loads. Two modifications of state determination for the nonlinear elements, step 4.4.2 of the algorithm presented in the previous section, account for the static response. For each nonlinear element:

- the tangent stiffness matrix,  $\mathbf{k}_T$ , for an element depends on the dynamic and static displacement,  $\mathbf{u} + \mathbf{u}_s$  (Step 4.4.2.1),
- the restoring force due to the dynamic and static displacements is  $-\mathbf{p}(\dot{\mathbf{u}}_{n+1}^k, \mathbf{u}_{n+1}^k + \mathbf{u}_s) + \mathbf{p}(\mathbf{u}_s)$ , which is assembled into  $\Delta \mathbf{P}^*$  (Step 4.4.2.2).

The static state,  $\mathbf{u}_s$  and  $\mathbf{p}(\mathbf{u}_s)$  for each nonlinear element, is computed from a static analysis of the entire system and stored for use in the state determination. If nonlinear response is expected under static loads then a nonlinear static analysis is performed.

# Chapter 4

## **DAM–WATER INTERACTION AND DAM–FOUNDATION INTERACTION**

### **4.1 Introduction**

The earthquake response of arch dams is substantially affected by the dynamic interaction between the dam, the impounded water, and the foundation rock. This chapter describes the methods adopted for including dam–water interaction and dam–foundation rock interaction in the nonlinear substructure analysis procedure.

### **4.2 Dam–Water Interaction**

Interaction between a concrete arch dam and the water impounded in the reservoir has a significant effect on the earthquake response of the dam. Recent studies show that water compressibility can be important in arch dam response (Fok and Chopra, 1987), as determined using a rigorous analytical procedure for interaction between the dam and compressible water (Fok and Chopra, 1985). However, including water compressibility requires a frequency domain solution of the equations of motion for the dam and water. This is only valid for a linear system, which is not the case for arch dams with opening and closing of joints.

If water compressibility is neglected, dam–water interaction can be represented by an added mass matrix and a time domain solution is possible. The added mass matrix, however, couples all DOF at the upstream face which would couple all substructures together. This section presents the formulation for an incompressible fluid and the approximations introduced for effective use of the substructure analysis procedure.

#### *4.2.1 Equations of Motion for Incompressible Fluids*

The finite element formulation for a fluid–structure system with incompressible fluid is summarized in this section (Kuo, 1982; Zienkiewics, 1977). Figure 4.1 shows the fluid–structure system.

The governing equation for hydrodynamic pressure of an incompressible fluid is:

$$\nabla^2 p = 0 \tag{4.1}$$

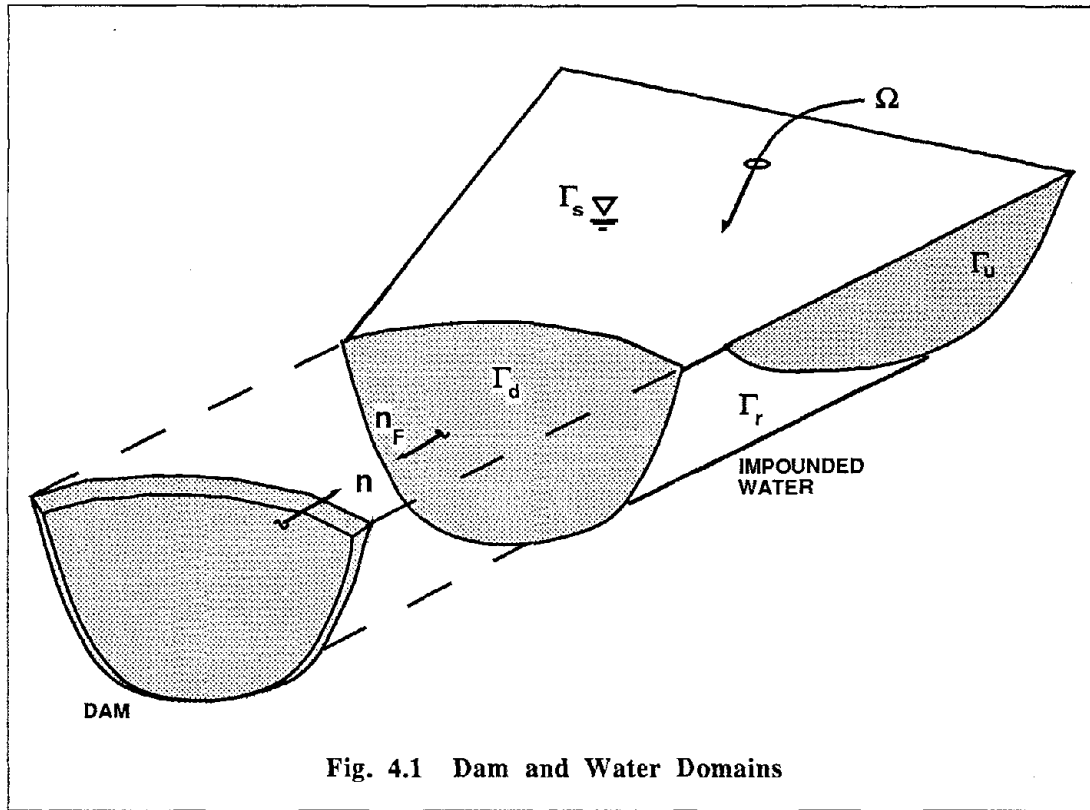


Fig. 4.1 Dam and Water Domains

where  $p=p(x,y,z,t)$  is the pressure in the fluid domain,  $\Omega$ . Normals to the boundaries,  $\Gamma$ , are defined positive pointing out of the fluid domain. The boundary condition at the free surface,  $\Gamma_s$ , neglecting surface waves is:

$$p = 0 \quad (4.2a)$$

The boundary condition for the reservoir boundary,  $\Gamma_r$ , is:

$$\frac{\partial p}{\partial n} = -\rho \ddot{u}_{nr} \quad (4.2b)$$

where  $\ddot{u}_{nr}$  is the normal component of the specified ground acceleration at the reservoir boundary. A similar boundary condition applies at the upstream face of the dam,  $\Gamma_d$ :

$$\frac{\partial p}{\partial n} = -\rho \ddot{u}_{nd} \quad (4.2c)$$

where  $\ddot{u}_{nd}$  is the total acceleration normal to the boundary at the upstream face of the dam. The finite element model of the fluid domain is truncated at some distance upstream of the dam. The condition at the truncated boundary,  $\Gamma_u$ , is:

$$\frac{\partial p}{\partial n} = -\rho \ddot{u}_{nu} \quad (4.2d)$$



where  $\ddot{u}_{nu}$  is the acceleration normal to the truncated boundary.

The acceleration,  $\ddot{u}_{nu}$ , could be determined using a closed form solution of the governing equation for incompressible water in a uniform, infinitely long channel upstream from the truncated boundary (Hall and Chopra, 1980). If the finite element model of the incompressible water is extended a sufficient distance upstream, however, the pressure at the dam is not substantially affected by the acceleration at the truncated boundary. Consequently, it is acceptable to assume  $\ddot{u}_{nu}$  is zero at the truncated boundary. The implication is that motion of the reservoir boundaries upstream from the truncated fluid domain has a small effect on the dam response: this is accurate if the upstream extent of water is greater than twice the dam height (Hall and Chopra, 1980).

The finite element solution for hydrodynamic pressure can be obtained from the weak form of the governing equation. The weak form of the hydrodynamic pressure equation, Eq. 4.1, is:

$$\int_{\Omega} \delta p \nabla^2 p d\Omega = 0 \quad (4.3)$$

where  $\delta p$  is an arbitrary pressure field that satisfies the boundary condition at the free surface (Eq. 4.2a),  $\delta p = 0$  on  $\Gamma_s$ . Use of the divergence theorem on Eq. 4.3 with the boundary conditions in Eqs. 4.2(b) to 4.2(d) gives:

$$\frac{1}{\rho} \int_{\Omega} \nabla \delta p \nabla p d\Omega + \int_{\Gamma_r} \delta p \ddot{u}_{nr} d\Gamma + \int_{\Gamma_d} \delta p \ddot{u}_{nd} d\Gamma = 0 \quad (4.4)$$

The finite element discretization of Eq. 4.4 is obtained by interpolating the pressure over an element:

$$p = \mathbf{N}_F \mathbf{p} \quad (4.5a)$$

$$\delta p = \mathbf{N}_F \delta \mathbf{p} \quad (4.5b)$$

where  $\mathbf{N}_F$  are shape functions for pressure and  $\mathbf{p}$  and  $\delta \mathbf{p}$  are vectors of pressure at the nodes. Substitution of Eq. 4.5 into Eq. 4.4 gives the discrete form of the hydrodynamic equation for arbitrary  $\delta \mathbf{p}$ :

$$\mathbf{g} \mathbf{p} = \mathbf{f}_d + \mathbf{f}_r \quad (4.6a)$$

$$\mathbf{g} = \frac{1}{\rho} \int_{\Omega} \nabla \mathbf{N}_F^T \nabla \mathbf{N}_F d\Omega \quad (4.6b)$$

$$\mathbf{f}_d = - \int_{\Gamma_d} \mathbf{N}_F^T \ddot{u}_{nd} d\Gamma \quad (4.6c)$$

$$\mathbf{f}_r = - \int_{\Gamma_r} \mathbf{N}_F^T \ddot{u}_{nr} d\Gamma \quad (4.6d)$$

The matrices  $\mathbf{g}$ ,  $\mathbf{f}_d$  and  $\mathbf{f}_r$  are assembled for each element in the fluid domain.

In the analysis of the coupled dam–water system, the pressure at the upstream face nodes is needed. Partitioning Eq. 4.6(a) into nodes at the upstream face and all other nodes in the fluid domain gives:

$$\begin{bmatrix} \mathbf{g}_{dd} & \mathbf{g}_{dr} \\ \mathbf{g}_{rd} & \mathbf{g}_{rr} \end{bmatrix} \begin{Bmatrix} \mathbf{p}_d \\ \mathbf{p}_r \end{Bmatrix} = \begin{Bmatrix} \mathbf{f}_d \\ \mathbf{0} \end{Bmatrix} + \begin{Bmatrix} \mathbf{0} \\ \mathbf{f}_r \end{Bmatrix} \quad (4.7)$$

where the quantities are associated with the upstream face ( $d$ ) or the reservoir plus other boundaries ( $r$ ). Elimination of the  $r$  quantities from Eq. 4.7 gives:

$$\bar{\mathbf{g}}\mathbf{p}_d = \mathbf{f}_d + \bar{\mathbf{f}}_r \quad (4.8a)$$

in which,

$$\bar{\mathbf{g}} = \mathbf{g}_{dd} - \mathbf{g}_{dr}\mathbf{g}_{rr}^{-1}\mathbf{g}_{rd} \quad (4.8b)$$

$$\bar{\mathbf{f}}_r = -\mathbf{g}_{dr}\mathbf{g}_{rr}^{-1}\mathbf{f}_r \quad (4.8c)$$

Whereas  $\mathbf{g}$  in Eq. 4.6 is a banded matrix, the reduced matrix  $\bar{\mathbf{g}}$  in Eq. 4.8(b) is full, coupling all pressure nodes at the upstream face of the dam.

#### 4.2.2 Fluid–Structure Coupling

The fluid equations, Eq. 4.8, are coupled to the equations of motion for the structure by equilibrium and compatibility at the fluid–structure interface, as shown in Fig. 4.2. The nonlinear equations of motion for a structure subjected to earthquake ground motion are:

$$\mathbf{m}\ddot{\mathbf{u}} + \mathbf{p}(\dot{\mathbf{u}}, \mathbf{u}) = -(\mathbf{m}\mathbf{r} + \mathbf{m}_g)\ddot{\mathbf{u}}_g + \mathbf{f} \quad (4.9)$$

where most of the quantities are defined in Chapter 3 and  $\mathbf{f}$  is a vector of hydrodynamic forces at the fluid–structure interface. The hydrodynamic forces can be computed in a consistent manner from the finite element equations for the fluid using the principle of virtual displacements:

$$\mathbf{f} = -\mathbf{h}^T \mathbf{p}_d \quad (4.10a)$$

in which the coupling matrix at the fluid–structure interface is:

$$\mathbf{h} = \int_{\Gamma_d} \mathbf{N}_F^T \mathbf{n}^T \mathbf{N} d\Gamma \quad (4.10b)$$

where  $\mathbf{N}$  are the shape functions for displacements in the dam elements and  $\mathbf{n}$  is the outward normal from the structure.

The forces on the right hand side of Eq. 4.8(a) can be expressed in terms of the acceleration at the upstream face of the dam and reservoir boundary. The total acceleration at the dam boundary of the fluid can be expressed in terms of the acceleration of the dam:

$$\ddot{\mathbf{u}}_{nd} = -\mathbf{n}^T \mathbf{N}(\ddot{\mathbf{u}} + \mathbf{r}\ddot{\mathbf{u}}_g) \quad (4.11)$$

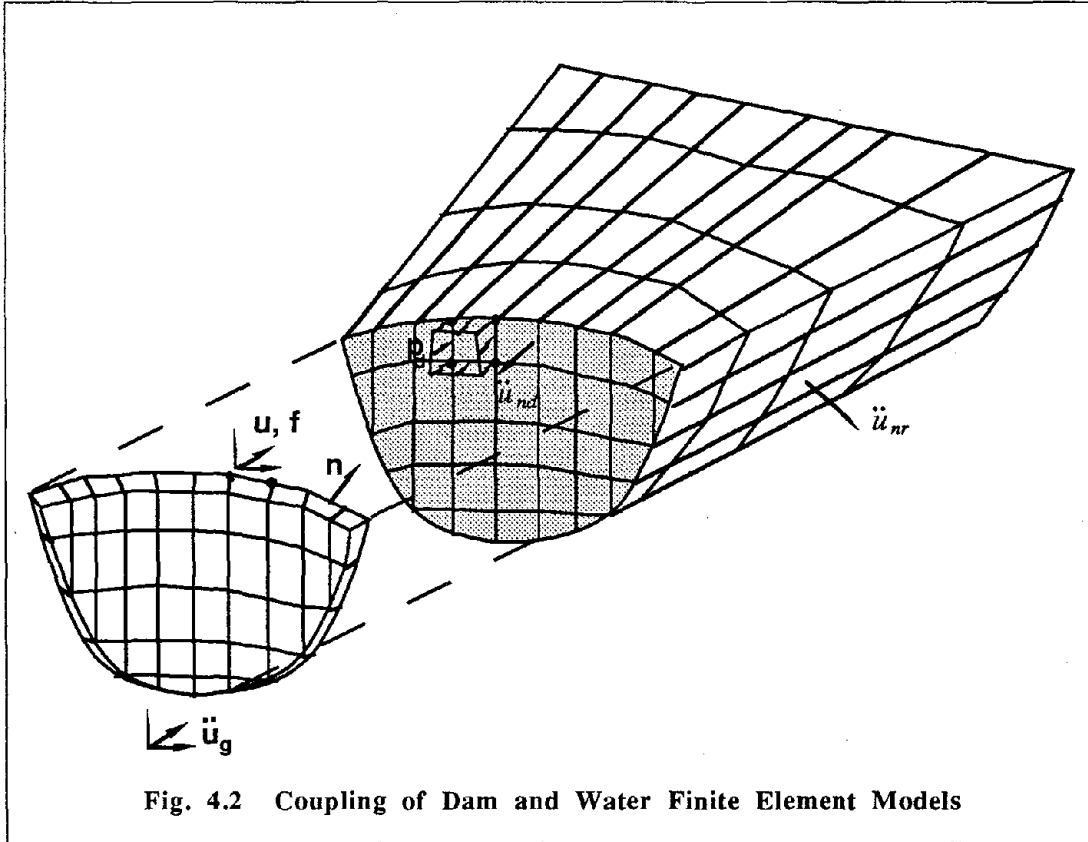


Fig. 4.2 Coupling of Dam and Water Finite Element Models

In Eq. 4.11, the interpolation on the second term is valid if  $\mathbf{r}$  represents rigid body motion of the structure because the shape functions must admit rigid body displacements. Substituting Eq. 4.11 into Eq. 4.6(c) gives:

$$\mathbf{f}_d = \mathbf{h}(\ddot{\mathbf{u}} + \mathbf{r}\ddot{\mathbf{u}}_g) \quad (4.12)$$

For rigid body motion of the reservoir bottom, Eq. 4.6(d) is:

$$\mathbf{f}_r = \mathbf{h}_r \ddot{\mathbf{u}}_g \quad (4.13a)$$

$$\mathbf{h}_r = \int_{\Gamma_r} \mathbf{N}_r^T \mathbf{n}_r^T d\Gamma \quad (4.13b)$$

The coupled fluid-structure equations can be written by substituting Eq. 4.10(a) into Eq. 4.9 and Eqs. 4.12 and 4.13 into Eq. 4.8:

$$\mathbf{m}\ddot{\mathbf{u}} + \mathbf{p}(\dot{\mathbf{u}}, \mathbf{u}) = -(\mathbf{m}\mathbf{r} + \mathbf{m}_g)\ddot{\mathbf{u}}_g - \mathbf{h}^T \mathbf{p}_d \quad (4.14a)$$

$$\bar{\mathbf{g}}\mathbf{p}_d = \mathbf{h}(\ddot{\mathbf{u}} + \mathbf{r}\ddot{\mathbf{u}}_g) + \bar{\mathbf{h}}_d \ddot{\mathbf{u}}_g \quad (4.14b)$$

where,

$$\bar{\mathbf{h}}_d = -\mathbf{g}_d \mathbf{g}_{rr}^{-1} \mathbf{h}_r \quad (4.14c)$$

### 4.2.3 Solution Procedures for Coupled Equations of Motion

Several solution strategies for the coupled equations of motion, Eq. 4.14, are possible. The selection of the solution method involves a compromise between accuracy and the computational efficiency of the nonlinear substructure procedure. The alternatives are briefly described in this section.

#### Direct Substitution

Eq. 4.14(b) can be solved for  $\mathbf{p}_d$  and substituted into Eq. 4.14(a):

$$(\mathbf{m} + \mathbf{m}_d)\ddot{\mathbf{u}} + \mathbf{p}(\dot{\mathbf{u}}, \mathbf{u}) = -[(\mathbf{m} + \mathbf{m}_d)\mathbf{r} + \mathbf{m}_g + \mathbf{m}_r]\ddot{\mathbf{u}}_g \quad (4.15a)$$

$$\mathbf{m}_d = \mathbf{h}^T \bar{\mathbf{g}}^{-1} \mathbf{h} \quad (4.15b)$$

$$\mathbf{m}_r = \mathbf{h}^T \bar{\mathbf{g}}^{-1} \bar{\mathbf{h}}_d \quad (4.15c)$$

The matrix  $\mathbf{m}_d$  is often referred to as an "added mass" that represents the effect of the incompressible fluid. This is the approach followed in the original version of ADAP and the reservoir program RESVOR (Kuo, 1982). However, the programs do not include the matrix  $\mathbf{m}_r$ , so the pressure on the dam due to motion of the reservoir boundary is neglected.

The difficulty with the direct substitution is that the added mass matrix is a full matrix that couples all DOF at the upstream face of the dam. The large bandwidth of the mass matrix results in a very inefficient nonlinear analysis. Furthermore, in the substructure procedure, the added mass matrix couples all substructures together, negating the major advantage of the substructure solution for the joint-opening mechanism.

#### Simultaneous Solution

Using nodal displacements and pressure as unknowns, Eq. 4.14 can be expressed in a form suitable for simultaneous solution:

$$\begin{bmatrix} \mathbf{m} & \mathbf{0} \\ -\mathbf{h} & \mathbf{0} \end{bmatrix} \begin{Bmatrix} \ddot{\mathbf{u}} \\ \ddot{\mathbf{p}}_d \end{Bmatrix} + \begin{bmatrix} \mathbf{0} & \mathbf{h}^T \\ \mathbf{0} & \bar{\mathbf{g}} \end{bmatrix} \begin{Bmatrix} \mathbf{u} \\ \mathbf{p}_d \end{Bmatrix} + \begin{Bmatrix} \mathbf{p}(\dot{\mathbf{u}}, \mathbf{u}) \\ \mathbf{0} \end{Bmatrix} = \begin{Bmatrix} -(\mathbf{m}\mathbf{r} + \mathbf{m}_g) \\ \mathbf{h}\mathbf{r} + \bar{\mathbf{h}}_d \end{Bmatrix} \ddot{\mathbf{u}}_g \quad (4.16)$$

The numerical solution of Eq. 4.16 has three disadvantages: (i) the matrices are unsymmetrical; (ii) the number of unknowns is increased substantially; and (iii) the matrices have a large bandwidth.

An earlier study of nonlinear arch dam response used the simultaneous solution with several modifications to mitigate the computational disadvantages (Dowling and Hall, 1989). Application of a numerical time integration operator and multiplication of the lower partition in Eq. 4.16 by a negative constant gives a symmetric matrix for the equivalent static problem. The matrix, however, may not be positive definite in all cases. To reduce the coupling introduced by the fluid, the bandwidth of  $\bar{\mathbf{g}}$  was reduced by neglecting some of the off-diagonal terms.

### Partitioned Solution

Partitioned analysis is an alternative solution method for dam–water interaction problems (Park and Felippa, 1984). Each set of equations in Eq. 4.14 is solved separately by staggering the solution for the dam, Eq. 4.14(a), with the solution for the water, Eq. 4.14(b). The solution for the dam response is unaffected by the water except for computing the hydrodynamic force. The water response is computed separately using the current estimate of dam acceleration. Iteration between the dam and water is required to obtain an equilibrium solution, but iteration is necessary for the nonlinear solution so the penalty is minor.

#### *4.2.4 Selection of Solution Procedure*

The principal goal of this investigation is to determine the effect of joint opening on the earthquake response of arch dams. Although dam–water interaction is very important, simplifications for including interaction effects are acceptable as long as the overall effect of the water is recognized. The simultaneous solution procedure increases the size of the numerical problem by about 25% and introduces additional coupling to the substructures. The partitioned solution procedure is promising, but its implementation is outside the scope of the current investigation. Consequently, an added mass solution was selected for including dam–water interaction in the nonlinear analysis. Because the added mass dramatically increases the bandwidth of the matrices and couples all the substructures together, the added mass matrix is diagonalized. This approach was used in an earlier nonlinear analysis of arch dams (Kuo, 1982).

The diagonalization of the added mass is based on a physical interpretation of the governing equations for the fluid. If the vector  $\mathbf{r}$  represents the rigid body acceleration of the dam in one direction, the hydrodynamic pressure at the upstream face is given by Eq. 4.14(b);

$$\bar{\mathbf{g}}\mathbf{p}_d = \mathbf{h}\mathbf{r} \quad (4.17a)$$

after neglecting the effect of the motion at the reservoir boundary. The hydrodynamic force on the upstream face of the dam in the direction  $\mathbf{r}$  is:

$$\mathbf{f} = -\mathbf{r}^T \mathbf{f} = \mathbf{r}^T \mathbf{h}^T \bar{\mathbf{g}}^{-1} \mathbf{h} \mathbf{r} = \mathbf{r}^T \mathbf{m}_d \mathbf{r} \quad (4.17b)$$

The diagonal terms of the added mass matrix,  $\mathbf{m}_d$ , corresponding to the direction  $\mathbf{r}$  are then scaled so that the sum of the diagonal terms is equal to  $f$ , and all the off–diagonal terms are set to zero. This procedure gives the correct total hydrodynamic force for rigid body acceleration of the dam. The diagonalization is performed separately for rigid body motion in the stream, cross–stream, and vertical directions.

The effect of the added mass matrix was evaluated using Morrow Point dam, which has been studied extensively with incompressible water (Kuo, 1982) and compressible water (Fok and Chopra, 1987), although only the incompressible case is considered here. Table 4.1 lists the

vibration frequencies of Morrow Point dam with the reservoir represented by the full added mass matrix and the diagonal added matrix, as described above. The vibration properties were obtained using the eigenvalue solution procedure in the program EADAP (Ghanaat and Clough, 1989).

TABLE 4.1 Effect of Incompressible Added Mass of Water on Vibration Frequencies of Morrow Point Dam

Mode	Vibration Frequency (rad/sec)		
	Empty Reservoir	Full Reservoir	Full Reservoir
		Full Added Mass	Diagonal Added Mass
1	20.31	17.60	15.73
2	22.34	19.00	16.43
3	35.40	29.06	22.85
4	37.47	30.28	25.00
5	40.40	36.29	27.50
6	43.60	39.57	31.77
7	48.22	46.41	33.50
8	54.12	49.99	37.84
9	60.58	54.43	42.13
10	60.80	56.65	44.13

The diagonal added mass matrix underestimates the frequency of the first vibration mode by 11% and the tenth mode by 22% compared with the full added mass matrix. The added mass matrix diagonalization does not have a substantial effect on the vibration mode shapes or the ordering of the modes. For the primary goal of investigating the joint mechanism, the diagonalization procedure represents the effect of the added water in an adequate manner and it does not decrease the efficiency of the nonlinear substructure solution procedure. It should be mentioned that the error in the incompressible water assumption may be greater than the error in the diagonalization. The response of Morrow Point Dam with compressible water shows more complex frequency response characteristics than with incompressible water; in particular, incompressible water overestimates the fundamental vibration frequency (Fok and Chopra, 1987).

### 4.3 Dam–Foundation Interaction

The interaction between a concrete arch dam and the supporting foundation rock has an important effect on the earthquake response, particularly on stresses in the dam near the dam–foundation rock interface. The modeling of the foundation region is complicated by the three-dimensional geometry of canyon sites and highly variable properties of the rock. The generally accepted practice in the earthquake analysis of concrete arch dams is to model the stiffness properties of a foundation rock region of a size approximately equal to the dimensions of the dam. Inertial properties, and hence the propagation of seismic waves through the foundation rock, are neglected in the massless model. Damping in the foundation is specified indirectly by stiffness proportional damping in the solution procedure.

The finite element model of the foundation rock region is one substructure with the far boundaries fixed. The stiffness matrix for the foundation region is statically condensed to the degree-of-freedom at the dam–foundation rock interface. This matrix could be used in the static and dynamic analysis of the system, but all the interface DOF would have to be included in the boundary partition for the nonlinear substructure procedure. The large number of additional DOF would adversely affect the computational effort.

The bandwidth of the condensed stiffness matrix for the foundation region is reduced by only retaining nonzero stiffness coefficients close to the diagonal, hence reducing the coupling of the substructures. Several numerical studies, static, dynamic, and eigenvalue, have shown that it is only necessary to retain the stiffness coupling with two immediately adjacent nodes on the dam–foundation interface. In effect then, each substructure is only coupled to its adjacent substructures through the foundation rock. A similar localization of the foundation rock stiffness matrix was used in an earlier study (Dowling and Hall, 1989).





# Chapter 5

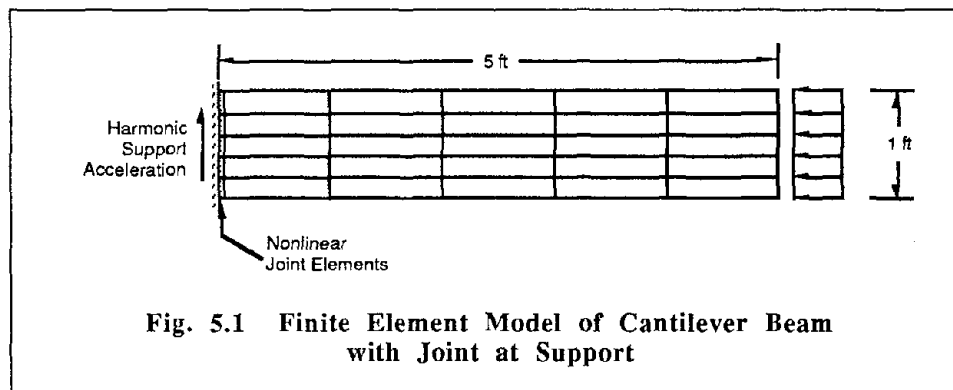
## STUDY OF CONTRACTION JOINT MODEL

### 5.1 Introduction

Two studies of the nonlinear joint element for modeling contraction joints in arch dams were undertaken. The first study involved a cantilever beam in which the joint at the fixed support can open. Additional understanding was obtained by comparing the response of a segmental arch rib recorded during shaking table experiments with the analytical response of a corresponding finite element model.

### 5.2 Cantilever Beam

Figure 5.1 shows the finite element model of a cantilever beam in which the support at the fixed end can open and close. The model consists of 25 solid elements and five joint elements. Out-of-plane displacements are restrained, so the beam is in a state of plane strain. The fundamental vibration frequency of the cantilever beam (with closed joint at the fixed end) is 64 Hz. Rayleigh damping in the beam provides a viscous damping ratio of 10% in the first and third vibration modes. Joint opening is allowed with a joint strength of  $q_0 = 0$  in the normal direction. The static load is a constant axial thrust at the free end, uniformly distributed over the beam cross section, which tends to close the joint at the support.

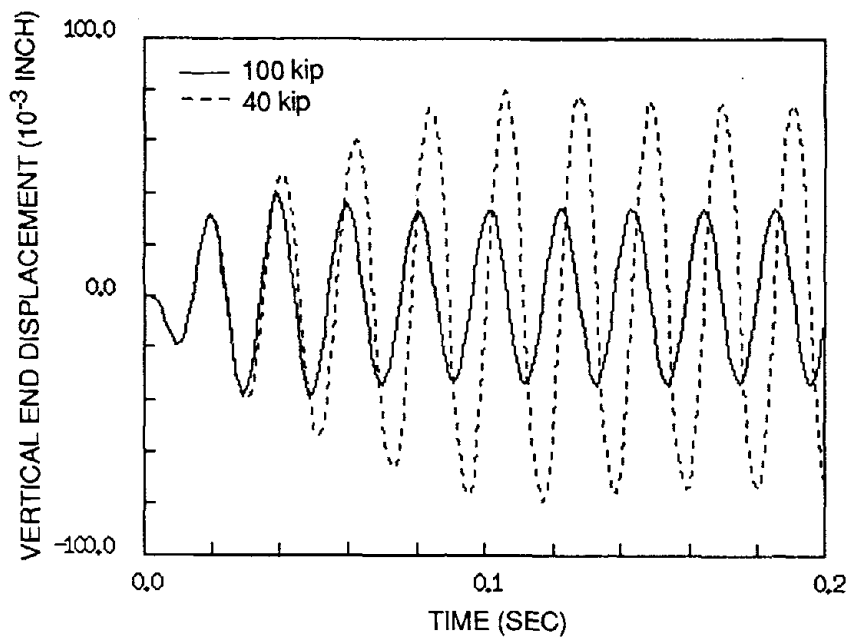


The beam is subjected to a harmonic vertical support acceleration with an amplitude of 1200 in/sec<sup>2</sup> at excitation frequencies of 48 Hz and 80 Hz. The steady-state response of the beam is computed for various values of axial thrust. Figures 5.2 and 5.4 show the vertical displacement at the free end of the beam subjected to support acceleration at frequencies 48 Hz and 80 Hz, respectively. Figures 5.3 and 5.5 show the horizontal displacement at the bottom of the joint for excitation frequencies 48 Hz and 80 Hz, respectively. In Figs. 5.3 and 5.5, positive displacement indicates an open joint and negative displacement indicates a closed joint.

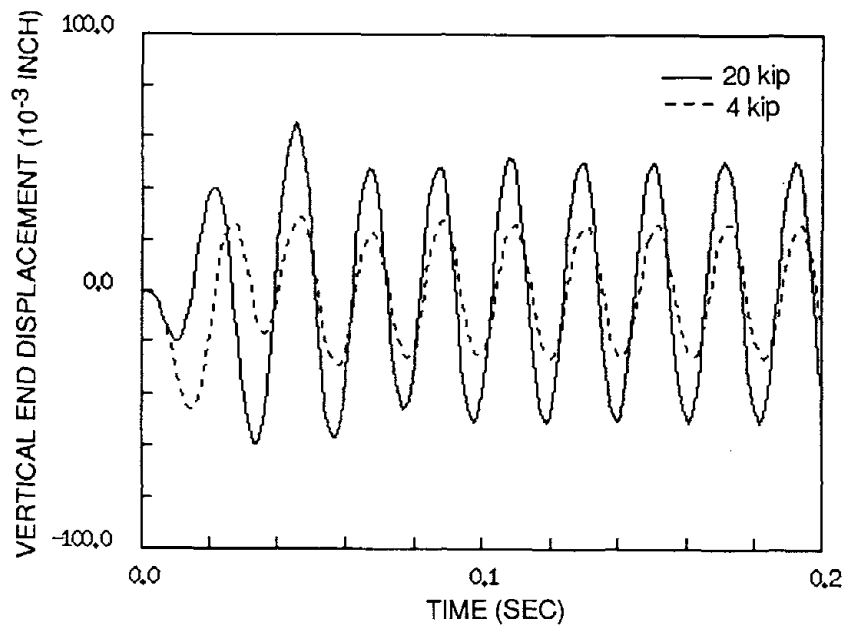
The thrust required to hold the joint closed during the dynamic response is 87 kip and 48 kip for excitation frequencies 48 Hz and 80 Hz, respectively. The response of the beam with a larger thrust is linear because the joint does not open. The joint remains closed with a thrust of 100 kip at 48 Hz (Fig. 5.2) and with a thrust of 50 kip at 64 Hz (Fig. 5.4).

An important aspect of the nonlinear response is that joint opening reduces the effective fundamental vibration frequency. For an excitation frequency of 48 Hz, reducing the thrust from 100 kip to 40 kip produces significant joint opening (Fig. 5.3a). The end displacement increases (Fig. 5.2a) because joint opening decreases the effective fundamental vibration frequency from 64 Hz, thus increasing the dynamic amplification for the harmonic load. The joint opening produced by further reduction of the thrust to 20 kip and 4 kip (Fig 5.3b) reduces the effective vibration frequency of the beam below 48 Hz, the frequency of maximum dynamic amplification, causing a decrease in the dynamic amplification and displacement at the free end (Fig. 5.2b).

The effect of the change of the vibration frequency on the dynamic amplification for the harmonic support acceleration is illustrated in Fig. 5.6. The plot shows the dynamic amplification function for a single degree-of-freedom system with a 10% viscous damping ratio. The ratio of the excitation frequency to the vibration frequency of the beam is related to the dynamic amplification for the steady state displacement of the beam. The response amplification for each case of the cantilever beam is illustrated in Fig. 5.6. Similar trends are apparent for an excitation frequency of 80 Hz, which is greater than the fundamental vibration frequency of the beam with a closed joint. Changing the axial thrust to 10 kip and 5 kip reduces the effective vibration frequency, thus reducing the dynamic amplification factor and the steady state displacement shown in Fig. 5.4. The reduction of dynamic amplification for this excitation frequency is also shown in Fig. 5.6.

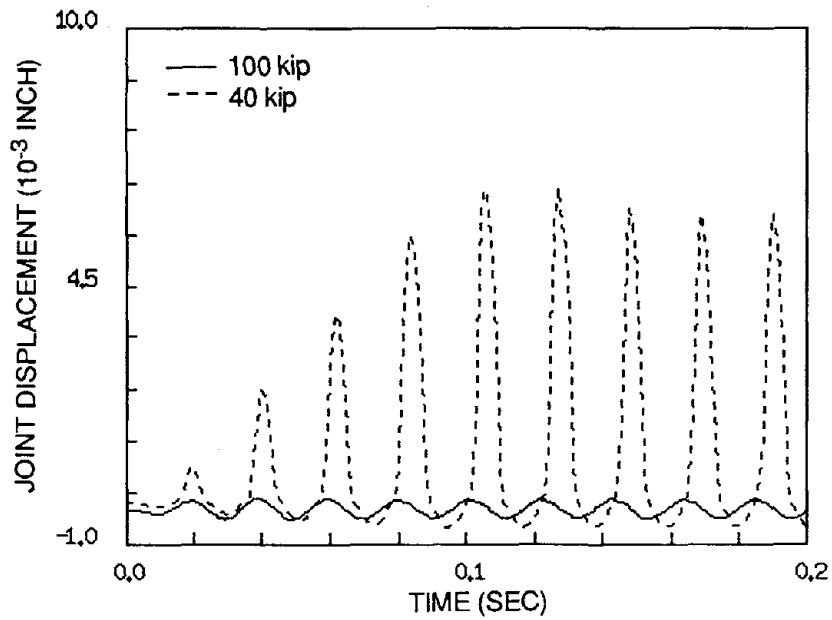


(a) Axial Thrust 100 kip and 40 kip

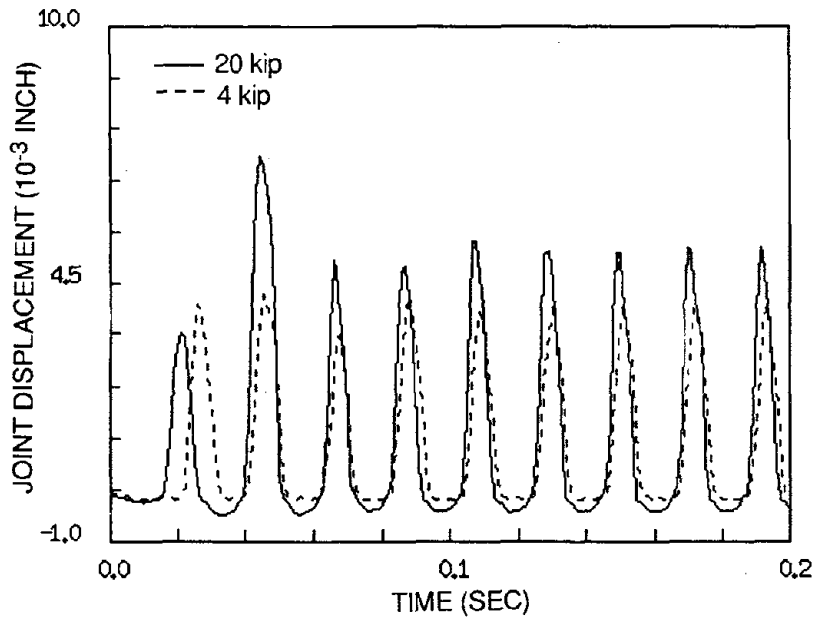


(b) Axial Thrust 20 kip and 4 kip

**Fig. 5.2 Vertical Displacement at Free End of Cantilever Beam Due to Harmonic Support Acceleration with  $f=48$  Hz**

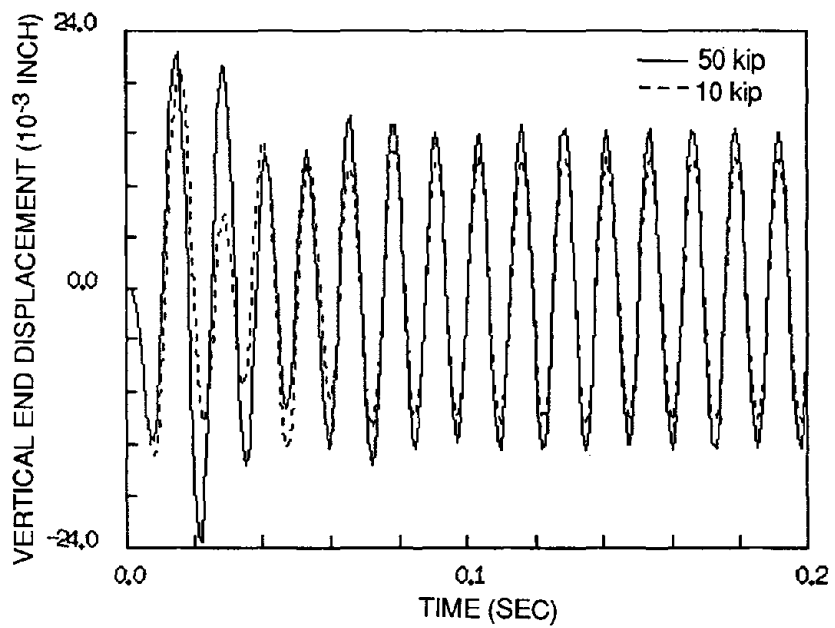


(a) Axial Thrust 100 kip and 40 kip

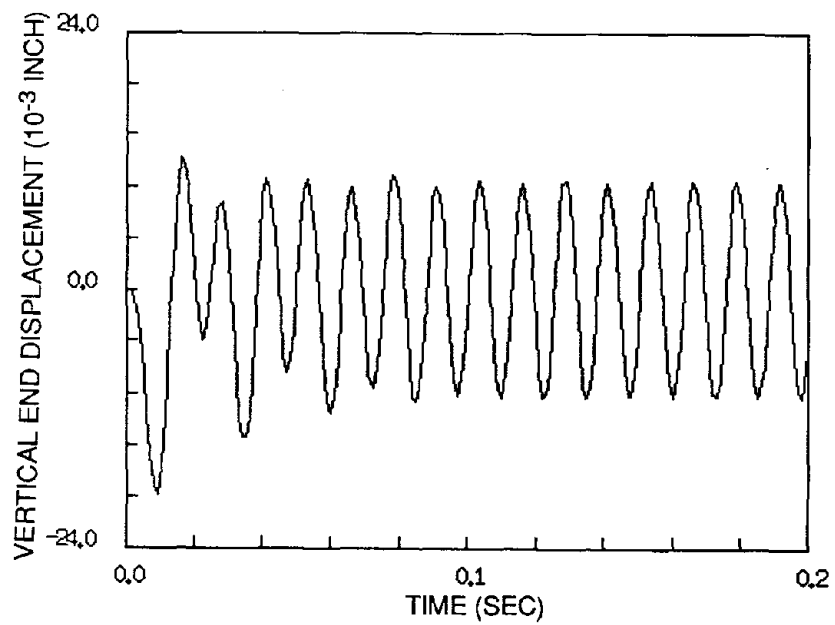


(b) Axial Thrust 20 kip and 4 kip

**Fig. 5.3 Joint Displacement at Bottom of Fixed End of Cantilever Beam Due to Harmonic Support Acceleration with  $f=48$  Hz**

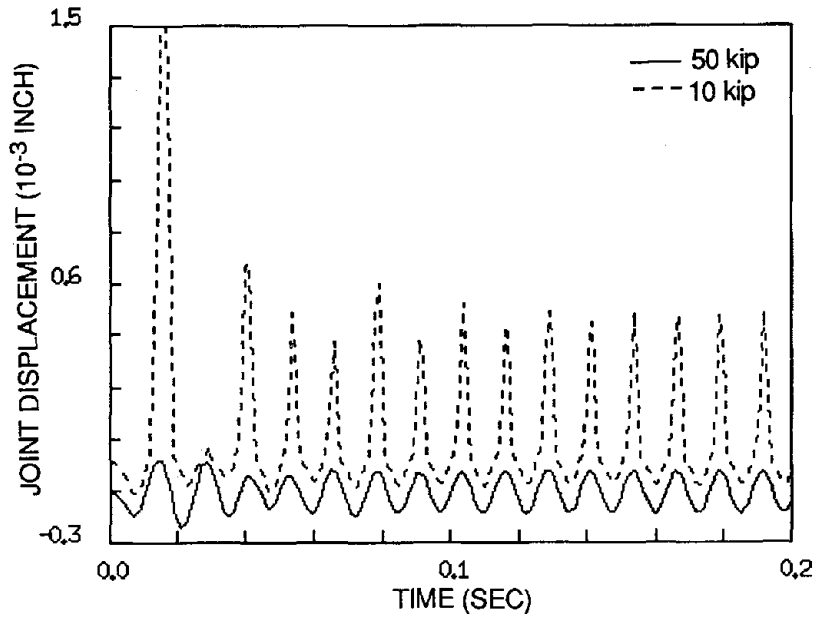


(a) Axial Thrust 50 kip and 10 kip

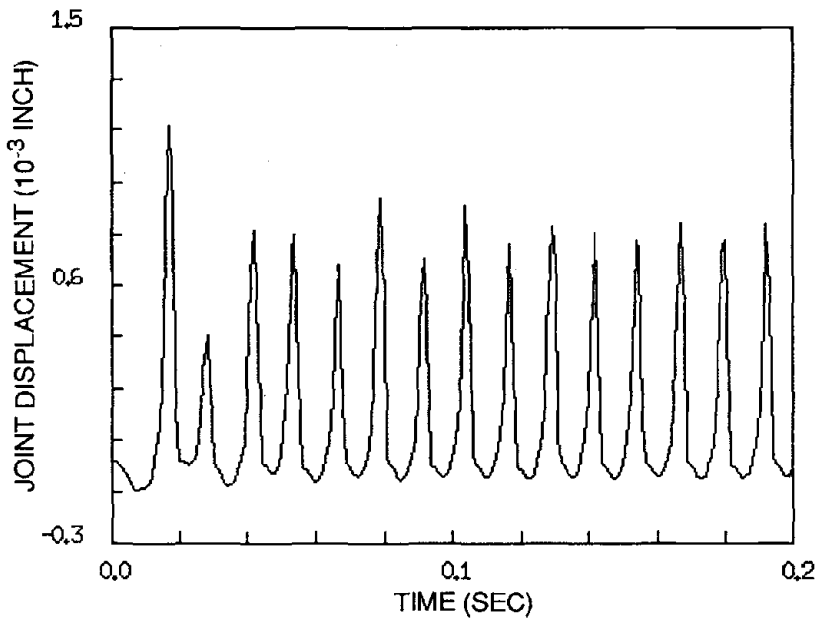


(b) Axial Thrust 5 kip

**Fig. 5.4 Vertical Displacement at Free End of Cantilever Beam Due to Harmonic Support Acceleration with  $f=80$  Hz**

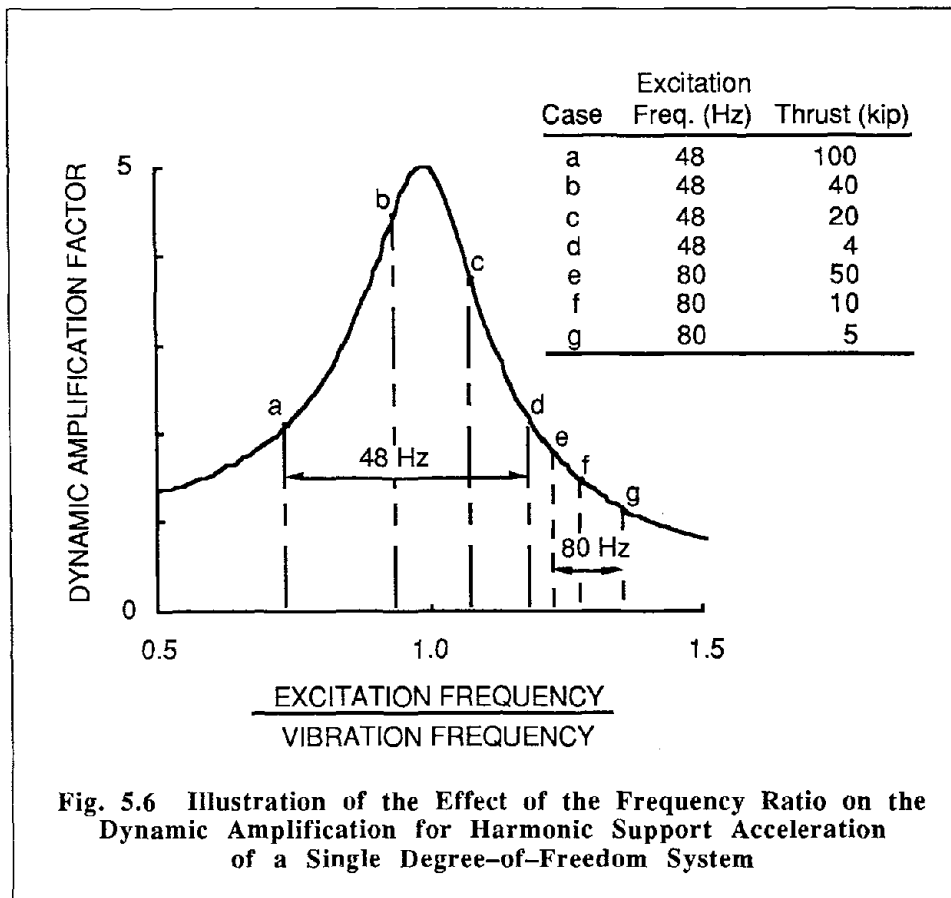


(a) Axial Thrust 50 kip and 10 kip



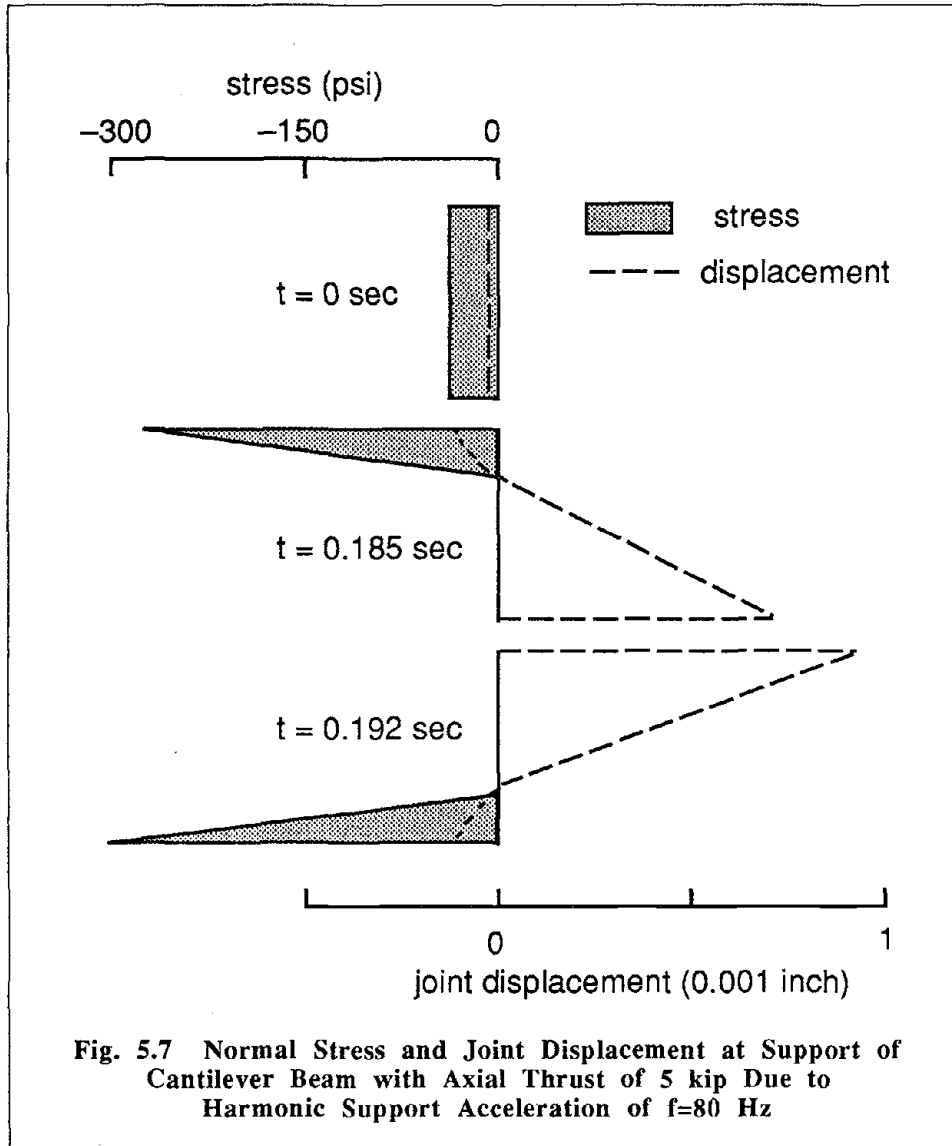
(b) Axial Thrust 5 kip

**Fig. 5.5 Joint Displacement at Bottom of Fixed End of Cantilever Beam Due to Harmonic Support Acceleration with  $f=80$  Hz**

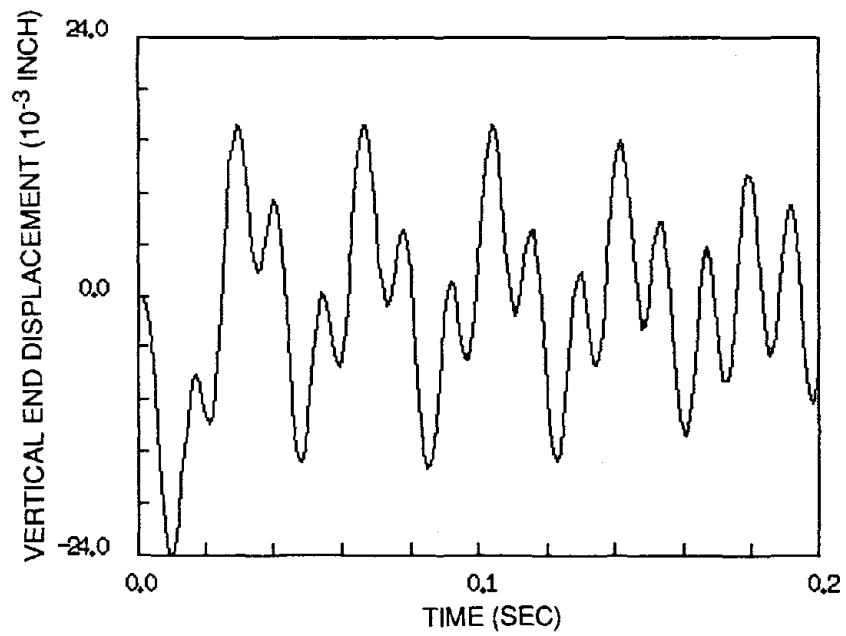


The distribution of normal stress at the fixed support of the beam with an axial thrust of 5 kip and an excitation frequency of 80 Hz is shown in Fig. 5.7. At time zero the stress is uniform because of the thrust. When joint opening is allowed there is no tensile stress and the compressive stress in the closed portion of the joint is large compared with the linear stress distribution. Figure 5.7 also shows the displacement of the joint, clearly demonstrating the opening. The small negative displacement represents the closed portion of the joint.

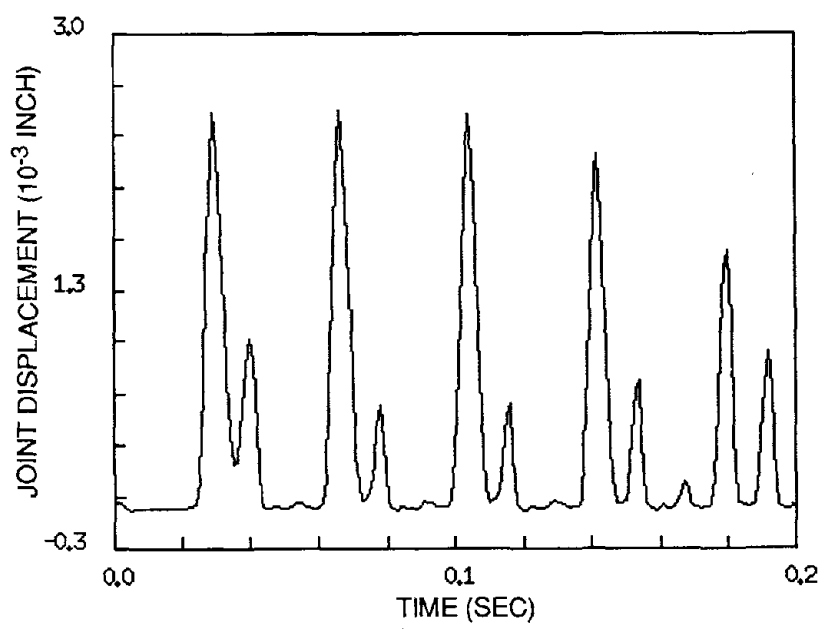
When the axial thrust is small enough, the beam is unstable under the dynamic load. The response with an axial thrust of 2 kip is shown in Fig. 5.8. The subharmonics in the vertical displacement response are caused by the large joint opening. The beam is on the borderline of stability; further reduction of the axial thrust results in unstable response.







(a) Vertical Displacement at Free End



(b) Joint Opening Displacement

**Fig. 5.8 Response of Cantilever Beam with Axial Thrust of 2 kip Due to Harmonic Support Acceleration of  $f=80$  Hz**

### 5.3 Experimental and Analytical Response of an Arch Rib

One of the few experimental investigations of the contraction joint behavior in arch dams was conducted at the shaking table facility of the Earthquake Engineering Research Center, University of California at Berkeley (Niwa and Clough, 1980). The rib was designed to approximate the geometry of an arch section of Techu Dam, Taiwan, with length scale of  $1/150$ . The model was constructed from a plaster mix formed into seven rectangular blocks with beveled edges. The plaster was proportioned so that the material properties preserve most of the similitude requirements.

#### 5.3.1 Experimental Model of Arch Rib

The arrangement of the arch rib model on the shaking table is shown in Fig. 5.9. Vertical weights develop the static forces in the arch. Vertical motion of the table simulates ground motion in the stream direction and horizontal table motion simulates cross-stream ground motion. The instrumentation recorded the radial and tangential displacements at the centers of the blocks and the joint opening displacement at the outer edge of each joint. The three lower modes of vibration determined from free vibration tests are shown in Fig. 5.10.

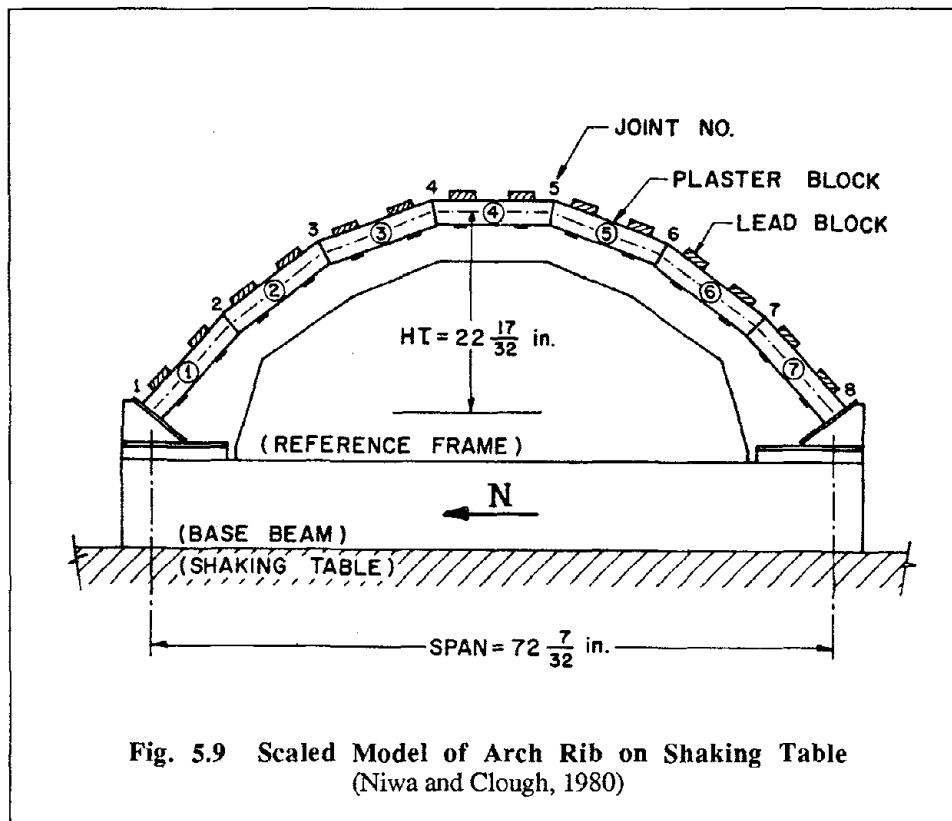
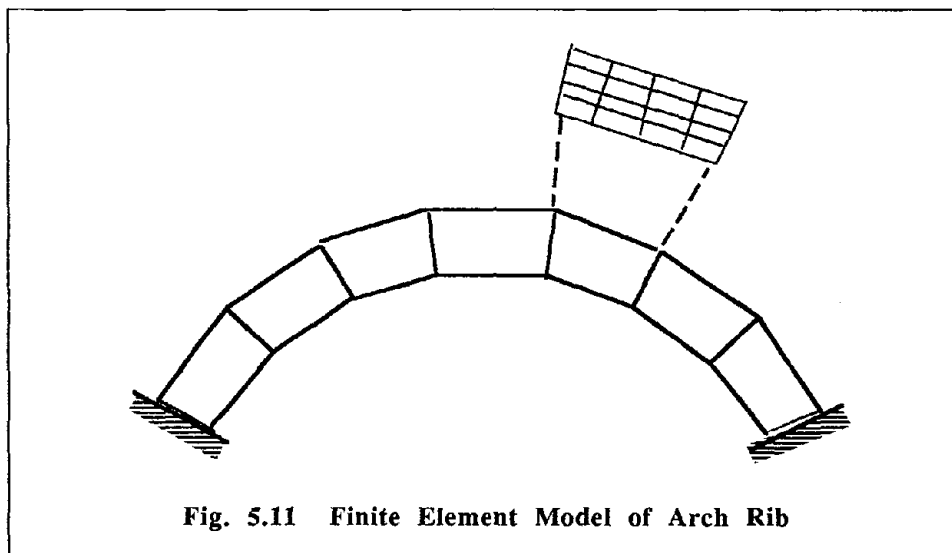
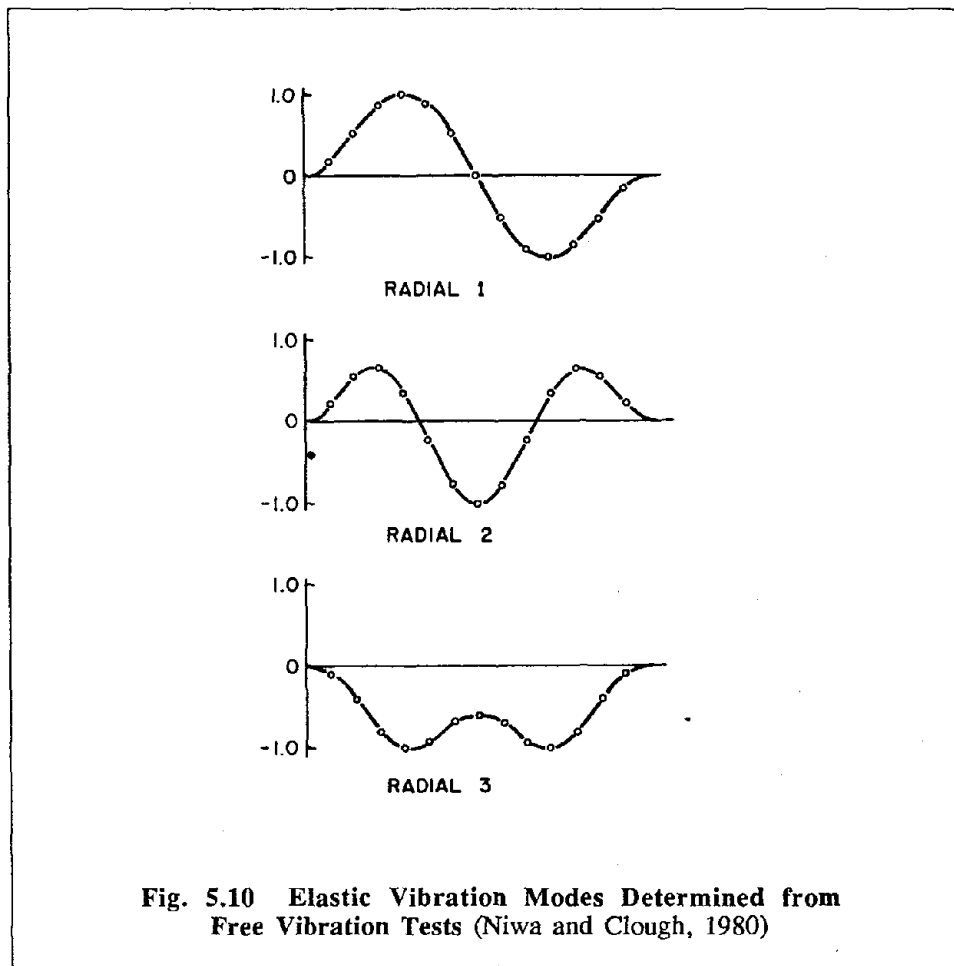


Fig. 5.9 Scaled Model of Arch Rib on Shaking Table  
(Niwa and Clough, 1980)



### 5.3.2 Finite Element Model of Arch Rib

The finite element model of the arch rib model consists of seven substructures connected by joints, as shown in Fig. 5.11. Each substructure consists of sixteen elements in a state of plane stress, and the linear elastic, isotropic material has a unit weight of 151 lb/ft<sup>3</sup>, which includes the effects of the gravity and hydrostatic loads on the arch, and an assumed Poisson's ratio of 0.2. An elastic modulus of 37,250 lb/in<sup>2</sup> provides an excellent match between the lower two vibration modes of the finite element model and the experimental model, as shown in Table 5.1. Three percent modal damping was measured in the free vibration tests and this is used in the finite element model.

### 5.3.3 Ground Motion

The horizontal ground motion obtained during the 1940 El Centro earthquake was used for the comparative study. The S00E component was applied in the horizontal direction (cross stream direction of arch) and the S90W component was applied in the vertical direction (stream direction of arch). The time scale of the records was speeded up by a factor of  $\sqrt{150}$  to maintain similitude with the prototype. The peak ground acceleration was scaled to provide different levels of excitation of the arch. Table 5.2 identifies the cases of earthquake excitation considered in the comparison of the analytical and experimental responses. The experimental study included cases 1, 2, and 4. Case 3 shows the effect of the level of cross stream excitation on the analytical response.

Table 5.1 Vibration Frequencies of Experimental and Analytical Models of Arch Rib

Mode	Mode Type	Vibration Frequency (Hz)	
		Experimental	Analytical
1	antisymmetric	12	12
2	symmetric	24	24
3	antisymmetric	—	43
4	symmetric	38	47

Table 5.2 Cases of El Centro Ground Motion Applied to Experimental and Analytical Models of Arch Rib

Case	Maximum Acceleration in g's	
	Horizontal (cross stream)	Vertical (stream)
1	0.039	—
2	0.152	—
3	0.740 <sup>a</sup>	—
4	0.740	0.788

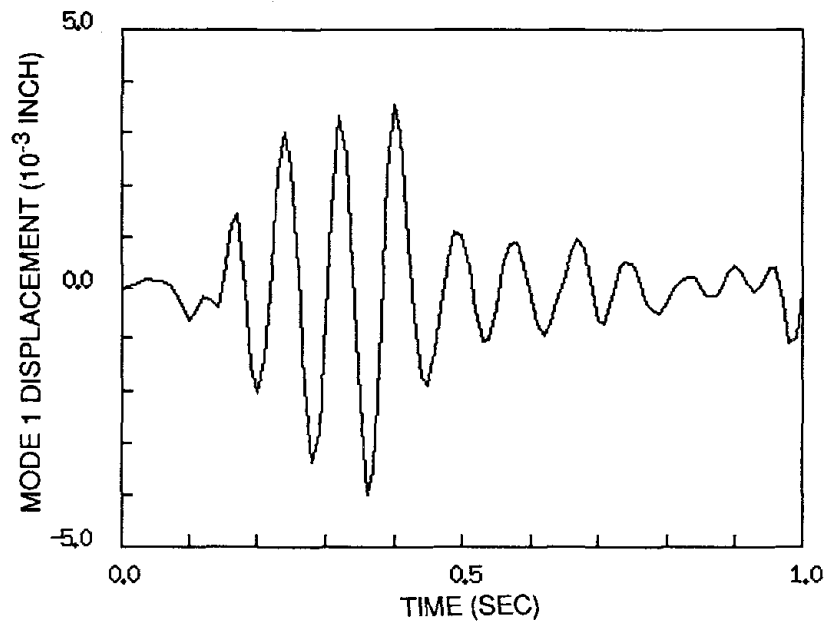
<sup>a</sup>Experimental response not available.

#### 5.3.4 Comparison of Experimental and Analytical Response

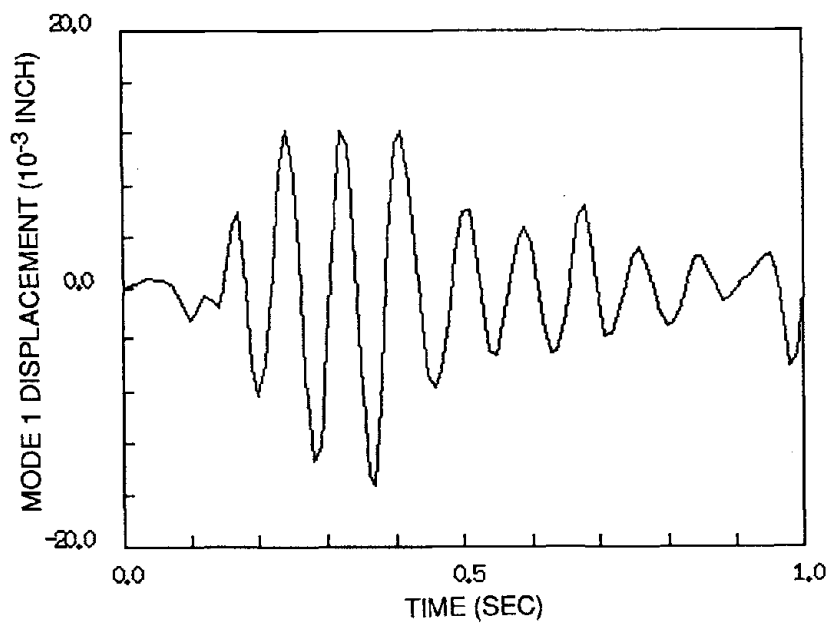
The responses of the experimental and analytical models to the earthquake excitation are presented as the amplitude of the first (antisymmetric) vibration mode (Niwa and Clough, 1980). The analytical modal response was determined from the nodal displacements of the finite element model using the three lowest vibration modes.

Figures 5.12 and 5.13 show the modal response of the experimental and analytical models, respectively, for cases 1 and 2. The response to the low-level ground motion (case 1) is essentially linear with both models showing a vibration frequency of 12 Hz. The maximum displacement of the analytical model underestimates the experimental response by about fifty percent. The response of the finite element model is similar to the analytical response computed for the original study (Niwa and Clough, 1980), with the same order of difference between the analytical and experimental responses.

Increasing the level of excitation (Case 2) increases the response of the rib as shown in Figs. 5.12 and 5.13. The experimental response indicates that the vibration frequency in the first antisymmetric mode reduces to 8 Hz because of joint opening (Fig. 5.13b). The analytical response shows only very small reduction in the vibration frequency (Fig. 5.12b) even though the joints open. Increasing the amplitude of the cross stream acceleration to a maximum value of 0.740 g (Case 3) causes larger nonlinear response of the finite element model and, as shown in Fig. 5.14, the effective vibration frequency reduces to about 8 Hz because of joint opening. The analytical and experimental responses to the high intensity biaxial excitation (case 4) are shown in Fig. 5.15. The experimental model shows a longer effective vibration period than does the analytical model as in the comparison for case 2.

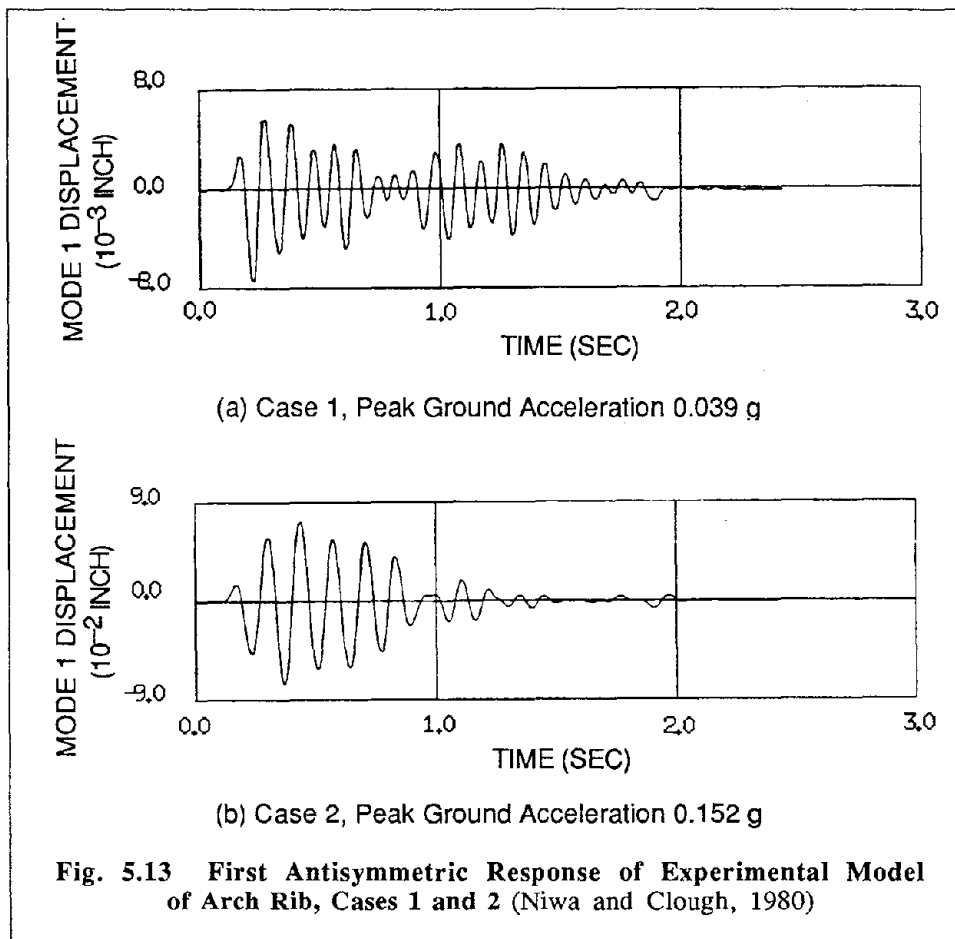


(a) Case 1, Peak Ground Acceleration 0.039 g



(b) Case 2, Peak Ground Acceleration 0.152 g

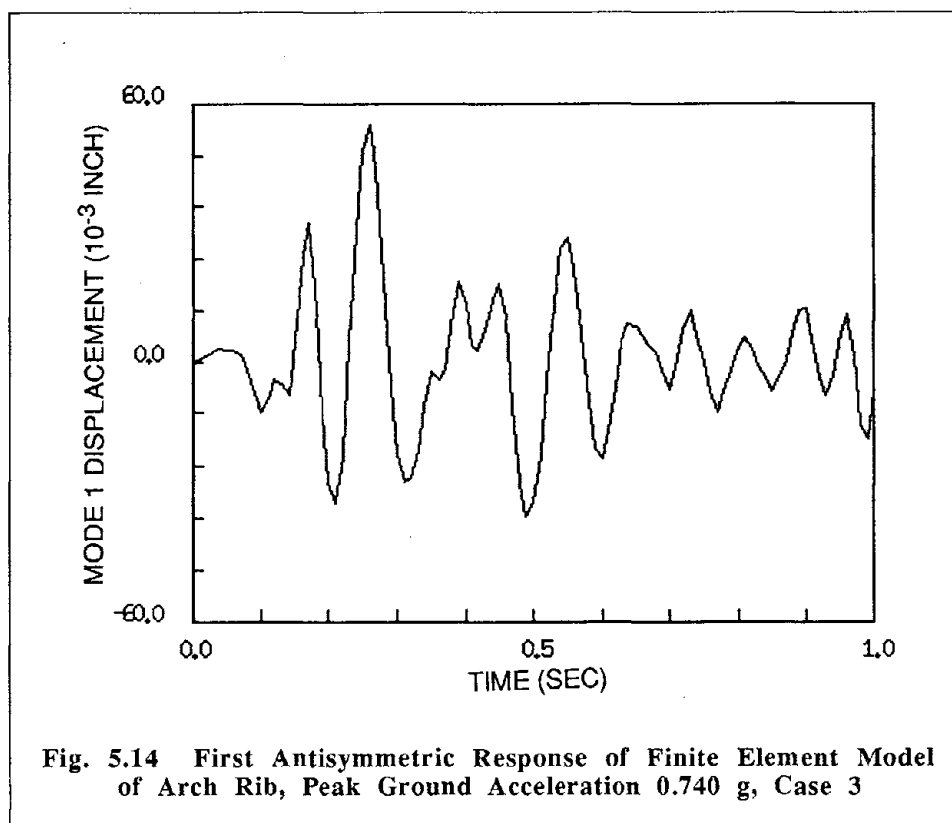
**Fig. 5.12 First Antisymmetric Response of Finite Element Model of Arch Rib, Cases 1 and 2**



### 5.3.5 Comparison of Joint Opening

During the shaking table testing of the rib, the opening displacement was recorded at two joints, and the analysis gives the joint opening of the finite element model. The joint opening is presented as a ratio of the open portion of the joint to the depth of the joint. The opening ratio for the joint at the left support is shown in Fig. 5.16, in which the analytical and experimental responses have similar qualitative joint response during the earthquake excitation.

From the viewpoint of the numerical solution, the nonlinear joint element and solution procedure perform very well. Convergence was achieved in three to five iterations per time step and the response does not show the high frequency oscillation often exhibited in the numerical solution of contact problems.

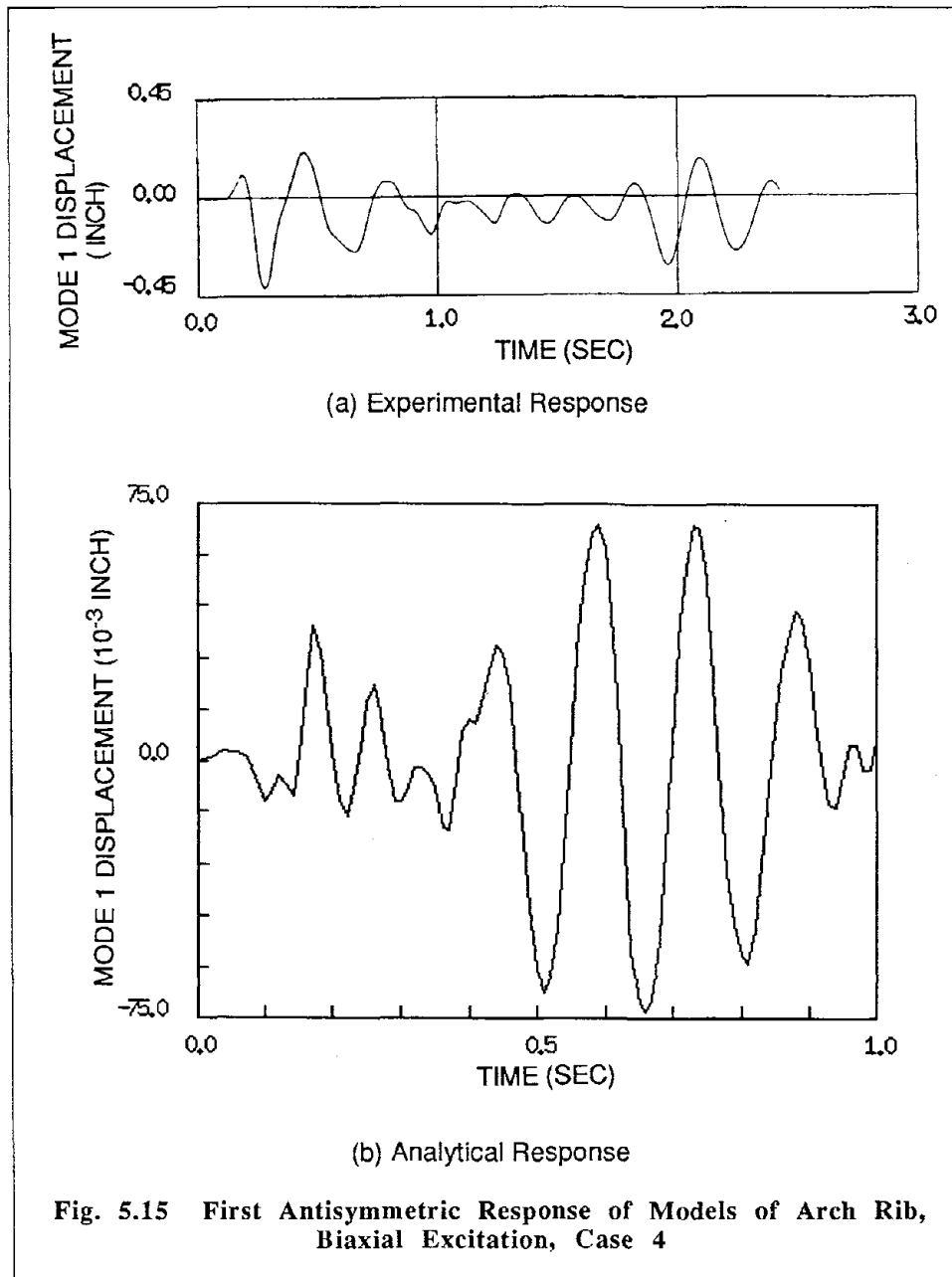


### 5.3.6 Discussion of Response Comparison

The purpose of the shaking table test of the arch rib was to investigate the effects of joint opening on the earthquake response of an idealized arch structure. Because of the problems in control of the model and accurate measurement of the response an exact comparison with an analytical model is probably not possible. Even in the linear range, the models underestimate the response of the arch rib observed in the shaking table tests.

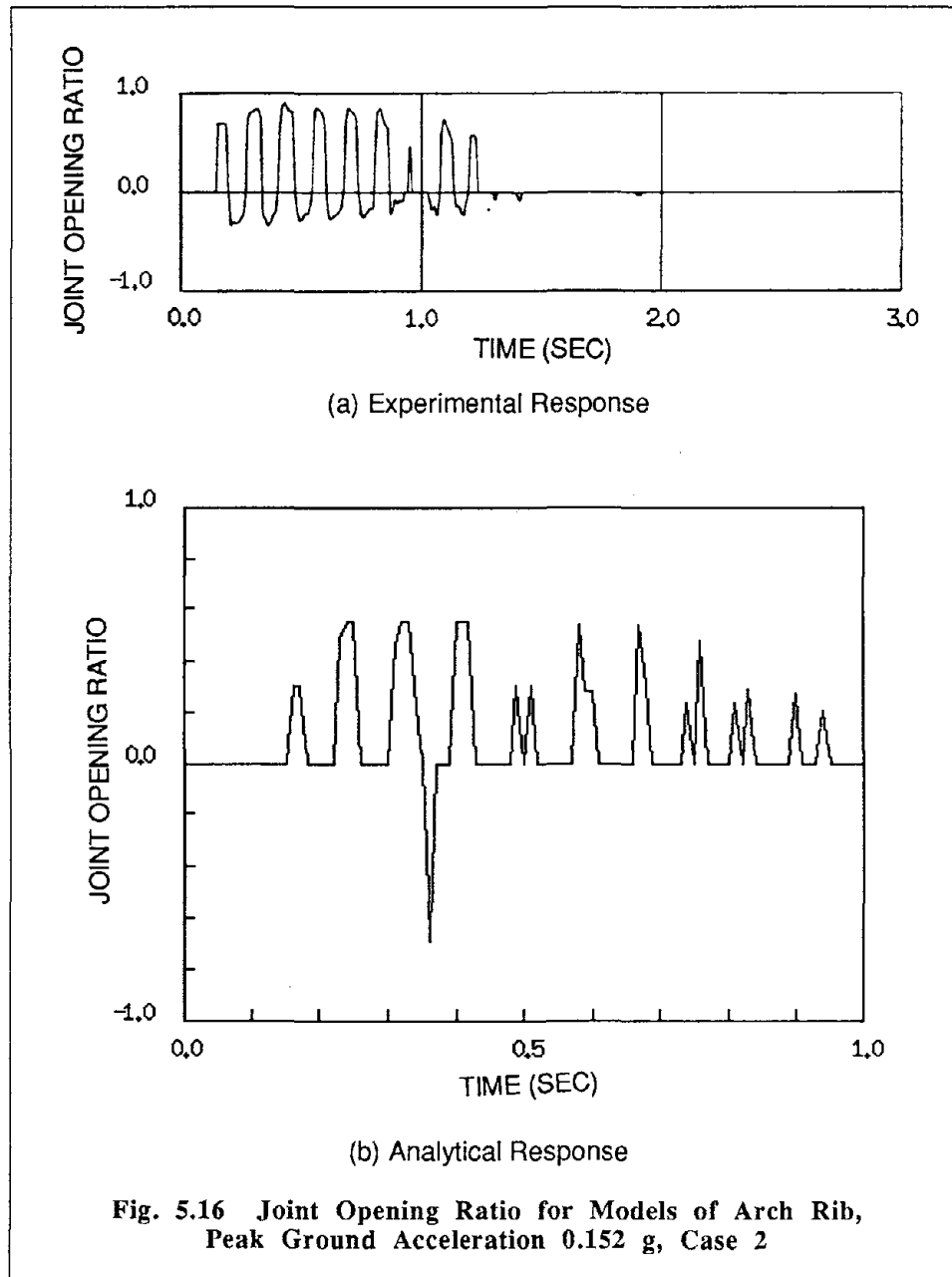
However, the analytical response does show an important effect of the joint opening mechanism that was observed in the tests: joint opening reduces the effective vibration frequency of the rib. Although the experimental and analytical models show this trend, the analytical model requires a higher level of excitation to accomplish the observed reduction in vibration frequency. Case 2 for the experimental test shows a reduction in the fundamental frequency of 33% (from 12 Hz to 8 Hz), whereas the excitation level must be increased in case 3 to produce the same reduction in the analytical model.

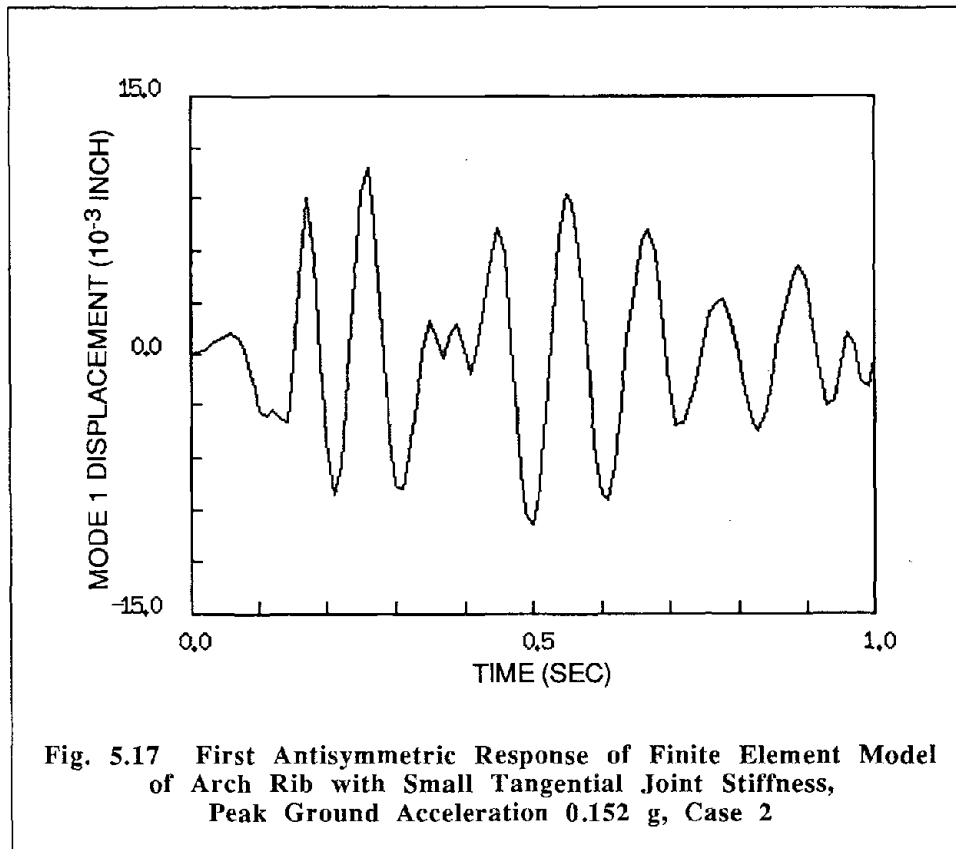




Although the trend in vibration frequency is represented by the analysis, the physical model of the rib is more flexible than accounted for in the finite element model. The major difference is that the joint element does not allow tangential motion between the blocks, whereas relative sliding of the blocks was observed during the tests (Clough, 1989). The nonlinear model for the joint could be modified to allow relative tangential motion of the joint with a force-displacement relationship that allows slippage (see Eq. 2.11). Although this was not done in the current study, the effect of joint slippage was simulated by using a small value for the stiffness in the tangential direction of

the joint, as shown in Fig. 5.17 for case 2. When tangential joint displacement is allowed, the effective fundamental frequency of the analytical model under this level of excitation decreases to 8 Hz as was the case for the experimental model.





#### 5.4 Summary

The analyses of a cantilever beam and single arch rib demonstrate the important characteristics of the joint opening mechanism on the response of structures. The numerical solution shows excellent convergence characteristics and the response does not show high frequency oscillations that often plague contact problems. The nonlinear joint elements represent the partial opening and closing of joints during a dynamic excitation. The effect of the joint mechanism on the vibration properties of the structure are accurately represented. The major shortcoming of the current study of the joint element is the constraint against tangential motion at the joint. The comparison of the experimental and analytical responses of the single arch rib demonstrate this effect. Although the formulation for the joint element can be modified to allow joint slippage, it was not done in this study.



# Chapter 6

## ***EARTHQUAKE ANALYSIS OF BIG TUJUNGA DAM***

### **6.1 Introduction**

The nonlinear analysis procedure described in the preceding chapters has been applied to the earthquake analysis of Big Tujunga dam, located in Big Tujunga canyon, Los Angeles County, California. The variable radius arch, shown in Fig. 6.1, has a crest length of 400 feet, the crest height is 251 feet above the foundation rock, and the thickness varies from 73 feet at the base to 8 feet at the crest. A concrete abutment block at the south end of the arch transfers the thrust into a highly fractured ridge, and a gravity section is used for a spillway at the north end. The dam was constructed in five foot lifts between full height contraction joints spaced approximately 50 feet along the crest. The earthquake response of Big Tujunga dam was thoroughly evaluated in an earlier study (Lindvall and Richter, 1975), which showed that a maximum credible earthquake produces maximum principal stresses in excess of 3000 psi. Because these large stresses cannot be transferred across contraction joints, it is expected that the joints will open during an earthquake. The objective of the present investigation is to examine the effect of joint opening on the earthquake response of Big Tujunga dam. This study does not supersede the earthquake analysis in an earlier report (Lindvall and Richter, 1975); the intent is to demonstrate the importance of the contraction joints in the earthquake response of this arch dam.

### **6.2 Finite Element Model and Ground Motion**

The present study uses a finite element model of the arch section of the dam only and a coarse mesh for the foundation rock region. The geometry of the arch is defined by thirteen design elevations, and the finite element mesh has six mesh elevations consisting of 12 thick shell elements and 18 3-D shell elements. This is a finer mesh than used in the earlier seismic evaluation (Lindvall and Richter, 1975). The foundation rock is modeled by one layer of 80 3-D solid elements to a depth of 240 feet.

To examine the effect of the number of contraction joints on the earthquake response of Big Tujunga dam, two models are analyzed:

- (i) one contraction joint, located at the crown section; and
- (ii) three contraction joints, located at the crown section and approximately the one-quarter points.

For each model the contraction joints are modeled by three joint elements through the thickness of the dam, and the transition region consists of three 3-D solid elements on each side of the contraction joint element. The mesh of the dam with three contraction joints has 48 nonlinear joint elements and 324 3-D solid elements. The finite element mesh for the model with three contraction joints is shown in Fig. 6.2.

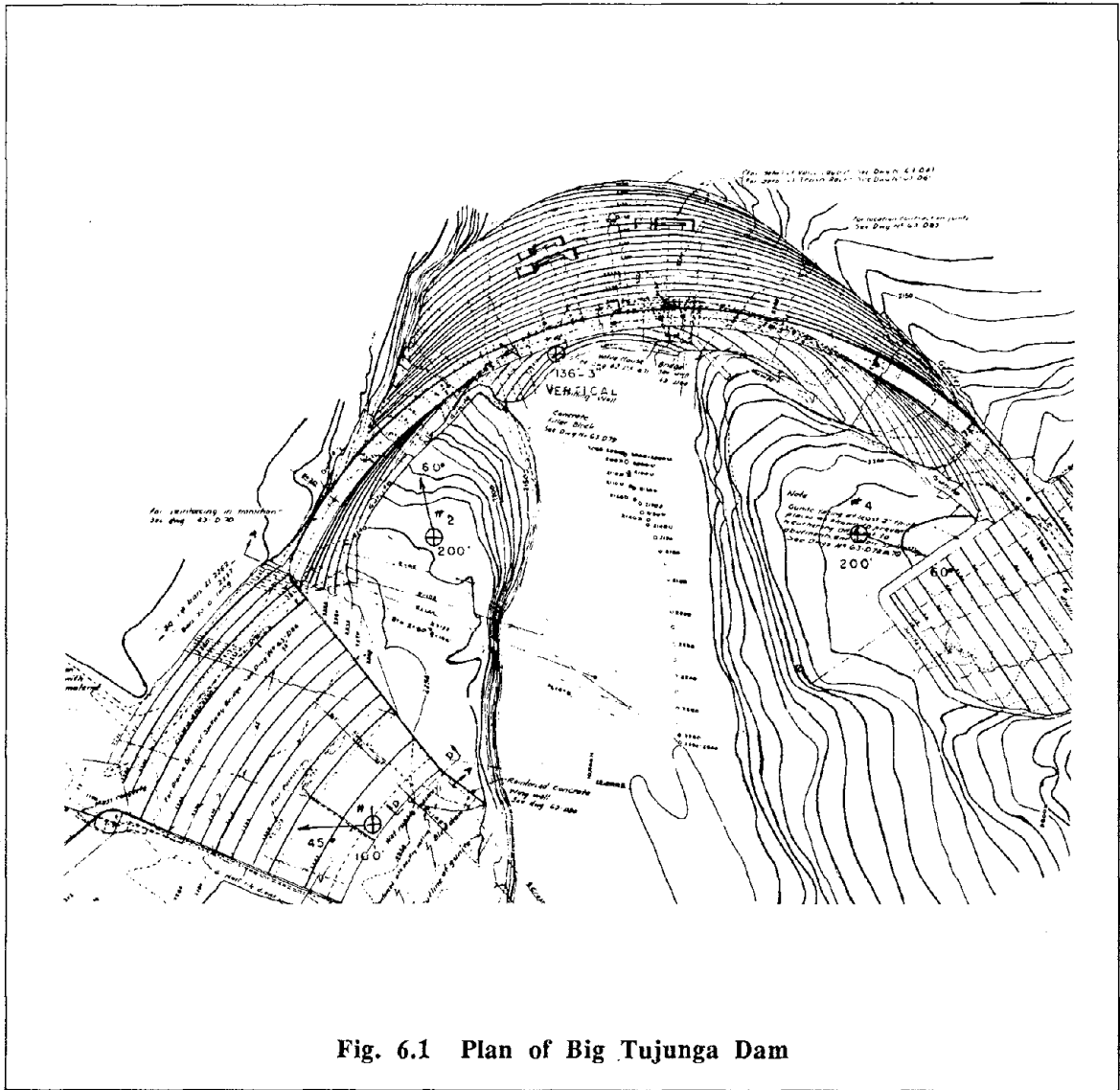
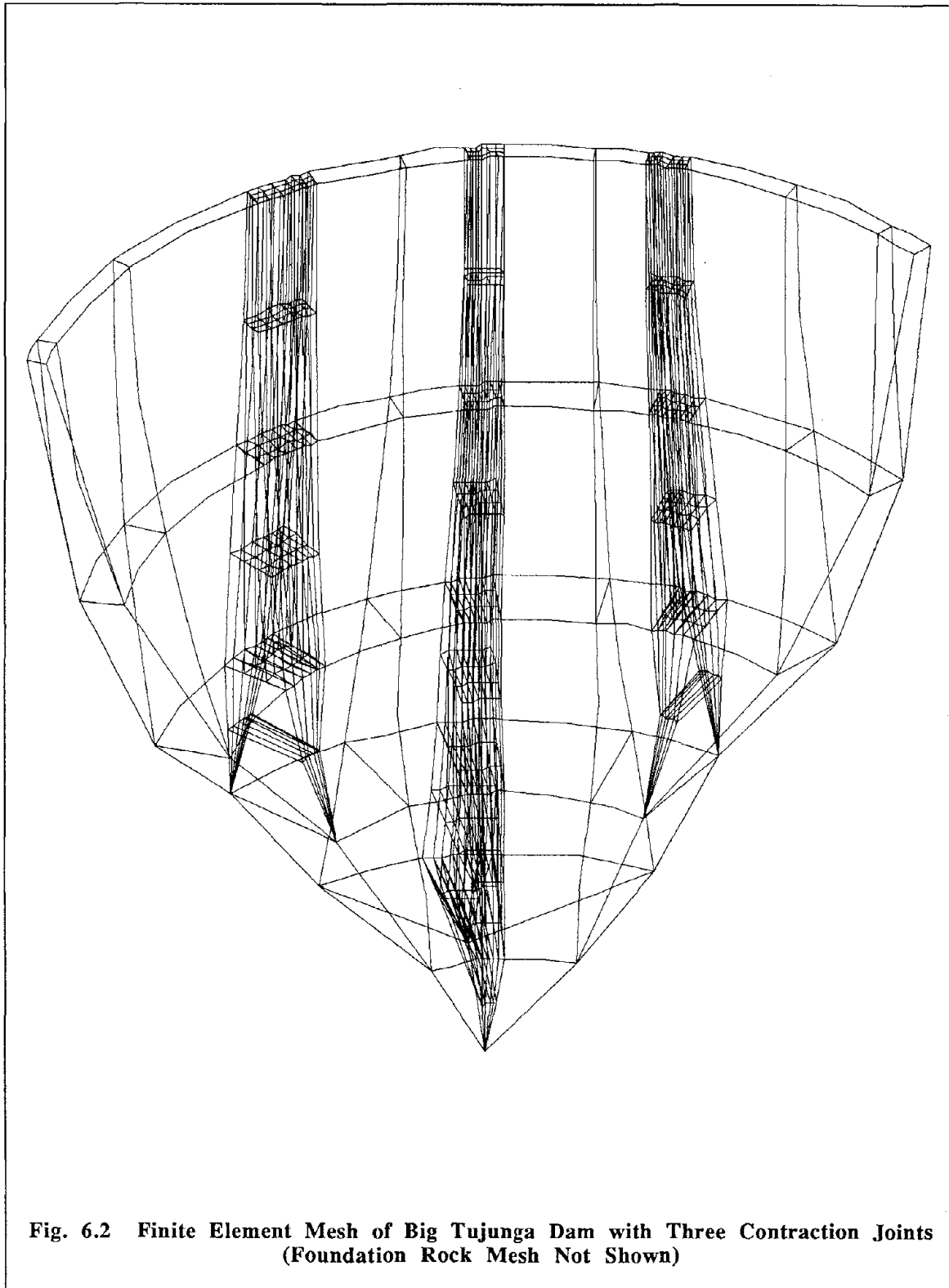


Fig. 6.1 Plan of Big Tujunga Dam



The response of the dam with two levels of water in the reservoir is considered: full reservoir with the water at elevation 230 feet above the foundation rock; one-third reservoir with the water at elevation 82 feet above the foundation rock. The cases considered in the earthquake analysis of Big Tujunga Dam are listed in Table 6.1.

TABLE 6.1 Cases for Earthquake Analysis of Big Tujunga Dam

Case	No. of Contraction Joints	Joint Opening Allowed	Water Level $H/H_s$
1	3	no	0.34
2	3	yes	0.34
3	3	no	0.96
4	3	yes	0.96
5	1	yes	0.96

The material properties for the concrete are: unit weight,  $0.154 \text{ k/ft}^3$ , modulus of elasticity,  $5.76 \times 10^5 \text{ k/ft}^2$ , Poisson's ratio, 0.20; for the foundation rock: unit weight,  $0.161 \text{ k/ft}^3$ , modulus of elasticity,  $3.74 \times 10^5 \text{ k/ft}^2$ , Poisson's ratio, 0.32; for the water, unit weight,  $0.0624 \text{ k/ft}^3$ . Joint opening is allowed with a normal strength of  $q_0=0$ ; joint opening is constrained with  $q_0=1 \times 10^9 \text{ k/ft}^2$ . The stiffness for the joint in the normal and tangential directions is  $k=1 \times 10^9 \text{ k/ft}^3$ . Rayleigh damping in the dam is represented by viscous damping ratios of 5% in the first and fifth modes of vibration. The vibration frequencies of the dam with joints closed and the diagonal added mass are given in Table 6.2, as determined from the program EADAP (Ghanaat and Clough, 1989).

The ground motion used in the earthquake analysis of Big Tujunga dam is the Lake Hughes No. 12 record obtained during the 1971 San Fernando earthquake. The three components of the ground motion are scaled such that the peak ground acceleration of the N21E component, acting in the cross-canyon direction, is 0.60 g. This scaled ground motion record is representative of a maximum credible earthquake at the site, as determined from a seismic-tectonic investigation (Lindvall and Richter, 1975). Figure 6.3 shows the three components of the ground motion used for the present earthquake analysis, and Fig. 6.4 gives the corresponding linear, elastic pseudo-acceleration spectra for 5% viscous damping.

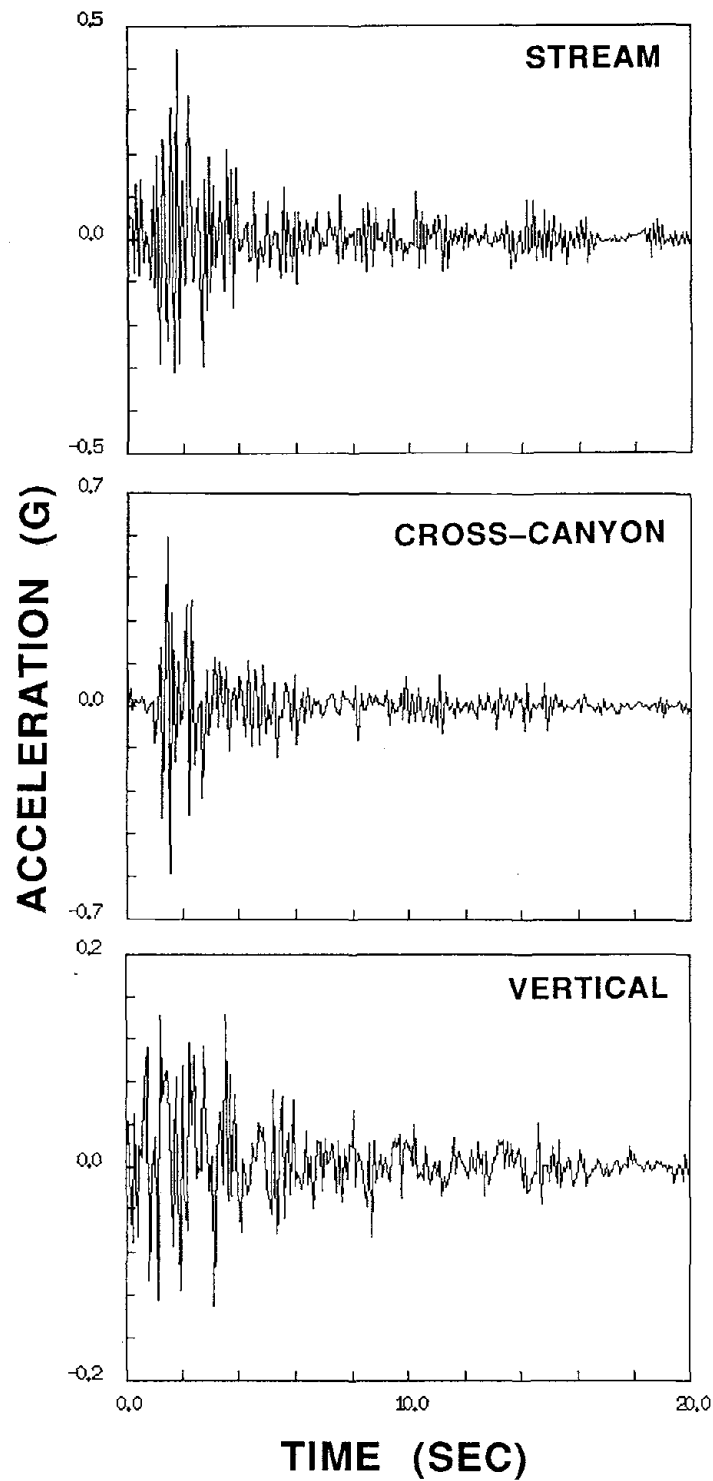


TABLE 6.2 Vibration Frequencies of Big Tujunga Dam with Flexible Foundation Rock

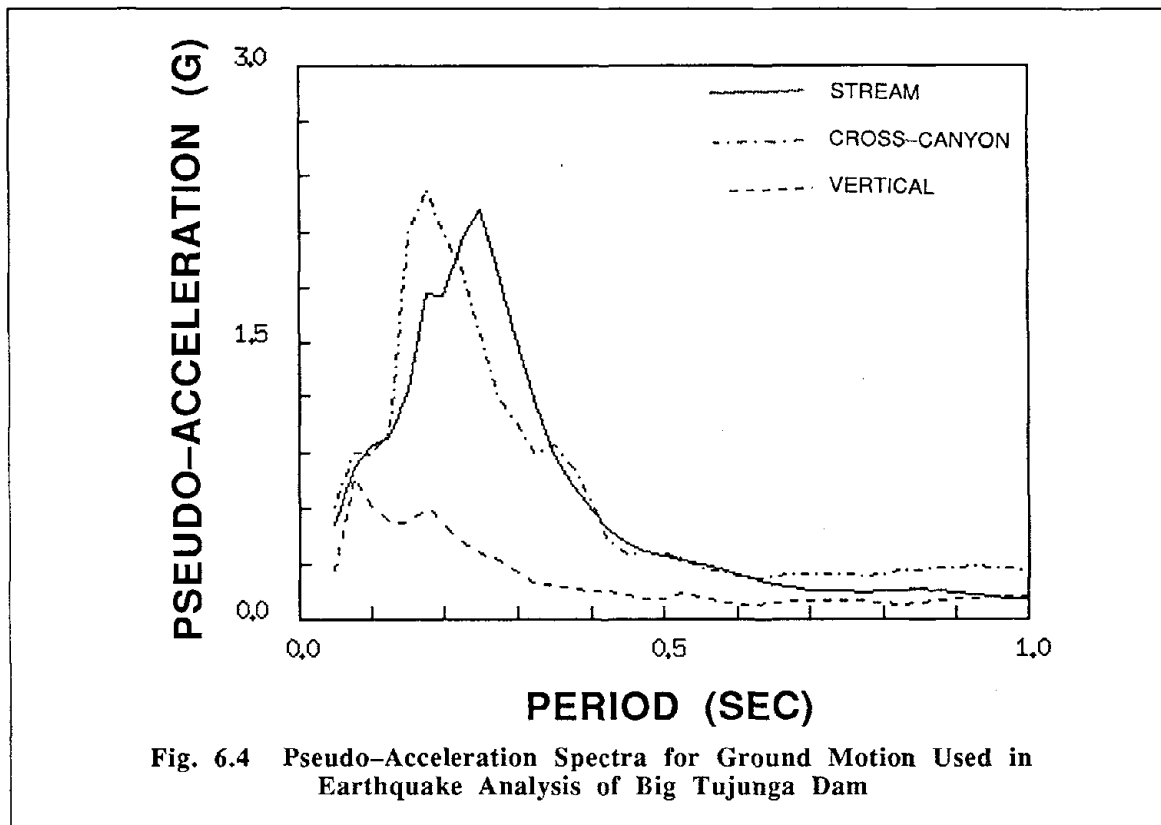
Mode	Vibration Frequency (rad/sec)	
	1/3 Reservoir	Full Reservoir
1	36.6	26.4
2	40.3	27.3
3	51.2	38.7
4	54.9	39.7
5	55.6	48.3
6	58.6	50.8
7	66.7	53.1
8	67.9	54.1
9	68.8	56.1
10	69.0	61.9

### 6.3 Static Response

The static state of stress affects the earthquake response when contraction joint opening is allowed. Figures 6.5 to 6.8 show the envelopes of maximum stress in the arch direction and cantilever direction at the upstream and downstream faces for the cases listed in Table 6.1. Although the dam is not symmetric, the envelopes are only shown for the right-half of the dam looking in the downstream direction. The joint opening does not have a large effect on the arch stresses, although the joints relieve tensile stress near the crest with the low water level, as shown in Fig. 6.5. In the case with a full reservoir the arch stresses are compressive, as shown in Fig. 6.7, and joint opening is minimal. The joints have a negligible effect on the cantilever stresses for either water level (Figs. 6.6 and 6.8). Figure 6.9 shows the opening of the contraction joints under the gravity and hydrostatic loads, in which the three joints are numbered from right to left, looking in the downstream direction. Even with the full reservoir, the joints open near the crest but the normal displacements across the joint are minimal.



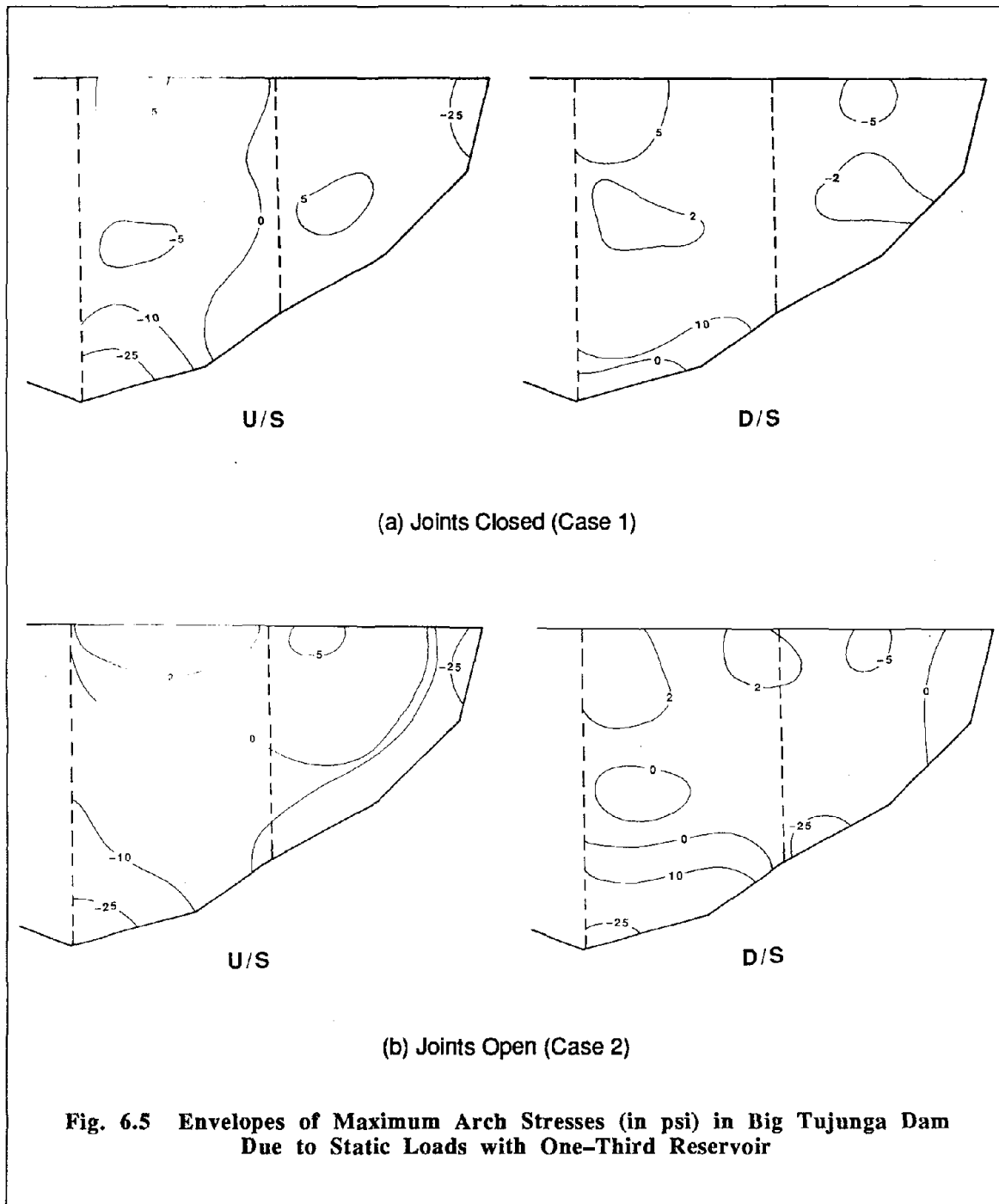
**Fig. 6.3** Ground Motion for Earthquake Analysis of Big Tujunga Dam, as Scaled From Lake Hughes No. 12 Records

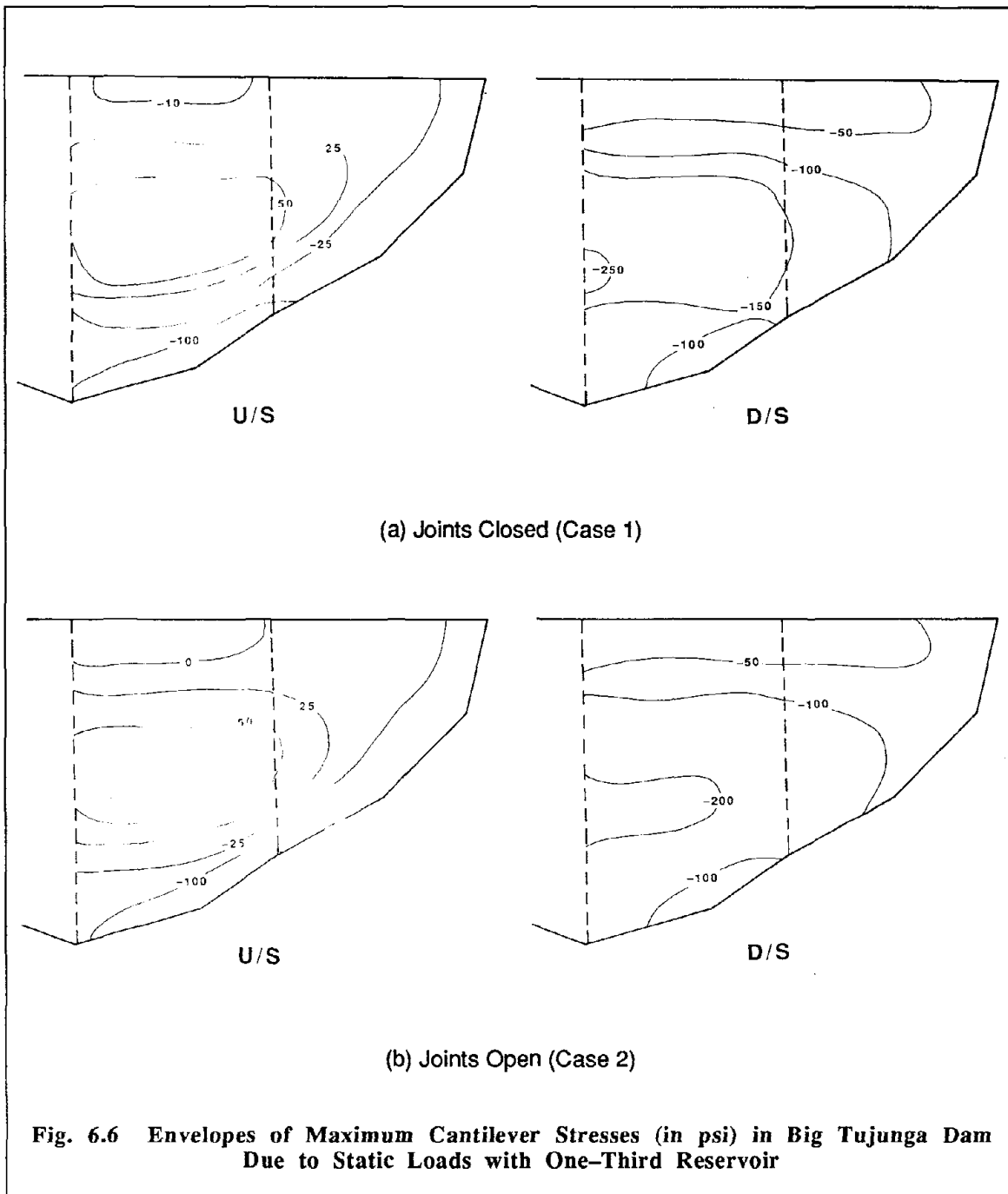


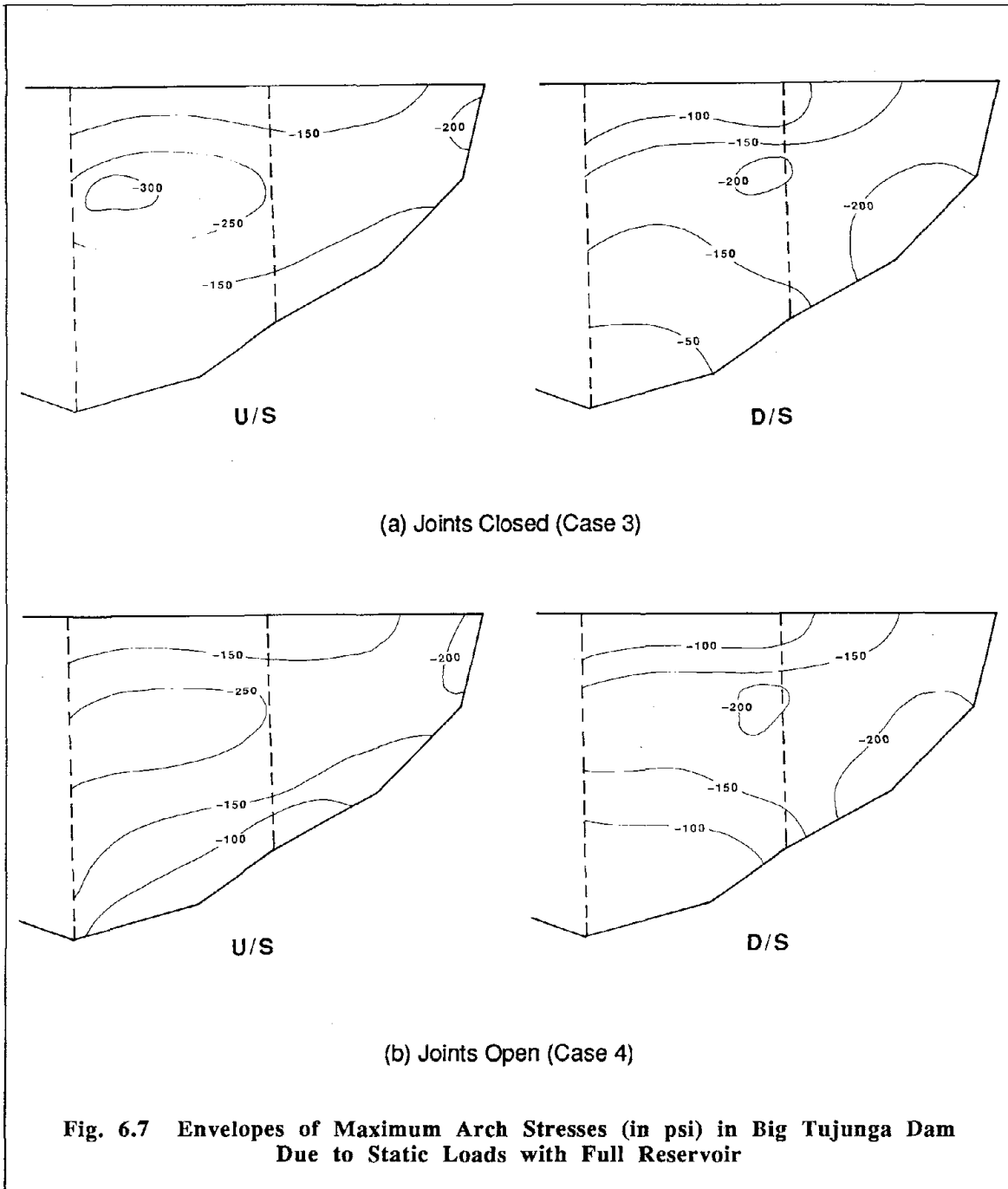
#### 6.4 Earthquake Response

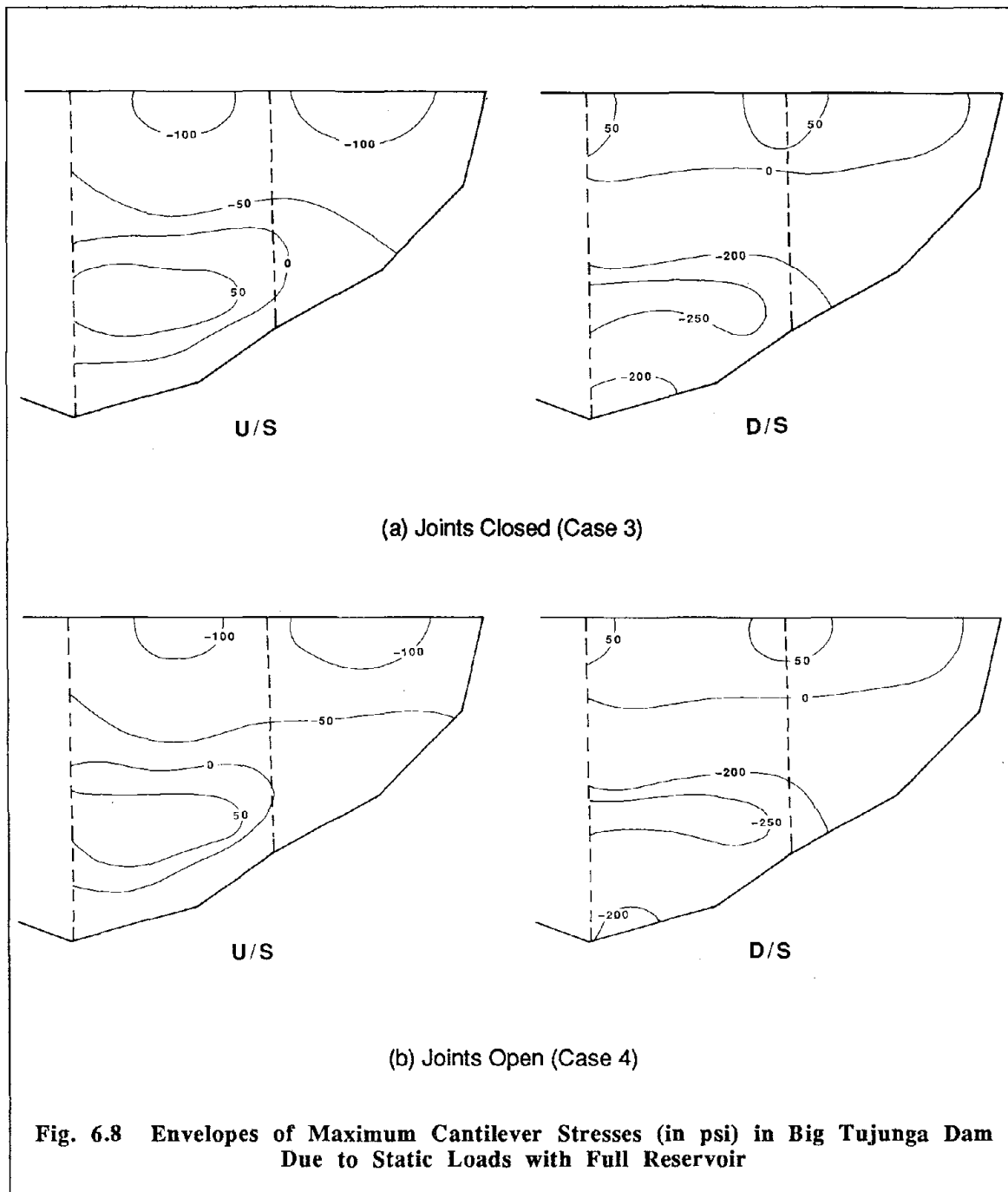
The earthquake response of the dam–water–foundation rock system to the three components of ground motion is computed using the average acceleration method,  $\gamma=0.50$  and  $\beta=0.25$  (see Chapter 3), with a time step of  $\Delta t=0.010$  sec for a duration of 7.0 seconds.

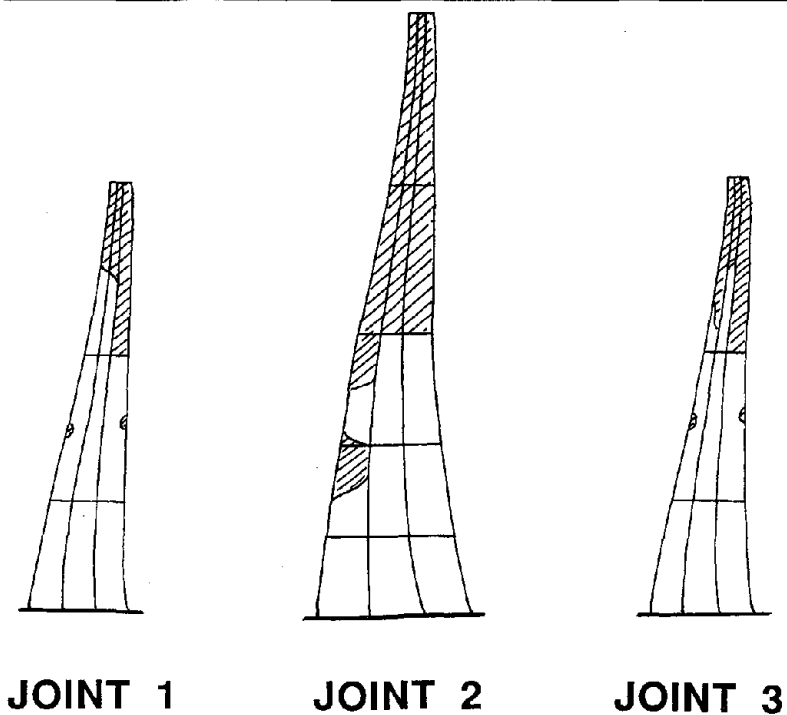
In the case of the dam with the low water level and joints closed (Case 1), the maximum tensile arch stress is 900 psi at the upstream face and the joints transmit significant tensile stresses as shown in Fig. 6.10(a). When opening of the contraction joint is allowed (Case 2), the arch tensile stresses at the upstream face reduce to a maximum of 300 psi and the contours in Fig. 6.10(b) show that the large tensile stresses do not cross the joints included in the model. Although the maximum arch stresses at the downstream face are not as large as at the upstream face, joint opening relieves the tensile stresses near the joint regions. Joint opening slightly reduces the cantilever stresses at the downstream face and there is a very large reduction in cantilever stresses at the upstream face, as shown in Fig. 6.11. When joint opening is included in the model, the maximum arch and cantilever stresses are similar, with the tensile stresses in the cantilever direction of the upstream face slightly larger than the stresses in the arch direction at the upstream face.



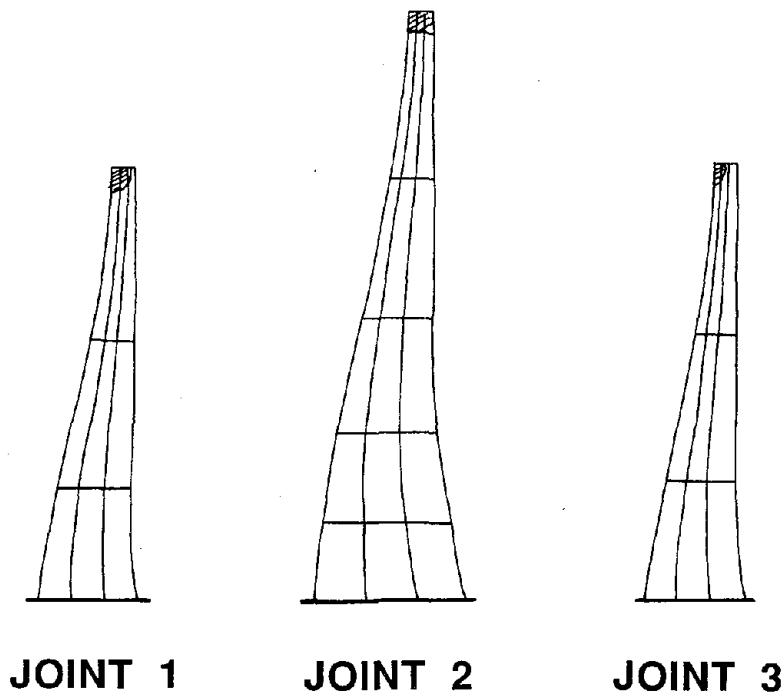








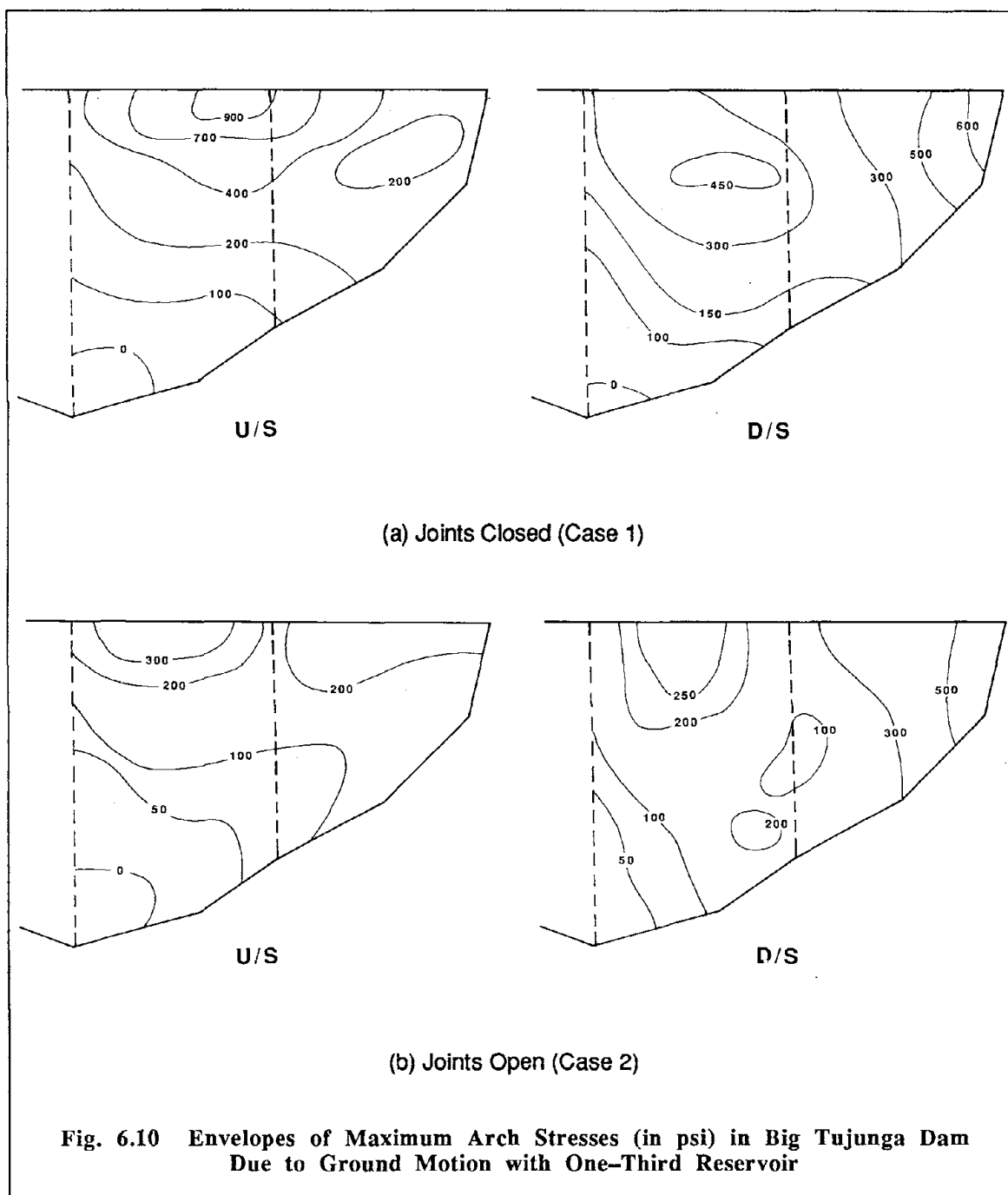
(a) One-Third Reservoir (Case 2)

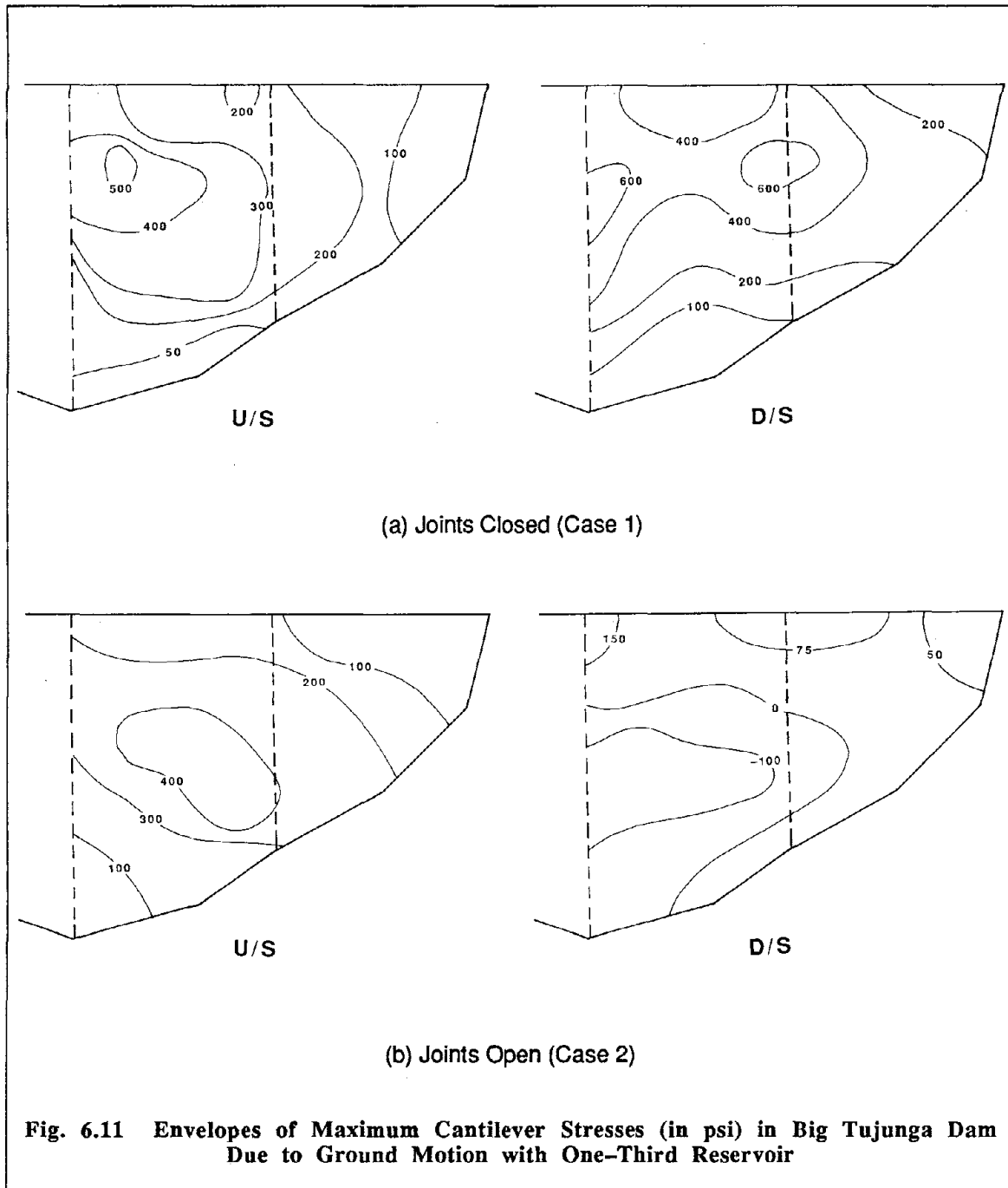


(b) Full Reservoir (Case 4)

Fig. 6.9 Regions of Joint Opening in Big Tujung Dam Due to Static Loads





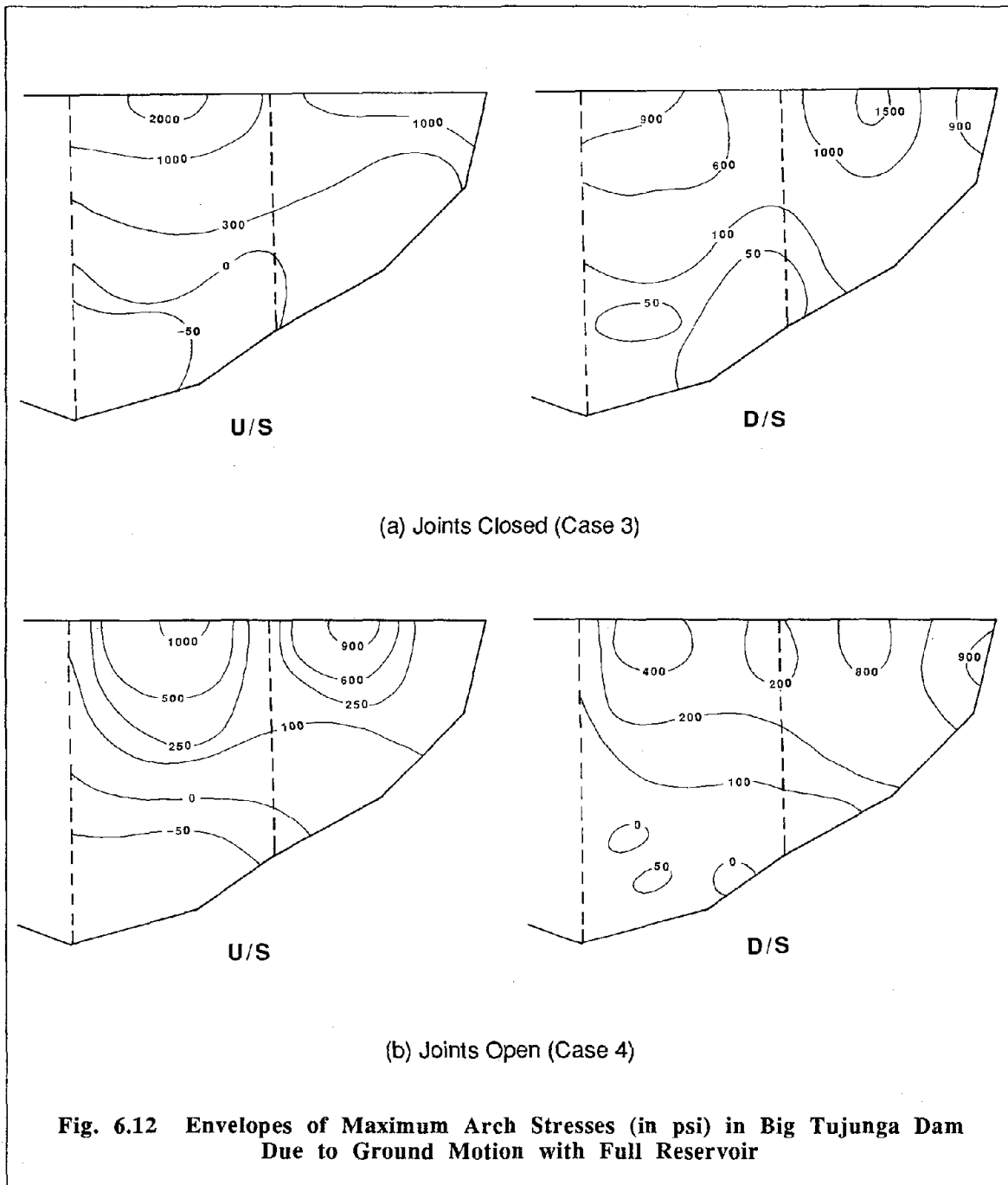


The maximum arch and cantilever stresses in the earthquake response of Big Tujunga dam with full reservoir are shown in Figs. 6.12 and 6.13, respectively. Joint opening reduces the maximum arch stress from over 2000 psi and 1500 psi at the upstream and downstream faces, respectively, to 1000 psi and 800 psi, respectively (Fig. 6.12). Again the contours of maximum arch stress tend to separate at the joint regions. The large reduction in tensile stresses occur near the crest, while the arch stresses in the lower part of the dam are not affected by the joints. As with the case of one-third full reservoir, the cantilever stresses at the upstream and downstream faces are reduced by more than fifty percent when joint opening is allowed, as shown in Fig. 6.13. The overall reduction in maximum tensile stresses occurs because joint opening lengthens the vibration periods and, for this ground motion, reduces the response. The fundamental period of the monolithic dam (closed joints) with full reservoir is 0.24 second, which is near the peak of the pseudo-acceleration spectra in Fig. 6.4 for the horizontal ground motion components. Joint opening lengthens the period, hence reducing the effective earthquake forces acting on the dam.

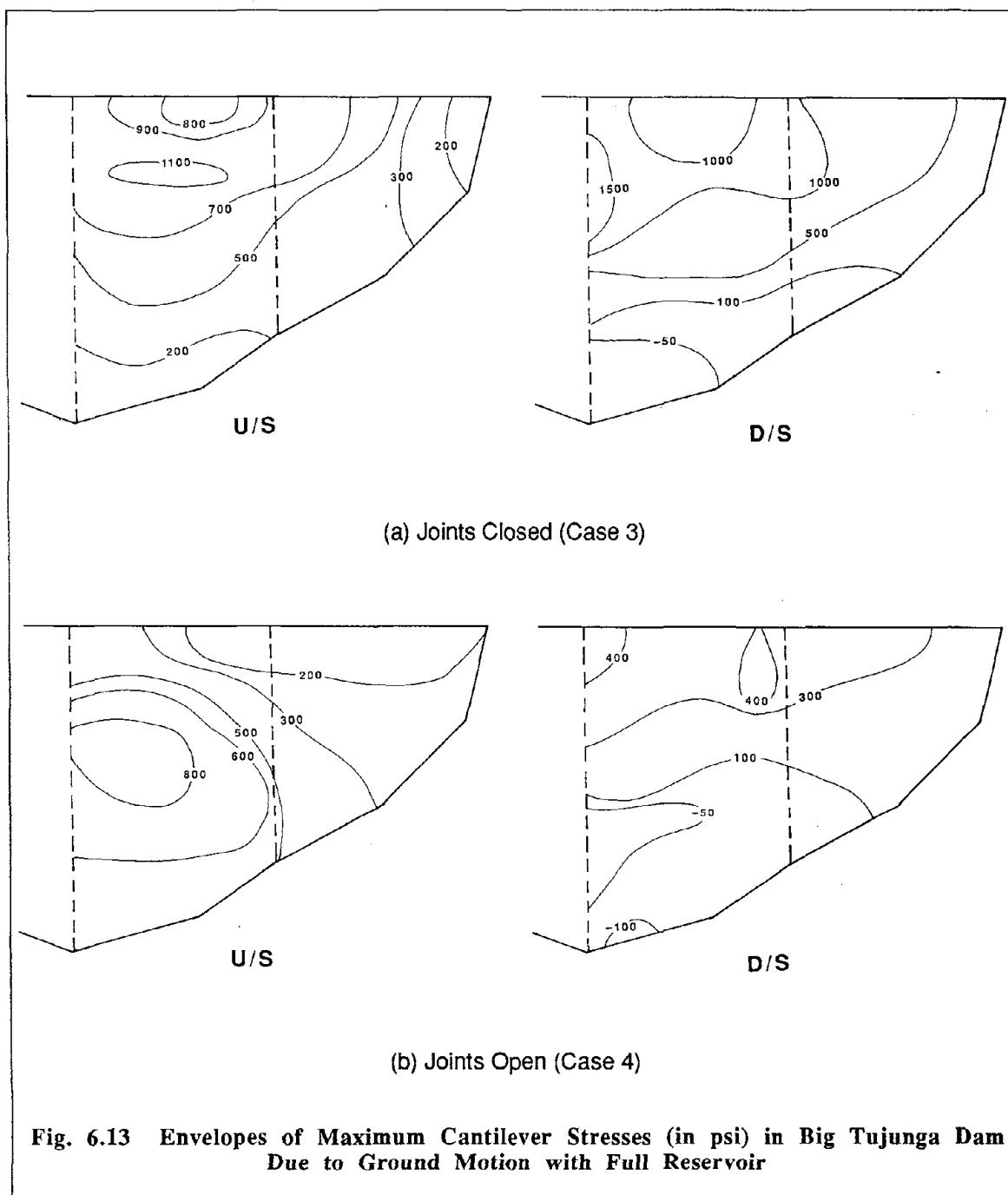
The history of upstream-downstream displacement of the dam mid-crest with full reservoir is shown in Fig. 6.14. With joint opening, the maximum displacement of the dam is slightly greater than in the case with joints closed and there are fewer cycles of large displacements occurring at a slightly longer vibration period. After the strong motion ends at about 3.5 seconds, the free vibration response of the dam with joint opening exhibits less damping and again a slightly longer vibration period. The displacements do not show high frequency oscillations that are sometimes exhibited with impact at joints, demonstrating the stability of the nonlinear joint element and time integration procedure.

The first three seconds of the displacement in the normal direction of the three joints for the dam with full reservoir (Case 4) is shown in Fig. 6.15, in which the opening displacement at the upstream end of the crest is plotted as a function of time for each joint. The joints periodically open to relieve tensile stresses and the maximum joint opening is 2.0 inches. At the time of maximum joint opening, the portion of the contraction joints that are open is shown in Fig. 6.16. The joints separate completely near the crest and this may conflict with the assumption for the joint element that tangential relative displacement at the joint is zero. The validity of this assumption depends on the presence and type of keys at the contraction joints; the effect of tangential motion at the contraction joint for unkeyed joints warrants further study.

An important question is the number of contraction joint regions in the model that are necessary to represent the regularly spaced contraction joints in arch dams. Figure 6.17 shows the maximum stresses for Big Tujunga with full reservoir but only one contraction joint at the crest included in the model (Case 5). Compared with the maximum stresses in the three joint model (Case 4), the tensile stresses near the crown joint are released but there are still large arch stresses,



in excess of 1500 psi in the middle third of the dam. The additional joints reduce these arch stresses, as shown in Figure 6.12(b). The maximum cantilever stresses for the three joint model, shown in Figure 6.13(b), are significantly less than the the cantilever stresses shown in Fig. 6.17



with one joint. It appears that at least three contraction joints are necessary to represent a realistic stress distribution, although further study is necessary to determine if more joints should be used in an earthquake analysis.

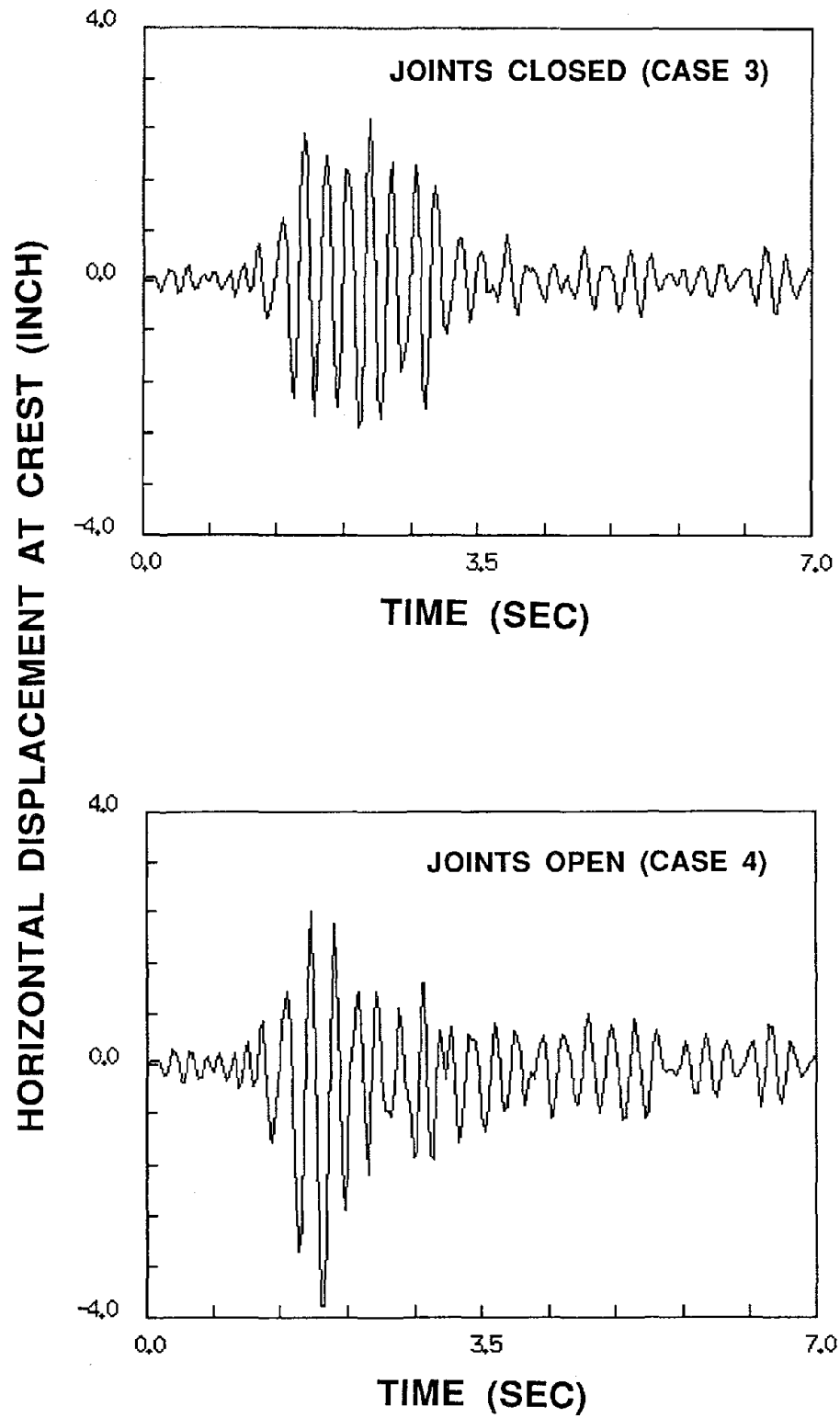
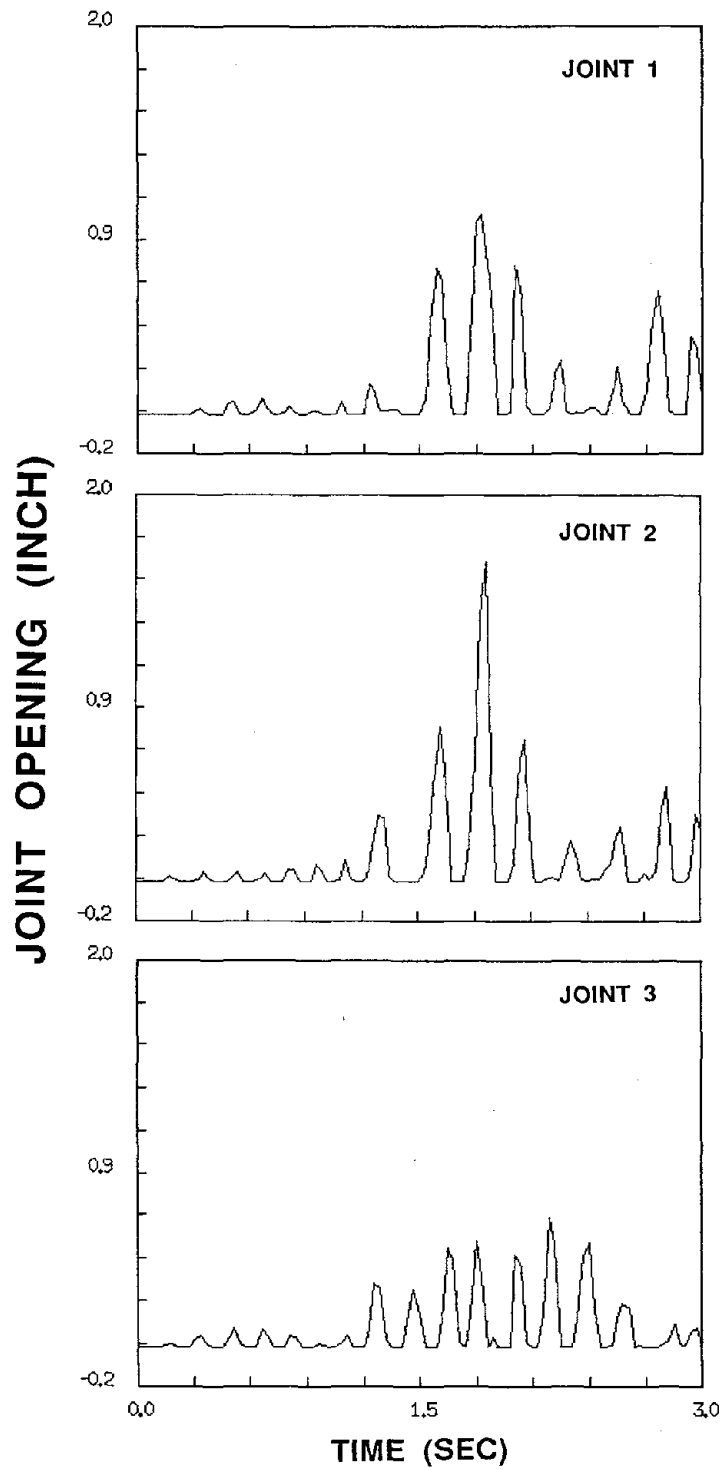
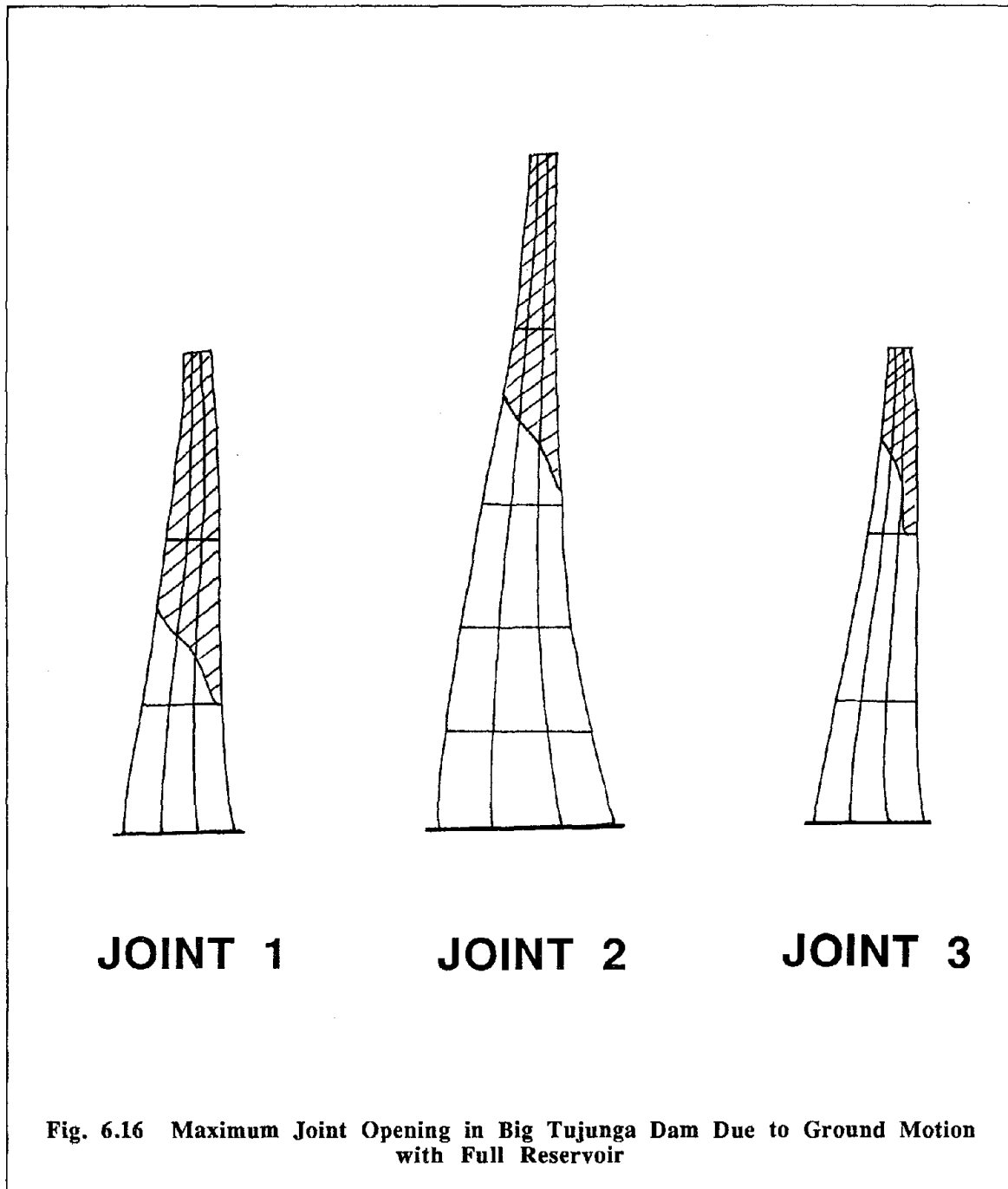


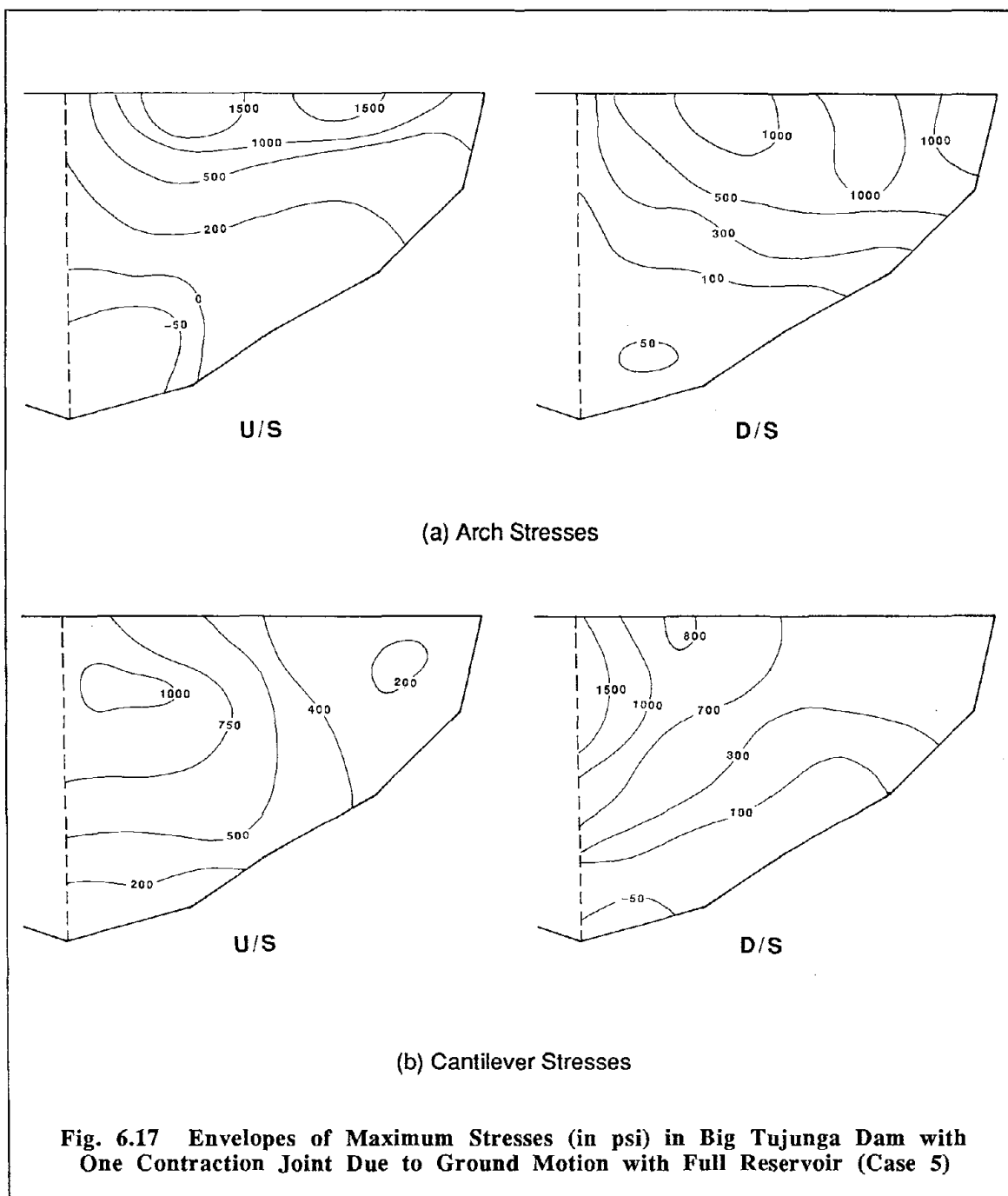
Fig. 6.14 Displacement at the Crest in the Stream Direction of Big Tujunga Dam Due to Ground Motion with Full Reservoir



**Fig. 6.15** Opening Displacement of Contraction Joints in Big Tujung Dam Due to Ground Motion with Full Reservoir









# Chapter 7

## CONCLUSIONS

A substructure procedure for nonlinear dynamic analysis has been implemented for computing the earthquake response of concrete arch dams including opening of contraction joints. The contraction joints are modeled by eight node nonlinear elements that allow partial opening and closing in the normal direction. In the current formulation the tangential displacement across the joint is constrained to zero, although sliding at the joint can be included. The time integration procedure for solving the equations of motion takes advantage of the fact that the nonlinear behavior in the model is concentrated at the joints, while the rest of the dam is assumed to respond in a linear elastic manner. The cantilevers are linear substructures, and the nonlinear equations of motion involve only the degrees-of-freedom associated with the joint element. The solution procedure is very efficient and it allows practical earthquake analysis of arch dams. Dam-water interaction is represented in an approximate manner using a diagonal added mass matrix derived from a finite element model of the water assuming an incompressible fluid. Further investigation is necessary, however, to improve the representation of the incompressible water without reducing the efficiency of the substructure solution procedure. Dam-foundation interaction is represented by a massless foundation region. The nonlinear analysis procedure does not include the effects of water compressibility nor wave propagation effects (and hence damping) in the foundation rock region.

A comprehensive study of the joint element and its ability to model joint opening in structures indicates that opening lengthens the vibration periods of a structure. The effect of the period increase on the maximum displacements and stresses depends on the frequency content of the excitation. An attempt was made to model the response of a single arch rib subjected to earthquake excitation on a shaking table. While the analytical response showed the general trends observed in the experiments, there was a significant difference in the amplitude of the responses. An important factor contributing to the difference is the relative tangential motion of the blocks in the rib. During the experiments sliding of the blocks was observed, whereas tangential displacement is prevented in the current formulation of the joint element. Future work is necessary to allow tangential displacement at the joints and another comparison with the experimental response of the arch rib should be performed.

Analysis of Big Tujunga dam, a typical concrete arch dam, subjected to ground motion representing a maximum credible earthquake illustrates the important effect of contraction joint opening on the earthquake response. In the case with full reservoir, the joints are essentially closed by the hydrostatic pressure of the impounded water. If joint opening is not allowed during the earthquake response, unrealistically large tensile stresses are produced, particularly in the arch direction. When joint opening is allowed, the large tensile stresses are relieved and the maximum arch stresses are reduced by fifty to sixty percent. Simultaneously, the cantilever stresses are reduced because, for this particular dam and ground motion, the period lengthening due to joint opening places the dam in the part of the spectrum with smaller pseudo-acceleration and hence smaller effective earthquake forces. The history of crest displacement shows slightly larger crest displacement when contraction joint opening is allowed. The increased displacement is mostly caused by the rotation of the cantilevers near the joints, which open as much as two inches at the upstream face and completely separate near the crest. This is a significant amount of opening and the joints would require sufficient displacement capacity to withstand this opening without damage. The large opening also brings into question the issue of keys at the contraction joints and the assumption of no tangential displacement. If the joints are not keyed then complete separation of the joint invalidates the assumption of no sliding and additional study is necessary to determine the effect of sliding. If the joints are keyed, they may still transfer a shear force depending on the size and shape of the keys. Even with a key, however, a two inch normal displacement may lead to some tangential displacement at the joint.

This study has demonstrated the importance of the joint opening mechanism on the earthquake response of concrete arch dams. Additional investigation is necessary to improve the understanding of the behavior of the joints and the effect on a variety of dams. The following issues require further research:

- Allow tangential displacement at the joint depending on the normal force or the normal displacement. Examine the effect of tangential motion at the joint on earthquake response.
- Examine the requirements for shear keys at joints, including the maximum displacement, forces, and number of cycles that the keys must withstand.
- Determine the number of contraction joints that should be included in the model to represent the effect of the closely spaced joints in actual dams.
- Investigate the role of arch geometry on the opening of contraction joints during an earthquake.
- Examine the effect of different ground motion parameters on the response of arch dams with joint opening.

The computer program ADAP-88 is an efficient and effective analysis tool for performing additional studies of arch dam response and it can be used in design evaluations of dams.

# Chapter 8

## REFERENCES

- Clough, R.W. (1980). "Nonlinear Mechanisms in the Seismic Response of Arch Dams," International Research Conference on Earthquake Engineering, Skopje, Yugoslavia.
- Clough, R.W. and Penzien, J. (1975). *Dynamics of Structures*, McGraw-Hill, New York, NY.
- Clough, R.W., Raphael, J.M. and Mojtahedi, S. (1973). "ADAP: A Computer Program for Static and Dynamic Analysis of Arch Dams," *Report No. UCB/EERC 73-14*, Earthquake Engineering Research Center, University of California at Berkeley, Berkeley, CA.
- Clough, R.W. and Wilson, E.L. (1979). "Dynamic Analysis of Large Structural Systems with Local Nonlinearities," *Computer Methods in Applied Mechanics and Engineering*, Vol. 17/18, No. 1, pp. 107-129.
- Dowling, M.J. and Hall, J.F. (1989). "Nonlinear Seismic Analysis of Arch Dams," *Journal of Engineering Mechanics*, ASCE, Vol. 115, No. 4, pp. 768-789.
- Fok, K.-L. and Chopra, A.K. (1985). "Earthquake Analysis and Response of Concrete Arch Dams," *Report No. UCB/EERC-85/07*, Earthquake Engineering Research Center, University of California at Berkeley, Berkeley, CA.
- Fok, K.-L. and Chopra, A.K. (1987). "Water Compressibility in Earthquake Response of Arch Dams," *Journal of Structural Engineering*, ASCE, Vol. 113, No. 5, pp. 958-975.
- Ghaboussi, J., Wilson, E.L. and Isenberg, J. (1973). "Finite Element for Rock Joints and Interfaces," *Journal of the Soil Mechanics and Foundations Division*, ASCE, Vol. 99, No. SM10, pp. 833-848.
- Ghaboussi, J., Wilson, E.L. and Taylor, R.L. (1971). "Isoparametric Finite Elements with Incompatible Deformation Modes," O.N.R. Symposium, University of Illinois, Urbana, IL.
- Ghanaat, Y. and Clough, R.W. (1989). "EADAP: Enhanced Arch Dam Analysis Program," *Report No. UCB/EERC-89/07*, Earthquake Engineering Research Center, University of California at Berkeley, Berkeley, CA.
- Goodman, R.E., Taylor, R.L. and Brekke, T.L. (1968). "A Model for the Mechanisms of Jointed Rock," *Journal of the Soil Mechanics Division*, ASCE, Vol. 94, No. SM3, pp. 637-659.
- Hall, J.F. and Chopra, A.K. (1980). "Dynamic Response of Embankment, Concrete Gravity and Arch Dams Including Hydrodynamic Interaction," *Report No. UCB/EERC-80/39*,

- Earthquake Engineering Research Center, University of California at Berkeley, Berkeley, CA.
- Hohberg, J.-M. and Bachman, H. (1988). "A Macro Joint Element for Nonlinear Arch Dam Analysis," *Numerical Methods in Geomechanics Innsbruck 1988*, Swoboda, G., ed., Sixth International Conference on Numerical Methods in Geomechanics, Innsbruck, pp. 829–834.
- Hughes, T.J.R. (1987). *The Finite Element Method: Linear Static and Dynamic Finite Element Analysis*, Prentice Hall, Englewood Cliffs, NJ.
- Hughes, T.J.R., Pister, K.S. and Taylor, R.L. (1979). "Implicit–Explicit Finite Elements in Nonlinear Transient Analysis," *Computer Methods in Applied Mechanics and Engineering*, Vol. 17/18, No. 1, pp. 159–182.
- Kuo, J. (1982). "Fluid–Structure Interactions: Added Mass Computations for Incompressible Fluid," *Report No. UCB/EERC–82/09*, Earthquake Engineering Research Center, University of California at Berkeley, Berkeley, CA.
- Kuo, J. (1982). "Joint Opening Nonlinear Mechanism: Interface Smeared Crack Model," *Report No. UCB/EERC–82/10*, Earthquake Engineering Research Center, University of California at Berkeley, Berkeley, CA.
- Lindvall and Richter, Associates. (1975). "Investigation and Re–Analysis of the Big Tujunga Dam," *Final Report, Parts I to III*, Los Angeles, CA.
- Mojtahedi, S., Noorishad, J. and Tsang, C.F. (1988). "Substructure Extension of a Hydroelastic Finite Element Method for Analysis of Fractured Rock Masses," unpublished report, Lawrence Berkeley Laboratory, Berkeley, CA.
- Niwa, A. and Clough, R.W. (1980). "Shaking Table Research on Concrete Dam Models," *Report No. UCB/EERC–80/05*, Earthquake Engineering Research Center, University of California at Berkeley, Berkeley, CA.
- Park, K.C. and Felippa, C.A. (1984). "Recent Developments in Coupled Field Analysis Methods," *Numerical Methods in Coupled Systems*, Lewis, R.W., et al, eds., John Wiley & Sons, Chichester, pp. 327–351.
- Pawsey, S.F. (1970). "The Analysis of Moderately Thick to Thin Shells by the Finite Element Method," *Report No. UC/SESM–70/12*, Structural Engineering Laboratory, University of California at Berkeley, Berkeley, CA.
- Row, D. and Schrieker, V. (1983). "Analysis of Earthquake Induced Response for Structures with Localized Nonlinearities," *Report to NSF*, SSD, Inc., Berkeley, CA,
- Row, D. and Schrieker, V. (1984). "Seismic Analysis of Structures with Localized Nonlinearities," Eighth World Conference on Earthquake Engineering, San Francisco, CA, Vol. IV, pp. 475–482.
- Zienkiewicz, O.C. (1977). *The Finite Element Method*, McGraw–Hill, New York, NY.

# Appendix A

## USER GUIDE FOR ADAP-88

### A.1 Introduction

The ADAP-88 computer program implements the nonlinear analysis procedure for concrete arch dams described in the report. A description of the program capabilities and the requirements for input data are presented in this appendix.

### A.2 Mesh Generation

ADAP-88 includes a finite element mesh generator for three-centered arch dams of arbitrary geometry with contraction joints. The coordinates of the nodal point generated by the program can be modified with coordinates specified by the user to account for irregular geometric features. The foundation mesh generated by the program assumes a prismatic cross section for the valley.

This section presents a description of the terms and assumptions to assist the user with preparing input data for generating a finite element mesh of an arch dam. The mesh generation is similar to an earlier version of the program (Clough, et al., 1973). The program provides options for creating plots of the finite element mesh.

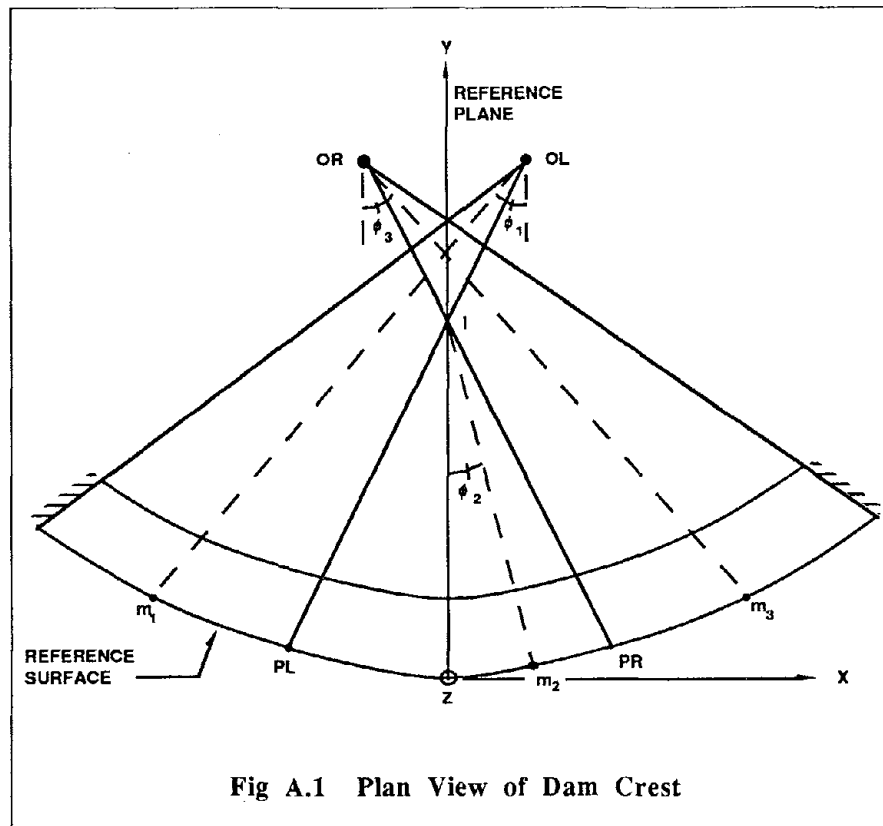
#### A.2.1 Definition of Mesh Generation Concepts

Figure A.1 shows the plan view of a dam crest. The *reference surface* is the vertical cylindrical surface that passes through the upstream edge of the crest. Points I, OR and OL are, respectively, the centers of inner, right-outer and left-outer portions of the reference surface. Points PR and PL are the points of compound curvature, points where the curvature changes. The *reference plane* is a vertical plane that passes through point I and the base of the dam. An angle to reference plane refers to the central angle between a point on the reference surface and the reference plane. Depending on the location of the point on the reference surface, center of inner, right-outer, or left-outer arc, is used in definition of the angle to reference plane. For points m1, m2, and m3 on the reference surface in Fig. A.1, the angles to the reference plane are  $\phi_1$ ,  $\phi_2$ , and  $\phi_3$ , respectively.

A right-hand, X-Y-Z global coordinate system is defined such that the Y-Z plane coincides with the reference plane with the Z-axes lying on the reference surface in the upward direction. The origin of the coordinate system is at the base of the dam.

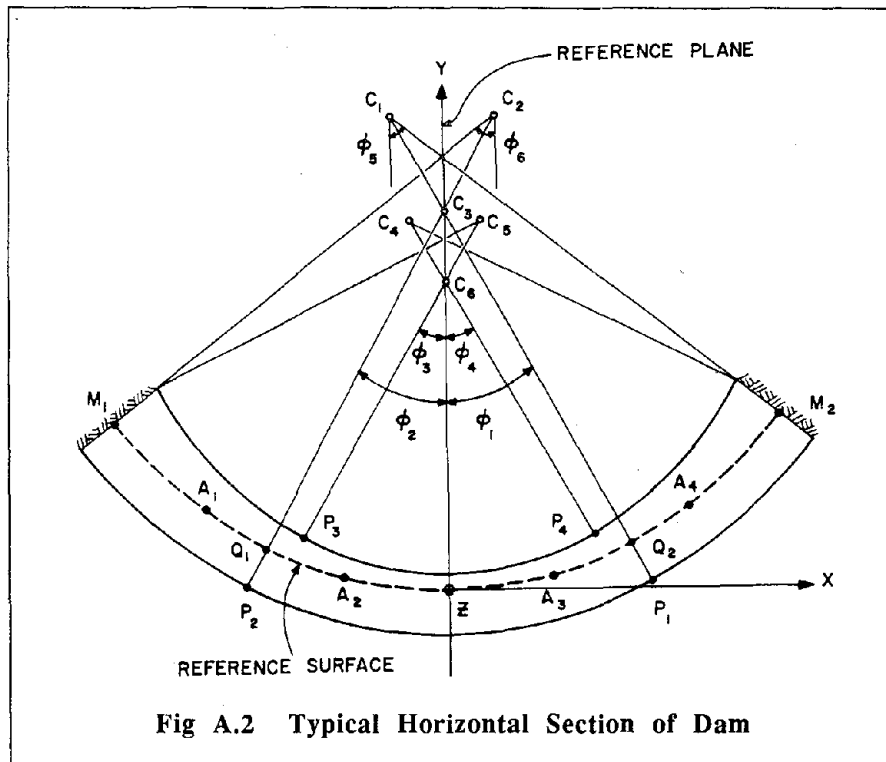
The geometry of the dam is specified at *design elevations*. Geometric properties of the dam at other elevations are computed from the data at the design elevations using cubic interpolation. A

typical horizontal cross section of a dam is shown in Fig. A.2. The centers of the inner upstream and downstream arcs may have arbitrary X and Y coordinates, although the centers illustrated in Fig. A.2 are on the Y-axis for clarity. The upstream and downstream arcs may be three-centered. Again with reference to Fig. A.2, the points of compound curvatures for the arcs, P1, P2, P3 and P4, are specified by *compounding angles*  $\phi_1$ ,  $\phi_2$ ,  $\phi_3$ , and  $\phi_4$  measured from lines parallel to the Y-axis. The abutment lines are assumed to be radial with respect to the upstream face and are specified by *angles to abutment*  $\phi_5$  and  $\phi_6$ .



The elevations of horizontal sections of the finite element mesh are *mesh elevations*. These are based on two different sets of elevations: (i) user-specified elevations, called *initial mesh elevations*, and (ii) elevations corresponding to the intersection of the joints and the abutment, called *joint-abutment elevations*. All joint-abutment elevations are used as mesh elevations, whereas certain initial mesh elevations may be disregarded as described in the next section.





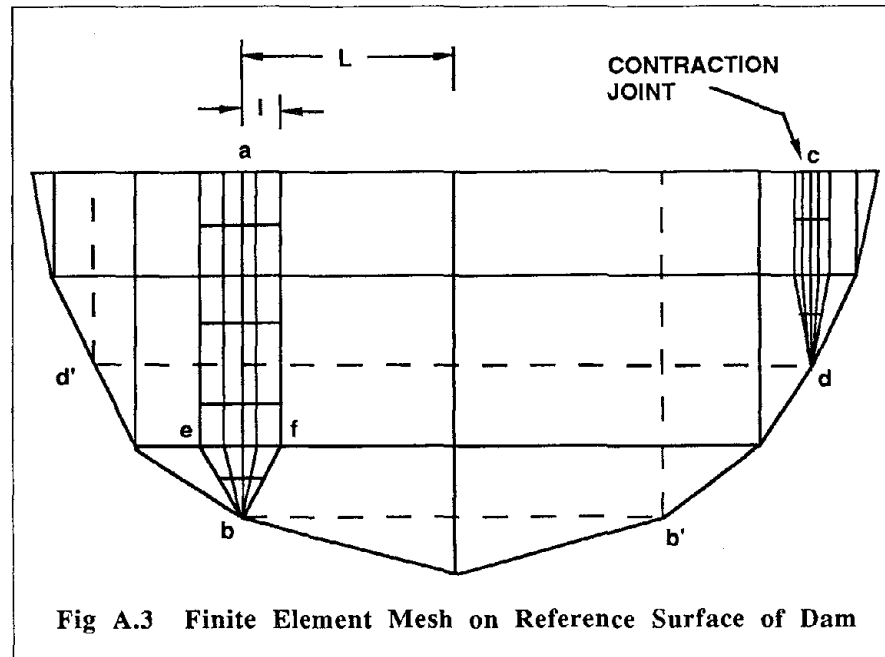
Each contraction joint is located normal to the upstream surface and is specified by an angle to the reference plane at the crest elevation. As described in Chapter 2, a contraction joint is modeled by joint elements and a portion of the dam on each side of a joint is discretized with 3-D solid elements to represent the stress distribution near the joint. A 3-D solid block is defined as the 3-D solid elements at one side of a joint. Thus, two 3-D solid blocks are associated with each contraction joint. The program assumes that each contraction joint is intersected by at least three mesh elevations. The user must provide this minimum number of initial elevations.

#### A.2.2 Generation of Dam Mesh

A preliminary dam mesh is generated as a grid of horizontal and vertical lines on the reference surface, as shown in Fig. A.3. The end points of the horizontal lines at the mesh elevations correspond to the intersection of the reference surface and abutment as shown by points M1 and M2 in Fig. A.2.

Lines ab and cd in Fig. A.3 are two joints in the dam which are located by angles to reference plane. Points b and d are the intersection of the joints and the abutment. The elevations of these points are computed by cubic interpolation from the design elevations for which the angles to the reference plane at abutment are available, as indicated in Fig. A.2.

Points  $b'$  and  $d'$  are two abutment nodes at the same elevations as points  $b$  and  $d$ , respectively. The angle between these points and the reference plane are computed using the same procedure for locating the abutment nodes ( $M1$  and  $M2$  in Fig. A.2).



The 3-D solid blocks are also represented in the reference surface as shown in Fig. A.3. The width of each block in the arch direction is controlled by the *width ratio*, a user-specified parameter. This ratio is defined as  $l/L$  where  $l$  is the width of the block and  $L$  is the distance from the joint to the next vertical line of the mesh as shown in Fig. A.3. Both  $l$  and  $L$  are measured on the reference surface.

After a two-dimensional mesh is generated on the reference surface, it is projected on the upstream and downstream faces to obtain a three-dimensional mesh of the dam. The centers of the upstream face are used in this projection to avoid difficulties associated with the irregular elements near the abutment.

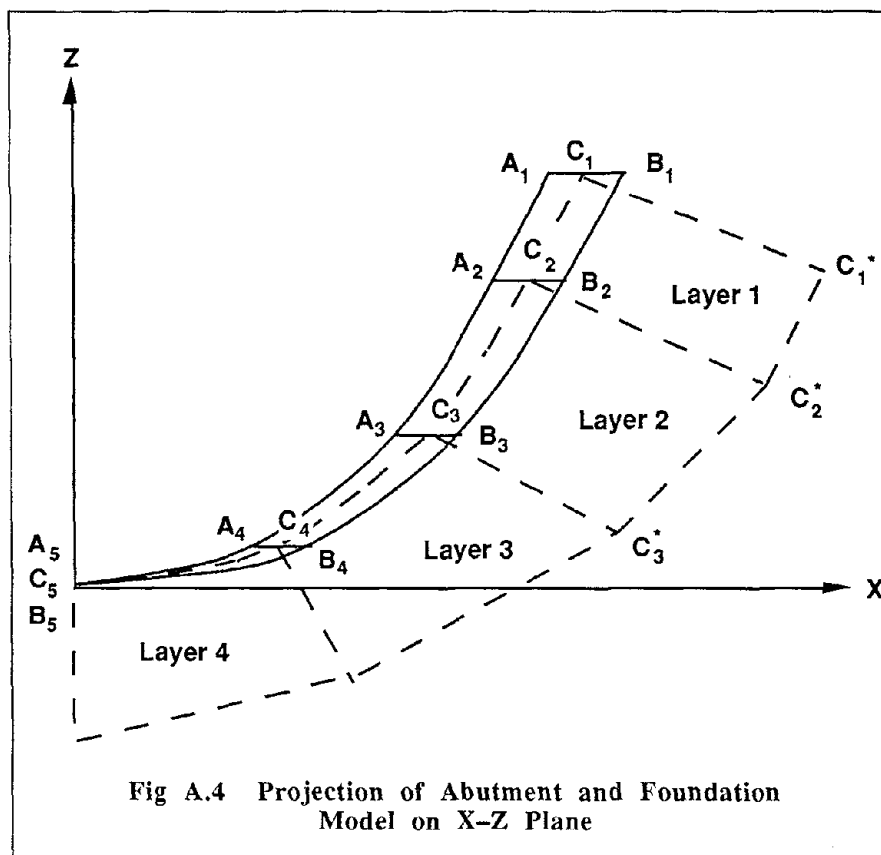
The nodal points of the shell elements are completely generated by the projection of the reference surface mesh on upstream and downstream faces. However, the 3-D elements in the projected mesh are further divided to obtain the appropriate number of 3-D elements in the thickness direction of the dam.

The mesh generation procedure may result in an excessive number of horizontal sections and inappropriate aspect ratios for the shell elements. To avoid this problem two measures are taken:

- A user-specified mesh elevation which is too close to any joint-abutment elevation is disregarded. The smallest distance is taken as one fifth of the smallest element size associated with the initial mesh elevations.
- If the joint-abutment elevations corresponding to a pair of joints at opposite sides of the crown are too close, the elevations are combined to give a nearly horizontal line on the reference surface. To avoid large slopes, this degeneration is allowed only for joint-abutment elevations that are within two consecutive user-specified mesh elevations.

### A.2.3 Generation of Foundation Mesh

The foundation mesh corresponds to a canyon with a prismatic cross section. Figure A.4 shows the projection of the right abutment on the X-Z plane. The abutment lines at various mesh elevations are shown by A<sub>1</sub>-B<sub>1</sub>, A<sub>2</sub>-B<sub>2</sub>, ..., and points C<sub>1</sub>, C<sub>2</sub>, ..., are the mid-points of these lines. The foundation model consists of several layers of 3-D solid elements. The interfaces of the layers are parallel to the Y-axis and they intersect the X-Z plane at right angles to the line passing through C<sub>1</sub>, C<sub>2</sub>, and so on. The interfaces of the layers are shown as C<sub>1</sub>-C<sub>1</sub><sup>\*</sup>, C<sub>2</sub>-C<sub>2</sub><sup>\*</sup>, ..., in Fig. A.4.



There are three foundation mesh types that differ in the volume of the foundation rock included in the model and the number of 3-D solid elements. Discretization of each layer at a typical dam–foundation interface is shown in Fig. A.5. Point C is the mid–point of the abutment line and points A and B are the projections of the upstream and downstream nodes of the abutment on the interface. The nodal points of the rigid support of the model are located on a semi–circle of radius  $R$  centered at the mid–point of the abutment lines. Values for  $R$  in terms of dam height,  $H$ , and also the number of 3–D elements in each layer are shown in Table A.1 for the three foundation mesh types.

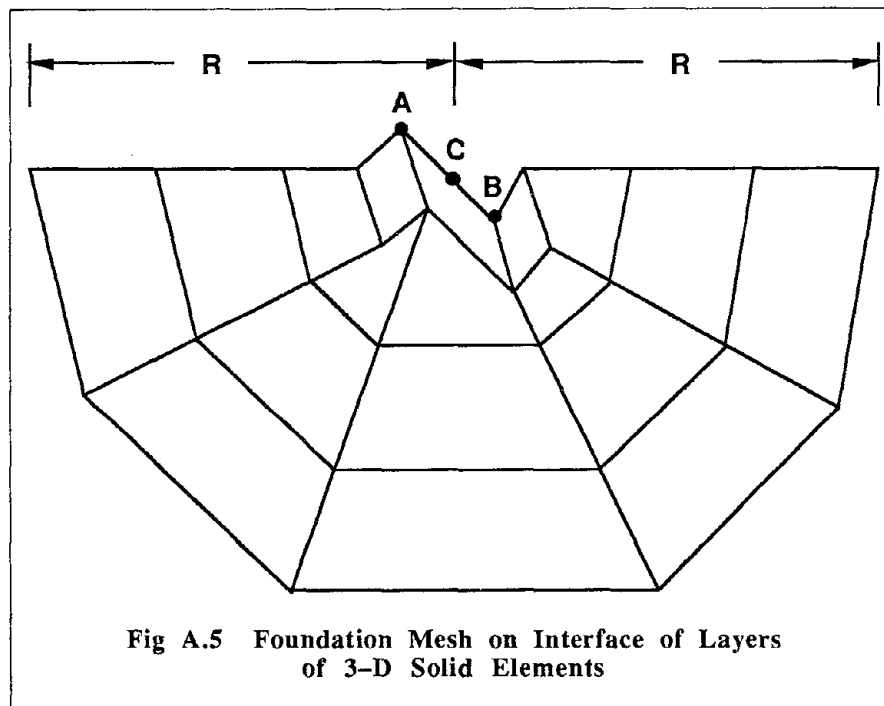


Table A.1 Parameters for Foundation Mesh Generation

Foundation Mesh Type	No. of 3-D Elements in Each Layer	Radius, $R$
1	8	$H$
2	13	$H$
3	18	$1.5H$

The mesh generator includes options for creating plots of the mesh by substructure, element type, or material type. The user specifies the plot options and a point in the global coordinate system from which to view the mesh.

### A.3 Parameters for Joint Elements

The nonlinear joint element is described in Chapter 2. The properties are specified in Records E and I of the input data. The parameters KN and Q0 correspond to the normal stiffness,  $k_n$ , and normal strength,  $q_{0i}$ , in Fig. 2.3, respectively. The tangential stiffness of the element is specified by the KS input parameter. Both KN and KS should have large values to enforce displacement continuity at the contraction joints. Excessively large values, however, may produce an ill-conditioned numerical solution because of large differences in the terms in the structural stiffness matrix. Appropriate values of KN and KS depend on the precision for floating point variables. The following value is recommended:

$$KN, KS = (n * E) / L$$

where  $E$  is the modulus of elasticity of the concrete and  $L$  is the length of the adjacent 3-D solid element in the direction normal to the joint. Depending on the floating point precision,  $n$  may range from 10 to 100 with larger values for higher precision floating point representation.

In the static or earthquake analysis, any tensile strength of the joints can be specified with an appropriate Q0 value. Q0 may be set equal to zero to specify no-tension property of the joints. To represent a dam as a monolithic structure a sufficiently large Q0 value should be specified so that the joints do not open.

### A.4 Static Analysis

Two different load cases can be included in the static analysis. The first load case corresponds to the gravity loads. The second load case corresponds to water and/or temperature loads acting on the entire dam.

In the static analysis for gravity loads, the construction sequence of the dam is represented by considering the dam as independent cantilevers, which are defined by the mesh generator. The gravity load analysis is performed for alternate cantilevers so that the response of each cantilever to its dead weight is independent of the other cantilevers. This type of gravity load analysis was used in the original version of ADAP (Clough, et al., 1973).

The current program uses a nonlinear solution procedure in the second static analysis to recognize opening of the contraction joints under hydrostatic and temperature loads. Usually a nonlinear static analysis can be performed in a single load step. A multi-load step solution procedure has also been implemented in the program, which should be used if the single load step fails to converge. In each step of the multi-step procedure, a fraction of static load is applied to the dam and the load is successively increased until the response under the full static load is obtained.

The type of static analysis is determined by item LSAT in Record D. The joint element properties and control parameters for the static analysis are given in Record I.

## A.5 Earthquake Analysis

The earthquake analysis is controlled by several parameters in Record D of the input data. The time integration procedure is determined by the parameters  $\beta$  and  $\gamma$  described in Section 3.2. The Newmark average acceleration procedure is recommended with  $\beta=0.25$  and  $\gamma=0.50$ . The time step for the integration procedure should be selected such that the high frequency components of the response are properly represented and the nonlinear solution procedure converges. Recommendations on the size of the time step are very problem dependent.

Control of the iterations for each time step is determined by parameters in Record D. NIT is the maximum number of iterations for each time step. If this limit is reached without convergence, an error message will be printed but the solution will proceed to the next time step. The criteria for convergence within a time step are determined by two input parameters, TOL1 and TOL2. If the earthquake analysis is preceded by a static analysis for water and/or temperature loads, convergence is achieved when the change in strain energy of the joints in the latest iteration is less than  $TOL1*U$ , where  $U$  is the strain energy of the joints under the static loads. If a static analysis is not performed (which is not recommended) TOL2 is the strain energy to use for convergence.

Appropriate values for TOL1 and TOL2 depend on the floating precision for the computer. For real variable lengths 4 and 8 bytes,  $TOL1=1.0e-8$  and  $TOL1=1.0e-15$  are recommended, respectively. When the first static load case is included in the analysis, the strain energy value will be printed by the program. This value may be used for TOL2 if no static analysis is performed prior to an earthquake analysis.

Care is required in selecting convergence tolerances because too small tolerances will prevent convergence, whereas too large tolerances will result in errors in the solution. The most suitable values should be determined from convergence studies of each problem. A linear earthquake analysis should require two iterations for each time step and generally the maximum number of iterations in each time step of a nonlinear earthquake analysis should not exceed ten.

As described in Chapter 4, the dam-water interaction effects in the earthquake analysis are represented by an added mass for the incompressible water. A diagonal added mass matrix for water should be provided on FORTRAN logical unit 16. The computer program RESVOR, which performs a finite element analysis of the impounded water (Kuo, 1982), is recommended for this purpose. RESVOR has been revised for computing a diagonal added mass matrix. The user guide for the revised version is given in Appendix B.

## A.6 Description of Input Data

The data in the input file consists of a number of records in free-format. Each record, which consists of several items, is processed by one free-format read statement in the FORTRAN 77

language. The items in a record can be separated by a comma or at least one space and they may be entered on any number of lines.

The user may select any physical units for the dimensional quantities in the input. The dimensions of the output quantities are consistent with the input units.

### **Record A — Title**

The title entered on one line is printed on the output for identification. The title is limited to 72 characters.

### **Record B — Master Control Parameters**

NLM      Number of initial mesh elevations  
 MESHFN    indicator for type of foundation mesh; =0 for rigid foundation; =1, =2, =3 for foundation mesh types 1, 2, and 3, respectively  
 WATL      z-coordinate of water level  
 WDEN      Weight density of water  
 GRAV      Acceleration due to gravity  
 REFT      Reference temperature for static analysis  
 NPLOT     Number of plots of finite element mesh; = 0, for no plots

### **Record C — Generation of Finite Element Mesh**

#### *Record C.1 — Control Parameters*

RI          Radius of inner portion of the reference surface  
 RO(1)     Radius of the right outer portion of the reference surface  
 RO(2)     Radius of the left outer portion of the reference surface  
 NL          Number of design elevations  
 IEL        =1 if the same compounding angles are specified for all elevations; =0 otherwise  
 IRL        =1 if the same compounding angles are specified for right and left portions of the dam; =0 otherwise  
 IIE        =1 if the same compounding angles are specified for intrados and extrados faces of the dam; =0 otherwise  
 NRL        =1 if the same radii are specified for right and left portions of the intrados and extrados arc; =0 otherwise  
 IPLT       =1 if the generated finite element mesh is to be plotted; =0 otherwise  
 FINC       width ratio of the 3-D block  
 NTAN       number of 3-D solid elements in arch direction of 3-D block

NTHK     number of 3-D solid elements through thickness of 3-D block

### *C.2 — Compounding Angles and Angles to Abutments*

One record is provided for each of NL design elevations in increasing order of elevations. If IEL=1, compounding angles for all elevations except the first may be entered as zero. If IRL=1, compounding angles for left arcs may be entered as zero. If IIE=1, compounding angles for extrados arcs may be entered as zero.

EL        Design elevation  
 FCI(1)    Compounding angle of the right intrados arc  
 FCI(2)    Compounding angle of the left intrados arc  
 FCE(1)    Compounding angle of the right extrados arc  
 FCE(2)    Compounding angle of the left extrados arc  
 FA(1)     Angle to right abutment  
 FA(2)     Angle to left abutment

### *C.3 — Contraction Joint Data*

In the current version, the total number of contraction joints is limited to eighteen (18).

#### C.3.1 — Contraction Joints to the Right of Crown Section

NJR        Number of contraction joints to the right of the crown section  
 ANGR(i)    Angles to the reference plane for contraction joint to the right of the crown section,  
               i=1,2...NJR, in increasing order.

#### C.3.1 — Contraction Joints to the Left of Crown Section

NJL        Number of contraction joints to the left of the crown section  
 ANGL(i)    Angles to the reference plane for contraction joint to the left of the crown section,  
               i=1,2...NJL, in increasing order.

### *C.4 — Temperature Data*

Two records are provided, the first for the upstream face and the second for the downstream face. Each record should list the temperature at the design elevations, in order of increasing elevation.

### *C.5 — Initial Mesh Elevations*

One record contains the initial elevations for the NLM mesh elevations in increasing order.



## *C.6—Intrados and Extrados Arcs*

### C.6.1—Y-coordinates of Centers and Radii of Arcs

For each design elevation, one record specifies the Y-coordinates of the centers and radii of the upstream and downstream face arcs. A total of NL records must be provided in order of increasing design elevations.

YII	y-coordinate of center of intrados inner arc
YEI	y-coordinate of center of extrados inner arc
RII	Radius of intrados inner arc
REI	Radius of extrados inner arc
RIO(1)	Radius of intrados right outer arc
REO(1)	Radius of extrados right outer arc
RIO(2)	Radius of intrados left outer arc
REO(2)	Radius of extrados left outer arc

### C.6.2—X-coordinates of the Centers of Inner Arcs

Two records are provided, the first for the downstream face and the second for the upstream face. Each record should list the X-coordinates of centers of the inner arcs at the design elevations, in order of increasing elevation.

## *C.7 Control for Mesh Plots*

Repeat the following data for each of the NPLOT mesh plots requested in Record B. Skip this record if NPLOT =0.

PTYPE	= 1, plot by substructure; = 2, plot by element type; = 3, plot by material type
OPLOT	= 1, X axis vertical in plot; = 2, Y axis vertical in plot, =3, Z axis vertical in plot
V(1), V(2), V(3)	X, Y, Z coordinates of view

### C.7.1 Plot by Substructure, PTYPE=1

N	Number of substructures to plot; = 0, plot all substructures and do not enter NSUB.
SUB(1)	First substructure number
•	
•	
SUB(N)	Last substructure number

### C.7.2 Plot by Element Type, PTYPE=2

N	Number of element sets to plot
---	--------------------------------

- ETYP(1) Element type identified as: joint elements, 1; 3-D solid elements, 2; 3-D shell elements, 3; thick shell elements, 4.
- FRM(1) First element number of specified type
- TO(1) Last element number of specified type
- 
- 
- 
- ETYP(N) Element type identified as follows: joint elements, 1; 3-D solid elements, 2; 3-D shell elements, 3; thick shell elements, 4.
- FRM(N) First element number of specified type
- TO(N) Last element number of specified type

### C.7.3 Plot by Material Type, PTYPE=3

- N Number of materials to plot
- ELM(1) First material number
- 
- 
- 
- FRM(N) Last material number

### **Record D — Control Parameters for Static and Earthquake Analysis**

- DT Time step for integration of equations of motion
- NT Number of time steps; enter zero to suppress earthquake analysis
- NIT Maximum number of iterations for each time step
- BETA  $\beta$  parameter for time integration; 0.25 is recommended
- GAMMA  $\gamma$  parameter for time integration; 0.50 is recommended
- B0  $b_0$  valued for Rayleigh damping
- B1  $b_1$  value for Rayleigh damping
- TOL1 Tolerance coefficient for iterations used when LSTAT(1)=1, that is when earthquake analysis is preceded by static analysis for water and/or temperature loads
- TOL2 Actual tolerance for iterations used when LSTAT(1)=0, that is no static analysis is performed for water and/or temperature loads
- IOUT Computed response is printed every IOUT time steps
- IPRS = 1, for printing information about iterations for each time step; =0, only print number of iterations for each time step. The number of iterations, history of joint opening, and equilibrium error measured by energy norm are printed when IPRS=1.

- NGM Number of ground motion components, = 1, = 2, or = 3
- IDIR NGM codes for directions of ground motion; enter 1, 2, 3 for ground motion in the X, Y, and Z directions, respectively
- NPLM Maximum number of time points used for any of the ground motion records
- LSTAT(1) = 1, perform static analysis for water load and/or temperature effects; = 0, otherwise
- LSTAT(2) = 1, perform static analysis for gravity loads; = 0, otherwise
- MWAT Control for dam-water interaction effects to be included in earthquake analysis; = 0, if interaction is neglected; = 1, if interaction is represented by a diagonal added mass matrix;
- NUMNS Total number of nodal points at upstream face used in computation of added mass; Enter zero if MWAT=0.
- NODSSW Number of nodal points at upstream face of each dam substructure used in the model of the reservoir; Enter one number for each substructure except for the foundation. If MWAT= 0, enter zero for each substructure. In the current version, NODSSW is limited to eighty (80) for each substructure.

### **Record E — Properties of Joint Elements for Earthquake Analysis**

- KN Normal stiffness for joint elements
- KS Tangential stiffness for joint elements
- Q0 Tensile strength for joint elements

### **Record F – Control of Output**

#### *F.1 – Control Parameters*

- ISEL Flag for stress envelopes from earthquake analysis: = 0 , envelopes are computed for selected elements; = 1, envelopes are computed for all elements.
- ISAVE Flag for saving the earthquake response: = 1, the earthquake response is saved for post processing; = 0, the response is not saved.
- IALL Flag for stresses from static analysis: = 0, static stresses computed only for elements for which earthquake stresses are requested (either envelope or history); = 1, static stresses computed for all elements.
- IPRST Flag for stresses and displacements from static analysis: = 0, print total static stresses only; = 1, in addition to total static stresses, for each static load case print element stresses, boundary and substructure displacements, joint displacements, and joint stresses.

### *F.2 – Request of Response Histories*

Five types of response histories from an earthquake analysis will be computed for:

- Nodal point displacements
- Joint displacements
- Stresses in 3–D solid elements
- Stresses in 3–D shell elements
- Stresses in thick shell elements

Details of the response output are given in Section A.7. Five records, one for each of the above types must be provided in the indicated order. A record has the following information:

NC        Number of items, displacement or stress components  
 ID(1)    Nodal point or element number for item 1  
 CMP(1)  Displacement or stress component number for item 1  
 •  
 •  
 •  
 ID(NC)   Nodal point or element number for item NC  
 CMP(NC) Displacement or stress component number for item NC

The element numbers must be entered in increasing order for the stresses of the 3–D solid, 3–D shell and thick shell elements.

### *F.3 – Request of Stress Envelopes*

Three records, one for each of three element types, must be provided if ISEL=0.

#### F.3.1 – 3–D Solid Elements

NEN3D    Number of 3–D solid elements for which envelopes are to be computed. In the current version, NEN3D is limited to 800.  
 NLD3D(i) Element numbers,  $i=1,2,\dots,NEN3D$ , in increasing order.

#### F.3.2 – 3–D Shell Elements

NENS1    Number of 3–D shell elements for which envelopes are to be computed. In the current version, NENS1 is limited to 50.  
 NLS1(i)  Element numbers,  $i=1,2,\dots,NENS1$ , in increasing order.

#### F.3.3 – Thick Shell Elements

NENS2    Number of thick shell elements for which envelopes are to be computed. In the current version, NENS2 is limited to 100.

NLS2(i) Element numbers,  $i=1,2,\dots,NENS2$ , in increasing order.

## Record G — Nodal Point Numbering at Dam–Water Interface

This record is skipped if dam–water interaction is neglected by setting  $MWAT=0$  in Record D. If  $MWAT=1$  then for each substructure, two records are required to specify the relationship between the numbering of the nodal points for the dam model in ADAP–88 and the nodal point numbering for the reservoir model in RESVOR. The order of the substructures should be the same as that for NODSSW in Record D.

### *G.1 — Upstream Nodal Points for Dam Model*

Enter nodal point numbers at the upstream face of the the reservoir model

### *G.2 — Upstream Nodal Points for Reservoir Model*

Enter the corresponding nodal point numbers at the upstream face of the dam model.

## Record H — Material Properties for Dam and Foundation

### *H.1 — 3–D Solid Elements*

One or two records are required depending if the foundation is modeled. The first record specifies material properties for 3–D elements in the dam body and should be supplied for all cases.

The second record specifies material properties for 3–D elements in the foundation if  $MESHF>0$ . Orthotropic material properties can be specified for the 3–D solid elements. This is intended to account for the different material properties of the foundation in vertical and horizontal directions. The axes of orthotropy is assumed to coincide with the global X–Y–Z axes.

An input item marked by an asterisk may be set to zero to indicate it has the same value as the previous item.

#### H.1.1 — Material Properties for Dam

MAT	Material identification, enter 1
ISOT	=0 for isotropic material, or =1 for orthotropic material
E(1)	Modulus of elasticity, $E_{xx}$
E(2)	Modulus of elasticity, $E_{yy}$ *
E(3)	Modulus of elasticity, $E_{zz}$ *
E(4)	Poisson's ratio, $\nu_{xy}$
E(5)	Poisson's ratio, $\nu_{xz}$ *

E(6)	Poisson's ratio, $\nu_{yz}$ *
E(7)	Shear modulus, $G_{xy}$
E(8)	Shear modulus, $G_{yz}$ *
E(9)	Shear modulus, $G_{zx}$ *
E(10)	Coefficient of thermal expansion for X-direction
E(11)	Coefficient of thermal expansion for Y-direction *
E(12)	Coefficient of thermal expansion for Z-direction *
E(13)	unit weight

### H.1.2 — Material Properties for Foundation

This record is not required if MESHFN=0.

MAT	Material identification, enter 2
ISOT	=0 for isotropic material, or =1 for orthotropic material
E(1)	Modulus of elasticity, $E_{xx}$
E(2)	Modulus of elasticity, $E_{yy}$ *
E(3)	Modulus of elasticity, $E_{zz}$ *
E(4)	Poisson's ratio, $\nu_{xy}$
E(5)	Poisson's ratio, $\nu_{xz}$ *
E(6)	Poisson's ratio, $\nu_{yz}$ *
E(7)	Shear modulus, $G_{xy}$
E(8)	Shear modulus, $G_{yz}$ *
E(9)	Shear modulus, $G_{zx}$ *
E(10)	Coefficient of thermal expansion for X-direction
E(11)	Coefficient of thermal expansion for Y-direction *
E(12)	Coefficient of thermal expansion for Z-direction *
E(13)	unit weight

### *H.2 — 3-D Shell and Thick Shell Elements*

EE	Modulus of elasticity
ENU	Poisson's ratio
RHO	unit weight
ALP	Coefficient of thermal expansion

### **Record I — Joint Element Properties and Control for Water/Temperature Analysis**

One record is required if a static analysis is performed for water and/or temperature loads. The load fraction for step  $i$  is  $i/NSTEP$ .

KN	Normal stiffness for joint elements
KS	Tangential stiffness for joint elements
Q0	Tensile strength for joint elements
NSTEP	Number of load steps
NIT	Maximum number of iterations for each step; execution terminates if solution does not converge

## Record J — Earthquake Ground Motion Records

Following the order specified by IDIR in Record D, three records should be provided for each of the NGM ground motion components.

### *J.1 — Title*

The title with a maximum of 64 characters is printed on the output for identification of the ground motion record

### *J.2 — Control Parameters*

NLP	Number of time points defining the ground motion record
SFTR	Scale factor for ground motion

### *J.3 — Ground Acceleration Values*

NLP pairs of data in order of increasing time:

T	Time value
P	Acceleration at time T

## A.7 Description of Earthquake Response Output

The user can request the program to print earthquake response histories for nodal point displacements, joint element displacements, stresses in 3-D solid elements, stresses in 3-D shell elements, and stresses in thick shell elements. Envelopes of the maximum and minimum arch, cantilever, and shear stresses for each element type (except joint elements) can also be requested. All stresses include the static and dynamic effects. This section describes the output quantities for each of these responses as controlled by the input parameters in Record F.

### *A.7.1 Nodal Point Displacements*

The nodal displacement component numbers 1 to 5 refer to the X-, Y-, and Z- displacements and the A- and B-rotations of the nodal points, respectively. The program computes and prints the displacements with respect to a rigid support. The displacements are only the dynamic response and exclude the displacements caused by the static loads.

### A.7.2 Joint Element Displacements

The displacements of a joint element are the relative normal displacements between two surfaces of the element, computed at the integration points. Positive displacement corresponds to opening of the joint. The tangential displacements are not printed and are not considered in numbering the joint displacements. In contrast to the nodal point displacements, the joint displacements include the effects of the earthquake as well as the temperature and/water loads, if such loads are included in the analysis.

Four integration points are used in computing stiffness and load vectors of a joint element. Thus, up to four displacement components can be requested for each joint element. The locations of these points are shown in Fig. A.6 and Table A.1.

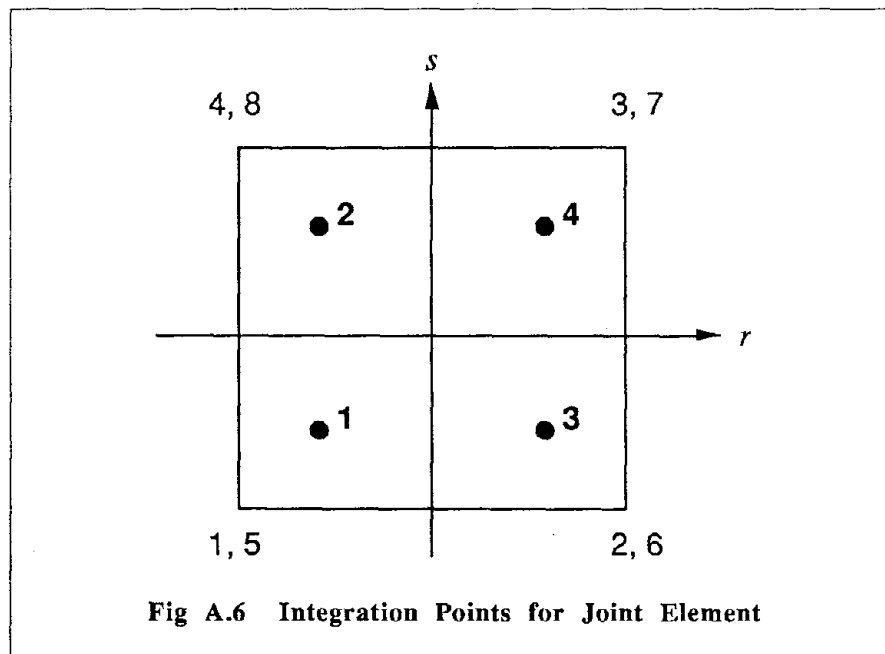




Table A.2 Natural Coordinates of Integration Points for Joint Element

Point	$r$	$s$
1	-0.5774	-0.5774
2	-0.5774	+0.5774
3	+0.5774	-0.5774
4	+0.5774	+0.5774

### A.7.3 Stresses in 3-D Solid Elements

Stresses are computed for dam elements only; stresses for foundation elements are not computed. The stresses of the 3-D solid elements immediately adjacent to shell elements are not computed either. The stress points are located at the center of upstream and downstream faces. Stresses are not computed for the interior elements if more than two elements are used through the dam thickness. Thus, a 3-D solid element will generally have only one stress point. For two special cases, an element has two stress points, one at the upstream face and one at the downstream face: (i) when one element is used through the dam thickness ( $NTHK=1$ ), and (ii) for the 3-D solid elements below the contraction joint (represented by triangle bef in Fig.A.3).

The numbering of the stress points is given in Table A.3. The second column in the table corresponds to the second stress point (downstream face) for the special cases mentioned above. Based on the definition of local coordinate system  $x-y-z$ ,  $\sigma_{xx}$ ,  $\sigma_{yy}$ , and  $\sigma_{xy}$  correspond to arch, cantilever and shear stresses, respectively, in the element.

Table A.3 Stress Components in 3-D Solid Elements

Stress Component	Point 1	Point 2
$\sigma_{xx}$	1	7
$\sigma_{yy}$	2	8
$\sigma_{zz}$	3	9
$\sigma_{xy}$	4	10
$\sigma_{yz}$	5	11
$\sigma_{zx}$	6	12

### A.7.4 Stresses in 3-D Shell Elements

The stresses in the 16-node 3-D shell element are given at ten points located at the upstream and downstream faces. The locations of these points in the natural coordinate system  $r$ - $s$ - $t$  are shown in Fig A.7. Points 1,3,5,7 and 9 are located at the upstream face, whereas, points 2,4,6,8 and 10 are located at the downstream face.

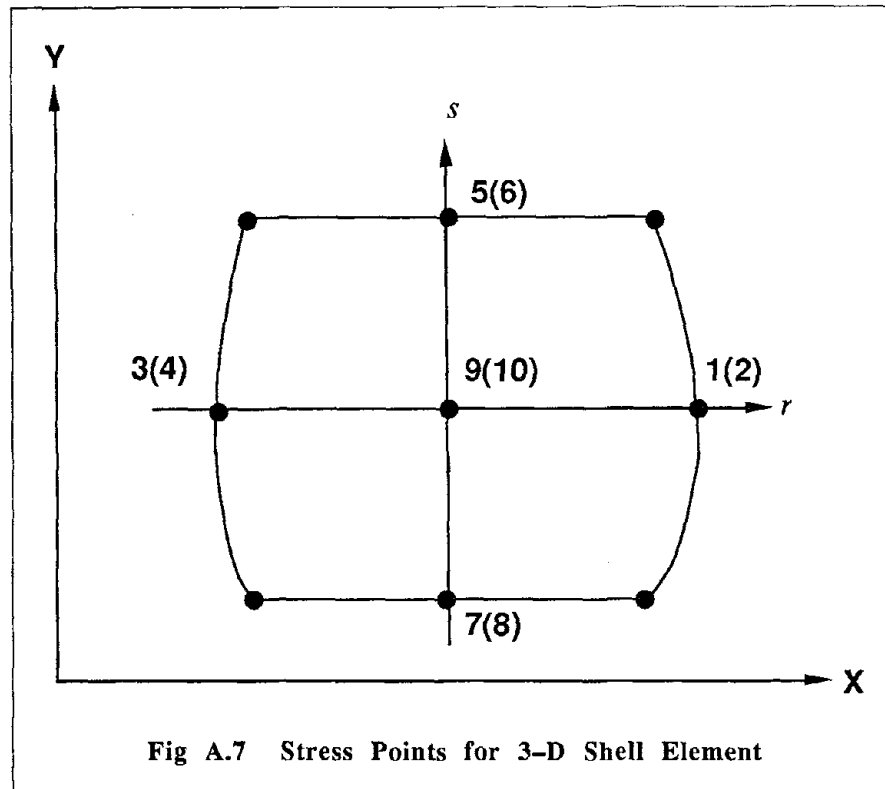


Fig A.7 Stress Points for 3-D Shell Element

The 12-node 3-D shell element used near the abutments is obtained from a 16-node element in which 6 nodes of a face degenerate into two nodes. Consequently, Fig. A.7 also identifies the stress points of the 12-node element. Stresses are not calculated at points 7 and 8 of a 12-node element, so a request of stresses of these points is not permitted.

Six stress components are associated with each stress point. Numbering of the sixty (60) stress components is given in Table A.4. Based on the definition of local coordinate system  $x$ - $y$ - $z$ ,  $\sigma_{xx}$ ,  $\sigma_{yy}$ , and  $\sigma_{xy}$  are approximations of the arch, cantilever and shear stresses, respectively.

Table A.4 Stress Components in 3-D Shell Elements

Stress Component	1	2	3	4	5	6	7	8	9	10
$\sigma_{xx}$	1	7	13	19	25	31	37	43	49	55
$\sigma_{yy}$	2	8	14	20	26	32	38	44	50	56
$\sigma_{zz}$	3	9	15	21	27	33	39	45	51	57
$\sigma_{xy}$	4	10	16	22	28	34	40	46	52	58
$\sigma_{yz}$	5	11	17	23	29	35	41	47	53	59
$\sigma_{zx}$	6	12	18	24	30	36	42	48	54	60

### A.7.5 Stresses in Thick Shell and Transition Elements

For these elements stresses are computed at eight stress points at the upstream and downstream faces. The locations of these points are given in Table A.5 and Fig A.8. Points 1,3,5 and 7 are at the downstream face, whereas, points 2,4,6 and 8 are at the upstream face.

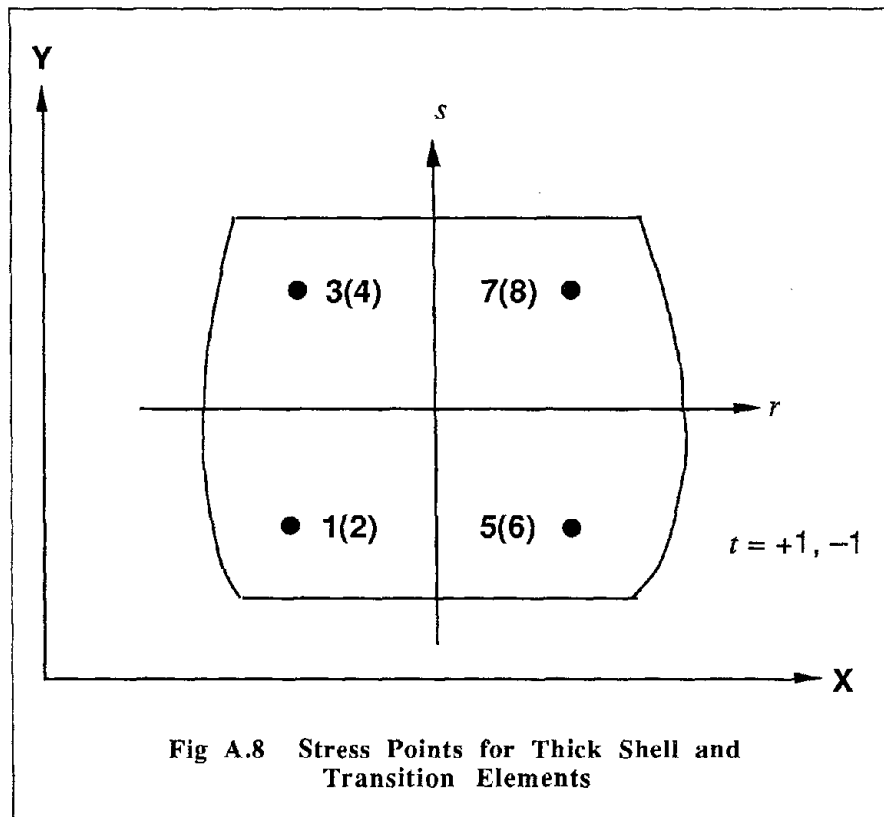


Table A.5 Natural Coordinates of Integration Points  
for Thick Shell and Transition Elements

Point	$r$	$s$	$t$
1	-0.5774	-0.5774	-1
2	-0.5774	-0.5774	+1
3	-0.5774	+0.5774	-1
4	-0.5774	+0.5774	+1
5	+0.5774	-0.5774	-1
6	+0.5774	-0.5774	+1
7	+0.5774	+0.5774	-1
8	+0.5774	+0.5774	+1

At each stress point five stress components are calculated ( $\sigma_{zz}$  is assumed to be zero). The numbering of the forty (40) stress components is given in Table A.6. Based on the definition of local coordinate system  $x$ - $y$ - $z$ ,  $\sigma_{xx}$ ,  $\sigma_{yy}$ , and  $\sigma_{xy}$  correspond to arch, cantilever and shear stresses, respectively.

Table A.6 Stress Components in Thick Shell and Transition Elements

Stress Component	1	2	3	4	5	6	7	8
$\sigma_{xx}$	1	6	11	16	21	26	31	36
$\sigma_{yy}$	2	7	12	17	22	27	32	37
$\sigma_{xy}$	3	8	13	18	23	28	33	38
$\sigma_{yz}$	4	9	14	19	24	29	34	39
$\sigma_{zx}$	5	10	15	20	25	30	35	40

## A.8 Saving Response Histories and Response Envelopes

Response histories and response envelopes requested in Record F can be saved for post-processing by specifying ISAVE=1 in Record F.1. The data is stored on FORTRAN logical unit 15 according to the following format.

### A.8.1 Response Histories

When the response histories are saved, two records are written for each of the five types of response histories requested in Record F.2.

*Record 1* — This record contains (i) the total number of displacement or stress components, (ii) element or nodal point numbers, and (iii) stress or displacement component numbers. These data are written in exactly the same order that they are specified in Record F.2.

*Record 2* — This record contains three items: (i) IOUT, the output interval from Record D, (ii) DT, the time step, and (iii) SHIS, the response history array. Row  $i$  of array SHIS is the response at time  $IOUT*DT*(i-1)$ . Columns of the array correspond to the requested response quantities in the order they are specified in Record F.2.

### A.8.2 Response Envelopes

When the envelopes of maximum and minimum stresses are saved, two records are written for each of the three response envelopes specified in Record F.3 .

*Record 1* — This record is similar to Record 1 above for the response histories. It contains: (i) the total number of stress components for which envelopes are requested, (ii) element numbers, and (iii) stress component numbers. Note that for the response histories this information is supplied in the input data, whereas for the response envelopes it is computed by the program.

*Record 2* — This record contains the array SV which has three rows. Each column contains values for a requested stress component in the sequence given by Record 1 (and also in the printed output for the response). The first row is the total static stress. The second and the third rows are the maximum and minimum values of the total (static plus earthquake) stresses, respectively.

## A.9 Installation of ADAP-88 Program

### A.9.1. Dynamic Storage Allocation

The large arrays in the program are stored in blank common and a memory manager allocates storage dynamically. The overall size of the problem that the program can analyze is determined by

the size of the blank common block. Within the program, the size of the blank common block is established by the size of integer array IA in the main program and by the corresponding variable MTOT. If the storage required for an analysis exceeds MTOT, the program will print a message indicating the storage deficit. Increasing the capacity involves increasing MTOT and the dimension of the IA array.

The dynamic storage allocation in the program can be adapted to computers with various word lengths. The storage allocation is a function of the ratio of the word length for real numbers to the word length for integers. These word lengths, which are called LREAL and LINTG in the program, depend on the compiler and the desired floating point precision (single or double). The values should be initialized in the main program during installation of the program.

### *A.9.2 Mesh Plotting*

The finite element mesh plotting is implemented using five subroutines supplied in the UNIX operating system library. If the library is available, it can be linked with the ADAP-88 program. If the library is not available, the subroutines must be implemented with system dependent functions to perform the plotting. The calls to the plotting subroutines used in ADAP-88 are defined as follows.

OPENPL()	open a plot file
CLOSEPL()	close plot file
SPACE (X1,Y1,X2,Y2)	Define view on the plot area with lower left corner (X1,Y1) and upper right corner (X2,Y2)
LINE (X1,Y1,X2,Y2)	Draw a line from (X1,Y1) to (X2,Y2)
MOVE (X1,Y1)	Move pen to (X1,Y1)

# Appendix B

## *USER GUIDE FOR RESVOR*

### **B.1 Introduction**

The RESVOR program performs a finite element analysis for computing the added mass matrix representing the incompressible water impounded in a reservoir. The program is described in (Kuo, 1982) and, as discussed in Chapter 4, the consistent added mass matrix is diagonalized for use in ADAP-88.

The diagonal terms of the final added mass matrix are written on FORTRAN logical unit 16, and this file should be available to ADAP-88 if dam-water interaction effects are included in the earthquake analysis.

The added mass matrix computed by RESVOR is associated with translational degrees-of-freedom of nodal points at the dam-water-interface. Thus, if NUMNS is the number of upstream nodes, the added mass will be saved as a one-dimensional array of order  $3 \times \text{NUMNS}$ . For the purpose of defining the added mass matrix for use in ADAP-88, the user must renumber the interface nodes following the sequence in which these nodes appear in the numbering of all the reservoir nodes. The new node numbers, 1 to NUMNS, should be used to prepare Record G of the input data for the ADAP-88 program.

### **B.2 Description of Input Data**

The data in the input file consist of a number of records in free-format. Each record, which consists of several items, is processed by one free-format read statement in the FORTRAN 77 language. The items in a record can be separated by a comma or at least one space and they may be entered on any number of lines.

The user may select any physical units for the dimensional quantities in the input. The dimensions of the output quantities are consistent with the input units.

#### **Record A - Title**

The title is entered on one line, and is limited to 80 characters.

#### **Record B - Master Control Parameters**

NUMNP	Total number of fluid nodal points in the reservoir
NUMNS	Number of fluid nodal points on the dam-water interface
N3DEL	Number of three-dimensional fluid elements

N2DEL	Number of two-dimensional fluid elements on the dam-water interface
WMASS	Mass density of water
GRAV	Acceleration due to gravity
WATL	Z-coordinate of free surface of reservoir
ICOMP	Control for comparison between finite element and Westergaard solutions. If ICOMP=1, 2 or 3, the nodal pressures and nodal forces due to uniform acceleration of the dam-water interface of dam in X, Y or Z direction are computed by the finite element methods as well as the generalized Westergaard formula. This computation is not performed if ICOMP=0.

### Record C – Nodal Coordinates and Boundary Conditions

One record is required for each node of the reservoir mesh except for nodes that are generated.

N	Node number
X	X-coordinate
Y	Y-coordinate
Z	Z-coordinate
IBC	Boundary condition code: = 0, for all nodes except those at the free surface and dam-water interface; = 1 for all nodes at the free surface except those on dam-water interface; = -1, for nodes on dam-water interface excluding nodes at water surface; = -2, for nodes at the free surface on the dam-water interface.
KN	Node generation increment

Nodal points located on a straight line between node N1 on the upstream end of the reservoir and node N2 on the dam-water interface can be generated. The boundary condition code for generated nodes will be the same as that for node N1. The record for node N1 should be entered followed by the record for node N2. The spacing of the nodes will be successively reduced towards the dam by a factor equal to 0.8. The node generation increment should be entered as KN for the N1 record and KN for the N2 record should be zero.

### Record D – Two-dimensional Elements on Dam-Water Interface

One record is required for each element. If the element is at the free surface and its upper nodes does not coincide with nodes of the dam model two records are required and the element number, NEL, is entered with a negative sign. The elements should be entered in increasing order of the actual element numbers.



*Record D.1 Data For All Elements*

NEL or -NEL	Element number
NCON(1)	Nodal point 1
NCON(2)	Nodal point 2
.	
.	
NCON(8)	Nodal point 8
NINT	Integration order, 2 or 3 ; NINT=2 is recommended

*Record D.2 Required If Element Number Is Negative*

Z2	Z-coordinate of the upper nodes of the corresponding dam element
Z0	Z-coordinate of the mid-height nodes of the corresponding dam element
Z1	Z-coordinate of the lower nodes of the corresponding dam element

Except for the nodes at the free surface, all of the reservoir nodes at the dam-water interface are assumed to coincide with nodes in the dam model.

**Record E - Three-dimensional Fluid Elements**

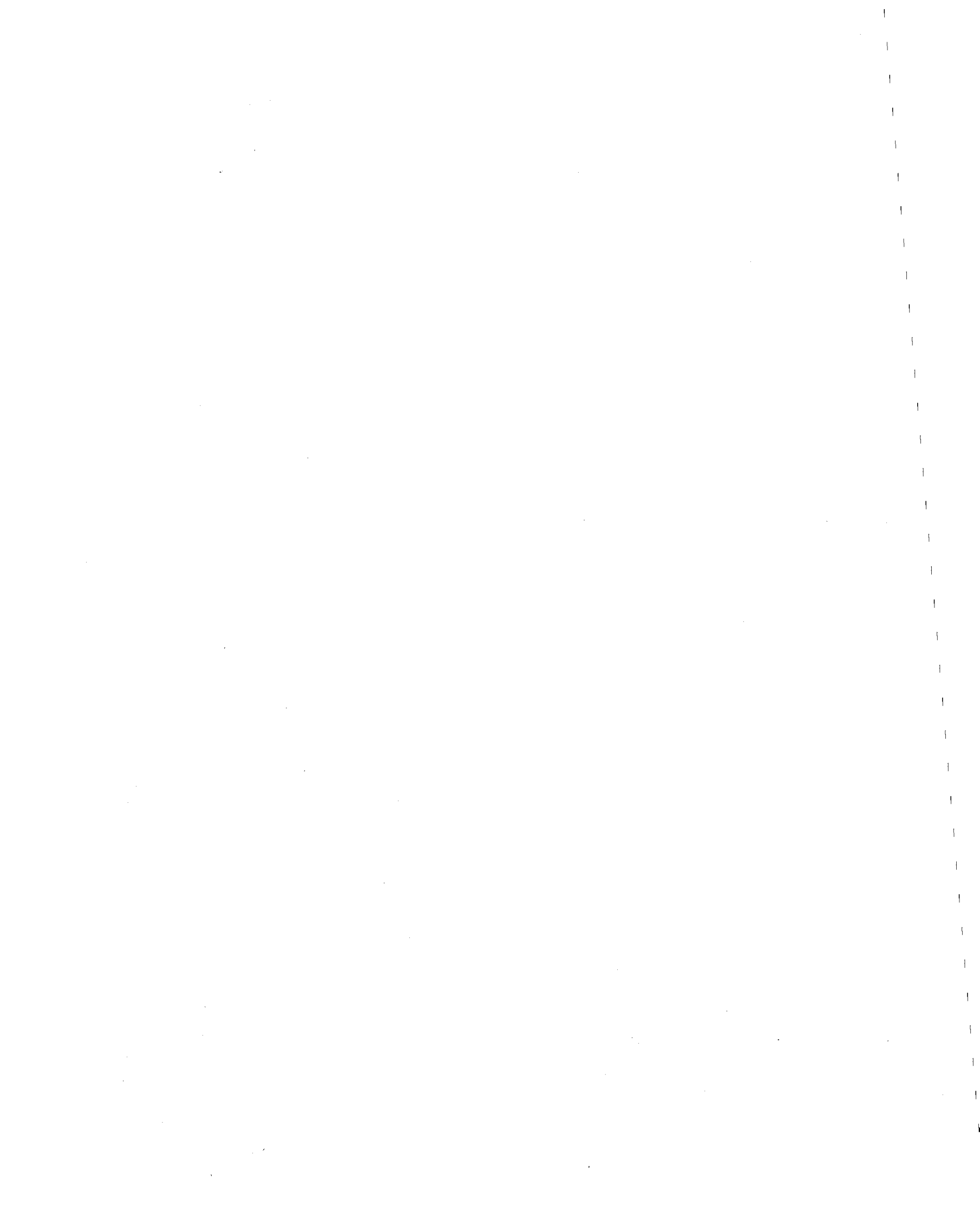
Two records are required for each element and elements are entered in increasing order of the element numbers.

*Record E.1 Element Number*

NE	Element number
NINT	Integration order, 2 or 3 ; NINT=2 is recommended

*Record E.2 Nodal Point Connectivity*

NP(1)	Nodal point 1
NP(2)	Nodal point 2
.	
.	
NP(16)	Nodal point 16



## EARTHQUAKE ENGINEERING RESEARCH CENTER REPORT SERIES

EERC reports are available from the National Information Service for Earthquake Engineering(NISEE) and from the National Technical Information Service(NTIS). Numbers in parentheses are Accession Numbers assigned by the National Technical Information Service; these are followed by a price code. Contact NTIS, 5285 Port Royal Road, Springfield Virginia, 22161 for more information. Reports without Accession Numbers were not available from NTIS at the time of printing. For a current complete list of EERC reports (from EERC 67-1) and availability information, please contact University of California, EERC, NISEE, 1301 South 46th Street, Richmond, California 94804.

- UCB/EERC-80/01 "Earthquake Response of Concrete Gravity Dams Including Hydrodynamic and Foundation Interaction Effects," by Chopra, A.K., Chakrabarti, P. and Gupta, S., January 1980, (AD-A087297)A10.
- UCB/EERC-80/02 "Rocking Response of Rigid Blocks to Earthquakes," by Yim, C.S., Chopra, A.K. and Penzien, J., January 1980, (PB80 166 002)A04.
- UCB/EERC-80/03 "Optimum Inelastic Design of Seismic-Resistant Reinforced Concrete Frame Structures," by Zagajski, S.W. and Bertero, V.V., January 1980, (PB80 164 635)A06.
- UCB/EERC-80/04 "Effects of Amount and Arrangement of Wall-Panel Reinforcement on Hysteretic Behavior of Reinforced Concrete Walls," by Iliya, R. and Bertero, V.V., February 1980, (PB81 122 525)A09.
- UCB/EERC-80/05 "Shaking Table Research on Concrete Dam Models," by Niwa, A. and Clough, R.W., September 1980, (PB81 122 368)A06.
- UCB/EERC-80/06 "The Design of Steel Energy-Absorbing Restrainers and their Incorporation into Nuclear Power Plants for Enhanced Safety (Vol 1a): Piping with Energy Absorbing Restrainers: Parameter Study on Small Systems," by Powell, G.H., Oughourlian, C. and Simons, J., June 1980.
- UCB/EERC-80/07 "Inelastic Torsional Response of Structures Subjected to Earthquake Ground Motions," by Yamazaki, Y., April 1980, (PB81 122 327)A08.
- UCB/EERC-80/08 "Study of X-Braced Steel Frame Structures under Earthquake Simulation," by Ghanaat, Y., April 1980, (PB81 122 335)A11.
- UCB/EERC-80/09 "Hybrid Modelling of Soil-Structure Interaction," by Gupta, S., Lin, T.W. and Penzien, J., May 1980, (PB81 122 319)A07.
- UCB/EERC-80/10 "General Applicability of a Nonlinear Model of a One Story Steel Frame," by Sveinsson, B.I. and McNiven, H.D., May 1980, (PB81 124 877)A06.
- UCB/EERC-80/11 "A Green-Function Method for Wave Interaction with a Submerged Body," by Kioka, W., April 1980, (PB81 122 269)A07.
- UCB/EERC-80/12 "Hydrodynamic Pressure and Added Mass for Axisymmetric Bodies," by Nilrat, F., May 1980, (PB81 122 343)A08.
- UCB/EERC-80/13 "Treatment of Non-Linear Drag Forces Acting on Offshore Platforms," by Dao, B.V. and Penzien, J., May 1980, (PB81 153 413)A07.
- UCB/EERC-80/14 "2D Plane/Axisymmetric Solid Element (Type 3-Elastic or Elastic-Perfectly Plastic)for the ANSR-II Program," by Mondkar, D.P. and Powell, G.H., July 1980, (PB81 122 350)A03.
- UCB/EERC-80/15 "A Response Spectrum Method for Random Vibrations," by Der Kiureghian, A., June 1981, (PB81 122 301)A03.
- UCB/EERC-80/16 "Cyclic Inelastic Buckling of Tubular Steel Braces," by Zayas, V.A., Popov, E.P. and Mahin, S.A., June 1981, (PB81 124 885)A10.
- UCB/EERC-80/17 "Dynamic Response of Simple Arch Dams Including Hydrodynamic Interaction," by Porter, C.S. and Chopra, A.K., July 1981, (PB81 124 000)A13.
- UCB/EERC-80/18 "Experimental Testing of a Friction Damped Aseismic Base Isolation System with Fail-Safe Characteristics," by Kelly, J.M., Beucke, K.E. and Skinner, M.S., July 1980, (PB81 148 595)A04.
- UCB/EERC-80/19 "The Design of Steel Energy-Absorbing Restrainers and their Incorporation into Nuclear Power Plants for Enhanced Safety (Vol.1B): Stochastic Seismic Analyses of Nuclear Power Plant Structures and Piping Systems Subjected to Multiple Supported Excitations," by Lee, M.C. and Penzien, J., June 1980, (PB82 201 872)A08.
- UCB/EERC-80/20 "The Design of Steel Energy-Absorbing Restrainers and their Incorporation into Nuclear Power Plants for Enhanced Safety (Vol 1C): Numerical Method for Dynamic Substructure Analysis," by Dickens, J.M. and Wilson, E.L., June 1980.
- UCB/EERC-80/21 "The Design of Steel Energy-Absorbing Restrainers and their Incorporation into Nuclear Power Plants for Enhanced Safety (Vol 2): Development and Testing of Restraints for Nuclear Piping Systems," by Kelly, J.M. and Skinner, M.S., June 1980.
- UCB/EERC-80/22 "3D Solid Element (Type 4-Elastic or Elastic-Perfectly-Plastic) for the ANSR-II Program," by Mondkar, D.P. and Powell, G.H., July 1980, (PB81 123 242)A03.
- UCB/EERC-80/23 "Gap-Friction Element (Type 5) for the Ansr-II Program," by Mondkar, D.P. and Powell, G.H., July 1980, (PB81 122 285)A03.
- UCB/EERC-80/24 "U-Bar Restraint Element (Type 11) for the ANSR-II Program," by Oughourlian, C. and Powell, G.H., July 1980, (PB81 122 293)A03.
- UCB/EERC-80/25 "Testing of a Natural Rubber Base Isolation System by an Explosively Simulated Earthquake," by Kelly, J.M., August 1980, (PB81 201 360)A04.
- UCB/EERC-80/26 "Input Identification from Structural Vibrational Response," by Hu, Y., August 1980, (PB81 152 308)A05.
- UCB/EERC-80/27 "Cyclic Inelastic Behavior of Steel Offshore Structures," by Zayas, V.A., Mahin, S.A. and Popov, E.P., August 1980, (PB81 196 180)A15.
- UCB/EERC-80/28 "Shaking Table Testing of a Reinforced Concrete Frame with Biaxial Response," by Oliva, M.G., October 1980, (PB81 154 304)A10.
- UCB/EERC-80/29 "Dynamic Properties of a Twelve-Story Prefabricated Panel Building," by Bouwkamp, J.G., Kollegger, J.P. and Stephen, R.M., October 1980, (PB82 138 777)A07.
- UCB/EERC-80/30 "Dynamic Properties of an Eight-Story Prefabricated Panel Building," by Bouwkamp, J.G., Kollegger, J.P. and Stephen, R.M., October 1980, (PB81 200 313)A05.
- UCB/EERC-80/31 "Predictive Dynamic Response of Panel Type Structures under Earthquakes," by Kollegger, J.P. and Bouwkamp, J.G., October 1980, (PB81 152 316)A04.
- UCB/EERC-80/32 "The Design of Steel Energy-Absorbing Restrainers and their Incorporation into Nuclear Power Plants for Enhanced Safety (Vol 3): Testing of Commercial Steels in Low-Cycle Torsional Fatigue," by Spanner, P., Parker, E.R., Jongewaard, E. and Dory, M., 1980.

- UCB/EERC-80/33 "The Design of Steel Energy-Absorbing Restrainers and their Incorporation into Nuclear Power Plants for Enhanced Safety (Vol 4): Shaking Table Tests of Piping Systems with Energy-Absorbing Restrainers," by Stierner, S.F. and Godden, W.G., September 1980, (PB82 201 880)A05.
- UCB/EERC-80/34 "The Design of Steel Energy-Absorbing Restrainers and their Incorporation into Nuclear Power Plants for Enhanced Safety (Vol 5): Summary Report," by Spencer, P., 1980.
- UCB/EERC-80/35 "Experimental Testing of an Energy-Absorbing Base Isolation System," by Kelly, J.M., Skinner, M.S. and Beucke, K.E., October 1980, (PB81 154 072)A04.
- UCB/EERC-80/36 "Simulating and Analyzing Artificial Non-Stationary Earth Ground Motions," by Nau, R.F., Oliver, R.M. and Pister, K.S., October 1980, (PB81 153 397)A04.
- UCB/EERC-80/37 "Earthquake Engineering at Berkeley - 1980," by , September 1980, (PB81 205 674)A09.
- UCB/EERC-80/38 "Inelastic Seismic Analysis of Large Panel Buildings," by Schricker, V. and Powell, G.H., September 1980, (PB81 154 338)A13.
- UCB/EERC-80/39 "Dynamic Response of Embankment, Concrete-Gavity and Arch Dams Including Hydrodynamic Interaction," by Hall, J.F. and Chopra, A.K., October 1980, (PB81 152 324)A11.
- UCB/EERC-80/40 "Inelastic Buckling of Steel Struts under Cyclic Load Reversal," by Black, R.G., Wenger, W.A. and Popov, E.P., October 1980, (PB81 154 312)A08.
- UCB/EERC-80/41 "Influence of Site Characteristics on Buildings Damage during the October 3,1974 Lima Earthquake," by Repetto, P., Arango, I. and Seed, H.B., September 1980, (PB81 161 739)A05.
- UCB/EERC-80/42 "Evaluation of a Shaking Table Test Program on Response Behavior of a Two Story Reinforced Concrete Frame," by Blondet, J.M., Clough, R.W. and Mahin, S.A., December 1980, (PB82 196 544)A11.
- UCB/EERC-80/43 "Modelling of Soil-Structure Interaction by Finite and Infinite Elements," by Medina, F., December 1980, (PB81 229 270)A04.
- UCB/EERC-81/01 "Control of Seismic Response of Piping Systems and Other Structures by Base Isolation," by Kelly, J.M., January 1981, (PB81 200 735)A05.
- UCB/EERC-81/02 "OPTNSR- An Interactive Software System for Optimal Design of Statically and Dynamically Loaded Structures with Nonlinear Response," by Bhatti, M.A., Ciampi, V. and Pister, K.S., January 1981, (PB81 218 851)A09.
- UCB/EERC-81/03 "Analysis of Local Variations in Free Field Seismic Ground Motions," by Chen, J.-C., Lysmer, J. and Seed, H.B., January 1981, (AD-A099508)A13.
- UCB/EERC-81/04 "Inelastic Structural Modeling of Braced Offshore Platforms for Seismic Loading," by Zayas, V.A., Shing, P.-S.B., Mahin, S.A. and Popov, E.P., January 1981, (PB82 138 777)A07.
- UCB/EERC-81/05 "Dynamic Response of Light Equipment in Structures," by Der Kiureghian, A., Sackman, J.L. and Nour-Omid, B., April 1981, (PB81 218 497)A04.
- UCB/EERC-81/06 "Preliminary Experimental Investigation of a Broad Base Liquid Storage Tank," by Bouwkamp, J.G., Kollegger, J.P. and Stephen, R.M., May 1981, (PB82 140 385)A03.
- UCB/EERC-81/07 "The Seismic Resistant Design of Reinforced Concrete Coupled Structural Walls," by Aktan, A.E. and Bertero, V.V., June 1981, (PB82 113 358)A11.
- UCB/EERC-81/08 "Unassigned," by Unassigned, 1981.
- UCB/EERC-81/09 "Experimental Behavior of a Spatial Piping System with Steel Energy Absorbers Subjected to a Simulated Differential Seismic Input," by Stierner, S.F., Godden, W.G. and Kelly, J.M., July 1981, (PB82 201 898)A04.
- UCB/EERC-81/10 "Evaluation of Seismic Design Provisions for Masonry in the United States," by Sveinsson, B.I., Mayes, R.L. and McNiven, H.D., August 1981, (PB82 166 075)A08.
- UCB/EERC-81/11 "Two-Dimensional Hybrid Modelling of Soil-Structure Interaction," by Tzong, T.-J., Gupta, S. and Penzien, J., August 1981, (PB82 142 118)A04.
- UCB/EERC-81/12 "Studies on Effects of Infills in Seismic Resistant R/C Construction," by Brokken, S. and Bertero, V.V., October 1981, (PB82 166 190)A09.
- UCB/EERC-81/13 "Linear Models to Predict the Nonlinear Seismic Behavior of a One-Story Steel Frame," by Valdimarsson, H., Shah, A.H. and McNiven, H.D., September 1981, (PB82 138 793)A07.
- UCB/EERC-81/14 "TLUSH: A Computer Program for the Three-Dimensional Dynamic Analysis of Earth Dams," by Kagawa, T., Mejia, L.H., Seed, H.B. and Lysmer, J., September 1981, (PB82 139 940)A06.
- UCB/EERC-81/15 "Three Dimensional Dynamic Response Analysis of Earth Dams," by Mejia, L.H. and Seed, H.B., September 1981, (PB82 137 274)A12.
- UCB/EERC-81/16 "Experimental Study of Lead and Elastomeric Dampers for Base Isolation Systems," by Kelly, J.M. and Hodder, S.B., October 1981, (PB82 166 182)A05.
- UCB/EERC-81/17 "The Influence of Base Isolation on the Seismic Response of Light Secondary Equipment," by Kelly, J.M., April 1981, (PB82 255 266)A04.
- UCB/EERC-81/18 "Studies on Evaluation of Shaking Table Response Analysis Procedures," by Blondet, J. M., November 1981, (PB82 197 278)A10.
- UCB/EERC-81/19 "DELIGHT.STRUCT: A Computer-Aided Design Environment for Structural Engineering," by Balling, R.J., Pister, K.S. and Polak, E., December 1981, (PB82 218 496)A07.
- UCB/EERC-81/20 "Optimal Design of Seismic-Resistant Planar Steel Frames," by Balling, R.J., Ciampi, V. and Pister, K.S., December 1981, (PB82 220 179)A07.
- UCB/EERC-82/01 "Dynamic Behavior of Ground for Seismic Analysis of Lifeline Systems," by Sato, T. and Der Kiureghian, A., January 1982, (PB82 218 926)A05.
- UCB/EERC-82/02 "Shaking Table Tests of a Tubular Steel Frame Model," by Ghanaat, Y. and Clough, R.W., January 1982, (PB82 220 161)A07.

- UCB/EERC-82/03 "Behavior of a Piping System under Seismic Excitation: Experimental Investigations of a Spatial Piping System supported by Mechanical Shock Arrestors," by Schneider, S., Lee, H.-M. and Godden, W. G., May 1982, (PB83 172 544)A09.
- UCB/EERC-82/04 "New Approaches for the Dynamic Analysis of Large Structural Systems," by Wilson, E.L., June 1982, (PB83 148 080)A05.
- UCB/EERC-82/05 "Model Study of Effects of Damage on the Vibration Properties of Steel Offshore Platforms," by Shahriver, F. and Bouwkamp, J.G., June 1982, (PB83 148 742)A10.
- UCB/EERC-82/06 "States of the Art and Practice in the Optimum Seismic Design and Analytical Response Prediction of R/C Frame Wall Structures," by Aktan, A.E. and Bertero, V.V., July 1982, (PB83 147 736)A05.
- UCB/EERC-82/07 "Further Study of the Earthquake Response of a Broad Cylindrical Liquid-Storage Tank Model," by Manos, G.C. and Clough, R.W., July 1982, (PB83 147 744)A11.
- UCB/EERC-82/08 "An Evaluation of the Design and Analytical Seismic Response of a Seven Story Reinforced Concrete Frame," by Charney, F.A. and Bertero, V.V., July 1982, (PB83 157 628)A09.
- UCB/EERC-82/09 "Fluid-Structure Interactions: Added Mass Computations for Incompressible Fluid," by Kuo, J.S.-H., August 1982, (PB83 156 281)A07.
- UCB/EERC-82/10 "Joint-Opening Nonlinear Mechanism: Interface Smeared Crack Model," by Kuo, J.S.-H., August 1982, (PB83 149 195)A05.
- UCB/EERC-82/11 "Dynamic Response Analysis of Teché Dam," by Clough, R.W., Stephen, R.M. and Kuo, J.S.-H., August 1982, (PB83 147 496)A06.
- UCB/EERC-82/12 "Prediction of the Seismic Response of R/C Frame-Coupled Wall Structures," by Aktan, A.E., Bertero, V.V. and Piazzi, M., August 1982, (PB83 149 203)A09.
- UCB/EERC-82/13 "Preliminary Report on the Smart 1 Strong Motion Array in Taiwan," by Bolt, B.A., Loh, C.H., Penzien, J. and Tsai, Y.B., August 1982, (PB83 159 400)A10.
- UCB/EERC-82/14 "Shaking-Table Studies of an Eccentrically X-Braced Steel Structure," by Yang, M.S., September 1982, (PB83 260 778)A12.
- UCB/EERC-82/15 "The Performance of Stairways in Earthquakes," by Roha, C., Axley, J.W. and Bertero, V.V., September 1982, (PB83 157 693)A07.
- UCB/EERC-82/16 "The Behavior of Submerged Multiple Bodies in Earthquakes," by Liao, W.-G., September 1982, (PB83 158 709)A07.
- UCB/EERC-82/17 "Effects of Concrete Types and Loading Conditions on Local Bond-Slip Relationships," by Cowell, A.D., Popov, E.P. and Bertero, V.V., September 1982, (PB83 153 577)A04.
- UCB/EERC-82/18 "Mechanical Behavior of Shear Wall Vertical Boundary Members: An Experimental Investigation," by Wagner, M.T. and Bertero, V.V., October 1982, (PB83 159 764)A05.
- UCB/EERC-82/19 "Experimental Studies of Multi-support Seismic Loading on Piping Systems," by Kelly, J.M. and Cowell, A.D., November 1982.
- UCB/EERC-82/20 "Generalized Plastic Hinge Concepts for 3D Beam-Column Elements," by Chen, P. F.-S. and Powell, G.H., November 1982, (PB83 247 981)A13.
- UCB/EERC-82/21 "ANSR-II: General Computer Program for Nonlinear Structural Analysis," by Oughourlian, C.V. and Powell, G.H., November 1982, (PB83 251 330)A12.
- UCB/EERC-82/22 "Solution Strategies for Statically Loaded Nonlinear Structures," by Simons, J.W. and Powell, G.H., November 1982, (PB83 197 970)A06.
- UCB/EERC-82/23 "Analytical Model of Deformed Bar Anchorages under Generalized Excitations," by Ciampi, V., Elgehausen, R., Bertero, V.V. and Popov, E.P., November 1982, (PB83 169 532)A06.
- UCB/EERC-82/24 "A Mathematical Model for the Response of Masonry Walls to Dynamic Excitations," by Sucuoglu, H., Mengi, Y. and McNiven, H.D., November 1982, (PB83 169 011)A07.
- UCB/EERC-82/25 "Earthquake Response Considerations of Broad Liquid Storage Tanks," by Cambra, F.J., November 1982, (PB83 251 215)A09.
- UCB/EERC-82/26 "Computational Models for Cyclic Plasticity, Rate Dependence and Creep," by Mosaddad, B. and Powell, G.H., November 1982, (PB83 245 829)A08.
- UCB/EERC-82/27 "Inelastic Analysis of Piping and Tubular Structures," by Mahasuverachai, M. and Powell, G.H., November 1982, (PB83 249 987)A07.
- UCB/EERC-83/01 "The Economic Feasibility of Seismic Rehabilitation of Buildings by Base Isolation," by Kelly, J.M., January 1983, (PB83 197 988)A05.
- UCB/EERC-83/02 "Seismic Moment Connections for Moment-Resisting Steel Frames," by Popov, E.P., January 1983, (PB83 195 412)A04.
- UCB/EERC-83/03 "Design of Links and Beam-to-Column Connections for Eccentrically Braced Steel Frames," by Popov, E.P. and Malley, J.O., January 1983, (PB83 194 811)A04.
- UCB/EERC-83/04 "Numerical Techniques for the Evaluation of Soil-Structure Interaction Effects in the Time Domain," by Bayo, E. and Wilson, E.L., February 1983, (PB83 245 605)A09.
- UCB/EERC-83/05 "A Transducer for Measuring the Internal Forces in the Columns of a Frame-Wall Reinforced Concrete Structure," by Sause, R. and Bertero, V.V., May 1983, (PB84 119 494)A06.
- UCB/EERC-83/06 "Dynamic Interactions Between Floating Ice and Offshore Structures," by Croteau, P., May 1983, (PB84 119 486)A16.
- UCB/EERC-83/07 "Dynamic Analysis of Multiply Tuned and Arbitrarily Supported Secondary Systems," by Igusa, T. and Der Kiureghian, A., July 1983, (PB84 118 272)A11.
- UCB/EERC-83/08 "A Laboratory Study of Submerged Multi-body Systems in Earthquakes," by Ansari, G.R., June 1983, (PB83 261 842)A17.
- UCB/EERC-83/09 "Effects of Transient Foundation Uplift on Earthquake Response of Structures," by Yim, C.-S. and Chopra, A.K., June 1983, (PB83 261 396)A07.
- UCB/EERC-83/10 "Optimal Design of Friction-Braced Frames under Seismic Loading," by Austin, M.A. and Pister, K.S., June 1983, (PB84 119 288)A06.
- UCB/EERC-83/11 "Shaking Table Study of Single-Story Masonry Houses: Dynamic Performance under Three Component Seismic Input and Recommendations," by Manos, G.C., Clough, R.W. and Mayes, R.L., July 1983, (UCB/EERC-83/11)A08.
- UCB/EERC-83/12 "Experimental Error Propagation in Pseudodynamic Testing," by Shiing, P.B. and Mahin, S.A., June 1983, (PB84 119 270)A09.
- UCB/EERC-83/13 "Experimental and Analytical Predictions of the Mechanical Characteristics of a 1/5-scale Model of a 7-story R/C Frame-Wall Building Structure," by Aktan, A.E., Bertero, V.V., Chowdhury, A.A. and Nagashima, T., June 1983, (PB84 119 213)A07.

- UCB/EERC-83/14 "Shaking Table Tests of Large-Panel Precast Concrete Building System Assemblages," by Oliva, M.G. and Clough, R.W., June 1983, (PB86 110 210/AS)A11.
- UCB/EERC-83/15 "Seismic Behavior of Active Beam Links in Eccentrically Braced Frames," by Hjelmstad, K.D. and Popov, E.P., July 1983, (PB84 119 676)A09.
- UCB/EERC-83/16 "System Identification of Structures with Joint Rotation," by Dimsdale, J.S., July 1983, (PB84 192 210)A06.
- UCB/EERC-83/17 "Construction of Inelastic Response Spectra for Single-Degree-of-Freedom Systems," by Mahin, S. and Lin, J., June 1983, (PB84 208 834)A05.
- UCB/EERC-83/18 "Interactive Computer Analysis Methods for Predicting the Inelastic Cyclic Behaviour of Structural Sections," by Kaba, S. and Mahin, S., July 1983, (PB84 192 012)A06.
- UCB/EERC-83/19 "Effects of Bond Deterioration on Hysteretic Behavior of Reinforced Concrete Joints," by Filippou, F.C., Popov, E.P. and Bertero, V.V., August 1983, (PB84 192 020)A10.
- UCB/EERC-83/20 "Correlation of Analytical and Experimental Responses of Large-Panel Precast Building Systems," by Oliva, M.G., Clough, R.W., Velkov, M. and Gavrilovic, P., May 1988.
- UCB/EERC-83/21 "Mechanical Characteristics of Materials Used in a 1/5 Scale Model of a 7-Story Reinforced Concrete Test Structure," by Bertero, V.V., Aktan, A.E., Harris, H.G. and Chowdhury, A.A., October 1983, (PB84 193 697)A05.
- UCB/EERC-83/22 "Hybrid Modelling of Soil-Structure Interaction in Layered Media," by Tzong, T.-J. and Penzien, J., October 1983, (PB84 192 178)A08.
- UCB/EERC-83/23 "Local Bond Stress-Slip Relationships of Deformed Bars under Generalized Excitations," by Elgehausen, R., Popov, E.P. and Bertero, V.V., October 1983, (PB84 192 848)A09.
- UCB/EERC-83/24 "Design Considerations for Shear Links in Eccentrically Braced Frames," by Malley, J.O. and Popov, E.P., November 1983, (PB84 192 186)A07.
- UCB/EERC-84/01 "Pseudodynamic Test Method for Seismic Performance Evaluation: Theory and Implementation," by Shing, P.-S.B. and Mahin, S.A., January 1984, (PB84 190 644)A08.
- UCB/EERC-84/02 "Dynamic Response Behavior of Kiang Hong Dian Dam," by Clough, R.W., Chang, K.-T., Chen, H.-Q. and Stephen, R.M., April 1984, (PB84 209 402)A08.
- UCB/EERC-84/03 "Refined Modelling of Reinforced Concrete Columns for Seismic Analysis," by Kaba, S.A. and Mahin, S.A., April 1984, (PB84 234 384)A06.
- UCB/EERC-84/04 "A New Floor Response Spectrum Method for Seismic Analysis of Multiply Supported Secondary Systems," by Asfura, A. and Der Kiureghian, A., June 1984, (PB84 239 417)A06.
- UCB/EERC-84/05 "Earthquake Simulation Tests and Associated Studies of a 1/5th-scale Model of a 7-Story R/C Frame-Wall Test Structure," by Bertero, V.V., Aktan, A.E., Charney, F.A. and Sause, R., June 1984, (PB84 239 409)A09.
- UCB/EERC-84/06 "R/C Structural Walls: Seismic Design for Shear," by Aktan, A.E. and Bertero, V.V., 1984.
- UCB/EERC-84/07 "Behavior of Interior and Exterior Flat-Plate Connections subjected to Inelastic Load Reversals," by Zee, H.L. and Moehle, J.P., August 1984, (PB86 117 629/AS)A07.
- UCB/EERC-84/08 "Experimental Study of the Seismic Behavior of a Two-Story Flat-Plate Structure," by Moehle, J.P. and Diebold, J.W., August 1984, (PB86 122 553/AS)A12.
- UCB/EERC-84/09 "Phenomenological Modeling of Steel Braces under Cyclic Loading," by Ikeda, K., Mahin, S.A. and Dermitzakis, S.N., May 1984, (PB86 132 198/AS)A08.
- UCB/EERC-84/10 "Earthquake Analysis and Response of Concrete Gravity Dams," by Fenves, G. and Chopra, A.K., August 1984, (PB85 193 902/AS)A11.
- UCB/EERC-84/11 "EAGD-84: A Computer Program for Earthquake Analysis of Concrete Gravity Dams," by Fenves, G. and Chopra, A.K., August 1984, (PB85 193 613/AS)A05.
- UCB/EERC-84/12 "A Refined Physical Theory Model for Predicting the Seismic Behavior of Braced Steel Frames," by Ikeda, K. and Mahin, S.A., July 1984, (PB85 191 450/AS)A09.
- UCB/EERC-84/13 "Earthquake Engineering Research at Berkeley - 1984," by , August 1984, (PB85 197 341/AS)A10.
- UCB/EERC-84/14 "Moduli and Damping Factors for Dynamic Analyses of Cohesionless Soils," by Seed, H.B., Wong, R.T., Idriss, I.M. and Tokimatsu, K., September 1984, (PB85 191 468/AS)A04.
- UCB/EERC-84/15 "The Influence of SPT Procedures in Soil Liquefaction Resistance Evaluations," by Seed, H.B., Tokimatsu, K., Harder, L.F. and Chung, R.M., October 1984, (PB85 191 732/AS)A04.
- UCB/EERC-84/16 "Simplified Procedures for the Evaluation of Settlements in Sands Due to Earthquake Shaking," by Tokimatsu, K. and Seed, H.B., October 1984, (PB85 197 887/AS)A03.
- UCB/EERC-84/17 "Evaluation of Energy Absorption Characteristics of Highway Bridges Under Seismic Conditions - Volume I and Volume II (Appendices)," by Imbsen, R.A. and Penzien, J., September 1986.
- UCB/EERC-84/18 "Structure-Foundation Interactions under Dynamic Loads," by Liu, W.D. and Penzien, J., November 1984, (PB87 124 889/AS)A11.
- UCB/EERC-84/19 "Seismic Modelling of Deep Foundations," by Chen, C.-H. and Penzien, J., November 1984, (PB87 124 798/AS)A07.
- UCB/EERC-84/20 "Dynamic Response Behavior of Quan Shui Dam," by Clough, R.W., Chang, K.-T., Chen, H.-Q., Stephen, R.M., Ghanaat, Y. and Qi, J.-H., November 1984, (PB86 115177/AS)A07.
- UCB/EERC-85/01 "Simplified Methods of Analysis for Earthquake Resistant Design of Buildings," by Cruz, E.F. and Chopra, A.K., February 1985, (PB86 112299/AS)A12.
- UCB/EERC-85/02 "Estimation of Seismic Wave Coherency and Rupture Velocity using the SMART 1 Strong-Motion Array Recordings," by Abrahamson, N.A., March 1985, (PB86 214 343)A07.

- UCB/EERC-85/03 "Dynamic Properties of a Thirty Story Condominium Tower Building," by Stephen, R.M., Wilson, E.L. and Stander, N., April 1985, (PB86 118965/AS)A06.
- UCB/EERC-85/04 "Development of Substructuring Techniques for On-Line Computer Controlled Seismic Performance Testing," by Dermitzakis, S. and Mahin, S., February 1985, (PB86 132941/AS)A08.
- UCB/EERC-85/05 "A Simple Model for Reinforcing Bar Anchorages under Cyclic Excitations," by Filiippou, F.C., March 1985, (PB86 112 919/AS)A05.
- UCB/EERC-85/06 "Racking Behavior of Wood-framed Gypsum Panels under Dynamic Load," by Oliva, M.G., June 1985.
- UCB/EERC-85/07 "Earthquake Analysis and Response of Concrete Arch Dams," by Fok, K.-L. and Chopra, A.K., June 1985, (PB86 139672/AS)A10.
- UCB/EERC-85/08 "Effect of Inelastic Behavior on the Analysis and Design of Earthquake Resistant Structures," by Lin, J.P. and Mahin, S.A., June 1985, (PB86 135340/AS)A08.
- UCB/EERC-85/09 "Earthquake Simulator Testing of a Base-Isolated Bridge Deck," by Kelly, J.M., Buckle, I.G. and Tsai, H.-C., January 1986, (PB87 124 152/AS)A06.
- UCB/EERC-85/10 "Simplified Analysis for Earthquake Resistant Design of Concrete Gravity Dams," by Fenves, G. and Chopra, A.K., June 1986, (PB87 124 160/AS)A08.
- UCB/EERC-85/11 "Dynamic Interaction Effects in Arch Dams," by Clough, R.W., Chang, K.-T., Chen, H.-Q. and Ghanaat, Y., October 1985, (PB86 135027/AS)A05.
- UCB/EERC-85/12 "Dynamic Response of Long Valley Dam in the Mammoth Lake Earthquake Series of May 25-27, 1980," by Lai, S. and Seed, H.B., November 1985, (PB86 142304/AS)A05.
- UCB/EERC-85/13 "A Methodology for Computer-Aided Design of Earthquake-Resistant Steel Structures," by Austin, M.A., Pister, K.S. and Mahin, S.A., December 1985, (PB86 159480/AS)A10.
- UCB/EERC-85/14 "Response of Tension-Leg Platforms to Vertical Seismic Excitations," by Liou, G.-S., Penzien, J. and Yeung, R.W., December 1985, (PB87 124 871/AS)A08.
- UCB/EERC-85/15 "Cyclic Loading Tests of Masonry Single Piers: Volume 4 - Additional Tests with Height to Width Ratio of 1," by Sveinsson, B., McNiven, H.D. and Sucuoglu, H., December 1985.
- UCB/EERC-85/16 "An Experimental Program for Studying the Dynamic Response of a Steel Frame with a Variety of Infill Partitions," by Yanev, B. and McNiven, H.D., December 1985.
- UCB/EERC-86/01 "A Study of Seismically Resistant Eccentrically Braced Steel Frame Systems," by Kasai, K. and Popov, E.P., January 1986, (PB87 124 178/AS)A14.
- UCB/EERC-86/02 "Design Problems in Soil Liquefaction," by Seed, H.B., February 1986, (PB87 124 186/AS)A03.
- UCB/EERC-86/03 "Implications of Recent Earthquakes and Research on Earthquake-Resistant Design and Construction of Buildings," by Bertero, V.V., March 1986, (PB87 124 194/AS)A05.
- UCB/EERC-86/04 "The Use of Load Dependent Vectors for Dynamic and Earthquake Analyses," by Leger, P., Wilson, E.L. and Clough, R.W., March 1986, (PB87 124 202/AS)A12.
- UCB/EERC-86/05 "Two Beam-To-Column Web Connections," by Tsai, K.-C. and Popov, E.P., April 1986, (PB87 124 301/AS)A04.
- UCB/EERC-86/06 "Determination of Penetration Resistance for Coarse-Grained Soils using the Becker Hammer Drill," by Harder, L.F. and Seed, H.B., May 1986, (PB87 124 210/AS)A07.
- UCB/EERC-86/07 "A Mathematical Model for Predicting the Nonlinear Response of Unreinforced Masonry Walls to In-Plane Earthquake Excitations," by Mengi, Y. and McNiven, H.D., May 1986, (PB87 124 780/AS)A06.
- UCB/EERC-86/08 "The 19 September 1985 Mexico Earthquake: Building Behavior," by Bertero, V.V., July 1986.
- UCB/EERC-86/09 "EACD-3D: A Computer Program for Three-Dimensional Earthquake Analysis of Concrete Dams," by Fok, K.-L., Hall, J.F. and Chopra, A.K., July 1986, (PB87 124 228/AS)A08.
- UCB/EERC-86/10 "Earthquake Simulation Tests and Associated Studies of a 0.3-Scale Model of a Six-Story Concentrically Braced Steel Structure," by Uang, C.-M. and Bertero, V.V., December 1986, (PB87 163 564/AS)A17.
- UCB/EERC-86/11 "Mechanical Characteristics of Base Isolation Bearings for a Bridge Deck Model Test," by Kelly, J.M., Buckle, I.G. and Koh, C.-G., November 1987.
- UCB/EERC-86/12 "Effects of Axial Load on Elastomeric Isolation Bearings," by Koh, C.-G. and Kelly, J.M., November 1987.
- UCB/EERC-87/01 "The FPS Earthquake Resisting System: Experimental Report," by Zayas, V.A., Low, S.S. and Mahin, S.A., June 1987.
- UCB/EERC-87/02 "Earthquake Simulator Tests and Associated Studies of a 0.3-Scale Model of a Six-Story Eccentrically Braced Steel Structure," by Whitaker, A., Uang, C.-M. and Bertero, V.V., July 1987.
- UCB/EERC-87/03 "A Displacement Control and Uplift Restraint Device for Base-Isolated Structures," by Kelly, J.M., Griffith, M.C. and Aiken, I.D., April 1987.
- UCB/EERC-87/04 "Earthquake Simulator Testing of a Combined Sliding Bearing and Rubber Bearing Isolation System," by Kelly, J.M. and Chalhoub, M.S., 1987.
- UCB/EERC-87/05 "Three-Dimensional Inelastic Analysis of Reinforced Concrete Frame-Wall Structures," by Moazzami, S. and Bertero, V.V., May 1987.
- UCB/EERC-87/06 "Experiments on Eccentrically Braced Frames with Composite Floors," by Ricles, J. and Popov, E., June 1987.
- UCB/EERC-87/07 "Dynamic Analysis of Seismically Resistant Eccentrically Braced Frames," by Ricles, J. and Popov, E., June 1987.
- UCB/EERC-87/08 "Undrained Cyclic Triaxial Testing of Gravels-The Effect of Membrane Compliance," by Evans, M.D. and Seed, H.B., July 1987.
- UCB/EERC-87/09 "Hybrid Solution Techniques for Generalized Pseudo-Dynamic Testing," by Thewalt, C. and Mahin, S.A., July 1987.
- UCB/EERC-87/10 "Ultimate Behavior of Butt Welded Splices in Heavy Rolled Steel Sections," by Bruneau, M., Mahin, S.A. and Popov, E.P., July 1987.
- UCB/EERC-87/11 "Residual Strength of Sand from Dam Failures in the Chilean Earthquake of March 3, 1985," by De Alba, P., Seed, H.B., Retamal, E. and Seed, R.B., September 1987.
- UCB/EERC-87/12 "Inelastic Seismic Response of Structures with Mass or Stiffness Eccentricities in Plan," by Bruneau, M. and Mahin, S.A., September 1987.

- UCB/EERC-87/13 "CSTRUCT: An Interactive Computer Environment for the Design and Analysis of Earthquake Resistant Steel Structures," by Austin, M.A., Mahin, S.A. and Pister, K.S., September 1987.
- UCB/EERC-87/14 "Experimental Study of Reinforced Concrete Columns Subjected to Multi-Axial Loading," by Low, S.S. and Moehle, J.P., September 1987.
- UCB/EERC-87/15 "Relationships between Soil Conditions and Earthquake Ground Motions in Mexico City in the Earthquake of Sept. 19, 1985," by Seed, H.B., Romo, M.P., Sun, J., Jaime, A. and Lysmer, J., October 1987.
- UCB/EERC-87/16 "Experimental Study of Seismic Response of R. C. Setback Buildings," by Shahrooz, B.M. and Moehle, J.P., October 1987.
- UCB/EERC-87/17 "The Effect of Slabs on the Flexural Behavior of Beams," by Pantazopoulou, S.J. and Moehle, J.P., October 1987.
- UCB/EERC-87/18 "Design Procedure for R-FBI Bearings," by Mostaghel, N. and Kelly, J.M., November 1987.
- UCB/EERC-87/19 "Analytical Models for Predicting the Lateral Response of R C Shear Walls: Evaluation of their Reliability," by Vulcano, A. and Bertero, V.V., November 1987.
- UCB/EERC-87/20 "Earthquake Response of Torsionally-Coupled Buildings," by Hejal, R. and Chopra, A.K., December 1987.
- UCB/EERC-87/21 "Dynamic Reservoir Interaction with Monticello Dam," by Clough, R.W., Ghanaat, Y. and Qiu, X-F., December 1987.
- UCB/EERC-87/22 "Strength Evaluation of Coarse-Grained Soils," by Siddiqi, F.H., Seed, R.B., Chan, C.K., Seed, H.B. and Pyke, R.M., December 1987.
- UCB/EERC-88/01 "Seismic Behavior of Concentrically Braced Steel Frames," by Khatib, I., Mahin, S.A. and Pister, K.S., January 1988.
- UCB/EERC-88/02 "Experimental Evaluation of Seismic Isolation of Medium-Rise Structures Subject to Uplift," by Griffith, M.C., Kelly, J.M., Coveney, V.A. and Koh, C.G., January 1988.
- UCB/EERC-88/03 "Cyclic Behavior of Steel Double Angle Connections," by Astaneh-Asl, A. and Nader, M.N., January 1988.
- UCB/EERC-88/04 "Re-evaluation of the Slide in the Lower San Fernando Dam in the Earthquake of Feb. 9, 1971," by Seed, H.B., Seed, R.B., Harder, L.F. and Jong, H.-L., April 1988.
- UCB/EERC-88/05 "Experimental Evaluation of Seismic Isolation of a Nine-Story Braced Steel Frame Subject to Uplift," by Griffith, M.C., Kelly, J.M. and Aiken, I.D., May 1988.
- UCB/EERC-88/06 "DRAIN-2DX User Guide," by Allahabadi, R. and Powell, G.H., March 1988.
- UCB/EERC-88/07 "Cylindrical Fluid Containers in Base-Isolated Structures," by Chalhoub, M.S. and Kelly, J.M., April 1988.
- UCB/EERC-88/08 "Analysis of Near-Source Waves: Separation of Wave Types using Strong Motion Array Recordings," by Darragh, R.B., June 1988.
- UCB/EERC-88/09 "Alternatives to Standard Mode Superposition for Analysis of Non-Classically Damped Systems," by Kusainov, A.A. and Clough, R.W., June 1988.
- UCB/EERC-88/10 "The Landslide at the Port of Nice on October 16, 1979," by Seed, H.B., Seed, R.B., Schlosser, F., Blondeau, F. and Juran, I., June 1988.
- UCB/EERC-88/11 "Liquefaction Potential of Sand Deposits Under Low Levels of Excitation," by Carter, D.P. and Seed, H.B., August 1988.
- UCB/EERC-88/12 "Nonlinear Analysis of Reinforced Concrete Frames Under Cyclic Load Reversals," by Filippou, F.C. and Issa, A., September 1988.
- UCB/EERC-88/13 "Implications of Recorded Earthquake Ground Motions on Seismic Design of Building Structures," by Uang, C.-M. and Bertero, V.V., November 1988.
- UCB/EERC-88/14 "An Experimental Study of the Behavior of Dual Steel Systems," by Whittaker, A.S., Uang, C.-M. and Bertero, V.V., September 1988.
- UCB/EERC-88/15 "Dynamic Moduli and Damping Ratios for Cohesive Soils," by Sun, J.I., Golsorkhi, R. and Seed, H.B., August 1988.
- UCB/EERC-88/16 "Reinforced Concrete Flat Plates Under Lateral Load: An Experimental Study Including Biaxial Effects," by Pan, A. and Moehle, J., October 1988.
- UCB/EERC-88/17 "Earthquake Engineering Research at Berkeley - 1988," by EERC, November 1988.
- UCB/EERC-88/18 "Use of Energy as a Design Criterion in Earthquake-Resistant Design," by Uang, C.-M. and Bertero, V.V., November 1988.
- UCB/EERC-88/19 "Steel Beam-Column Joints in Seismic Moment Resisting Frames," by Tsai, K.-C. and Popov, E.P., November 1988.
- UCB/EERC-88/20 "Base Isolation in Japan, 1988," by Kelly, J.M., December 1988.
- UCB/EERC-89/01 "Behavior of Long Links in Eccentrically Braced Frames," by Engelhardt, M.D. and Popov, E.P., January 1989.
- UCB/EERC-89/02 "Earthquake Simulator Testing of Steel Plate Added Damping and Stiffness Elements," by Whittaker, A., Bertero, V.V., Alonso, J. and Thompson, C., January 1989.
- UCB/EERC-89/03 "Implications of Site Effects in the Mexico City Earthquake of Sept. 19, 1985 for Earthquake-Resistant Design Criteria in the San Francisco Bay Area of California," by Seed, H.B. and Sun, J.I., March 1989.
- UCB/EERC-89/04 "Earthquake Analysis and Response of Intake-Outlet Towers," by Goyal, A. and Chopra, A.K., July 1989.
- UCB/EERC-89/05 "The 1985 Chile Earthquake: An Evaluation of Structural Requirements for Bearing Wall Buildings," by Wallace, J.W. and Moehle, J.P., July 1989.
- UCB/EERC-89/06 "Effects of Spatial Variation of Ground Motions on Large Multiply-Supported Structures," by Hao, H., July 1989.
- UCB/EERC-89/07 "EADAP - Enhanced Arch Dam Analysis Program: User's Manual," by Ghanaat, Y. and Clough, R.W., August 1989.
- UCB/EERC-89/08 "Seismic Performance of Steel Moment Frames Plastically Designed by Least Squares Stress Fields," by Ohi, K. and Mahin, S.A., August 1989.
- UCB/EERC-89/09 "Feasibility and Performance Studies on Improving the Earthquake Resistance of New and Existing Buildings Using the Friction Pendulum System," by Zayas, V., Low, S., Mahin, S.A. and Bozzo, L., July 1989.
- UCB/EERC-89/10 "Measurement and Elimination of Membrane Compliance Effects in Undrained Triaxial Testing," by Seed, R.B., Anwar, H. and Nicholson, P.G., September 1989.
- UCB/EERC-89/11 "Static Tilt Behavior of Unanchored Cylindrical Tanks," by Lau, D.T. and Clough, R.W., September 1989.
- UCB/EERC-89/12 "ADAP-88: A Computer Program for Nonlinear Earthquake Analysis of Concrete Arch Dams," by Fenves, G.L., Mojtahedi, S. and Reimer, R.B., September 1989.